

2m4

NASA CR-134541



BURNING RATE RESPONSE OF LIQUID MONOPROPELLANTS TO IMPOSED PRESSURE OSCILLATIONS

by

C. B. Allison

Mechanical Engineering Department
The Pennsylvania State University
University Park, Pennsylvania



prepared for

NATIONAL AERONAUTICS AND SPACE ADMINISTRATION

NASA Lewis Research Center
Contract NGR 39-009-077

Richard J. Priem, Program Manager and Technical Monitor

(NASA-CR-134541) BURNING RATE RESPONSE
OF LIQUID MONOPROPELLANTS TO IMPOSED
PRESSURE OSCILLATIONS (Pennsylvania State
Univ.) 138 p HC \$9.00 CSCL 21I

N74-16479

Unclas

G3/27 28328

154

NOTICE

This work was prepared as an account of Government sponsored work. Neither the United States, nor the National Aeronautics and Space Administration (NASA), nor any person acting on behalf of NASA:

- A.) Makes any warranty or representation, expressed or implied, with respect to the accuracy, completeness, or usefulness of the information contained in this report, or that the use of any information, apparatus, method, or process disclosed in this report may not infringe privately owned rights; or
- B.) Assumes any liabilities with respect to the use of, or for damages resulting from the use of any information, apparatus, method or process disclosed in this report.

As used above, "person acting on half of NASA" includes any employee or contractor of NASA, or employee of such contractor, to the extent that such employee or contractor of NASA, or employee of such contractor prepares, disseminates, or provides access to, any information pursuant to his employment or contract with NASA, or his employment with such contractor.

I

1. Report No. NASA CR-134541		2. Government Accession No.		3. Recipient's Catalog No.	
4. Title and Subtitle Burning Rate Response of Liquid Monopropellants to Imposed Pressure Oscillations				5. Report Date January 1974	
				6. Performing Organization Code	
7. Author(s) Carl B. Allison				8. Performing Organization Report No.	
9. Performing Organization Name and Address Mechanical Engineering Department The Pennsylvania State University University Park, Pennsylvania 16802				10. Work Unit No.	
				11. Contract or Grant No. NGR 39-009-077	
12. Sponsoring Agency Name and Address National Aeronautics and Space Administration Washington, D.C. 20546				13. Type of Report and Period Covered Contractor Report	
				14. Sponsoring Agency Code	
15. Supplementary Notes Program Manager and Technical Monitor, Richard J. Priem, Chemical Rocket Division NASA Lewis Research Center, Cleveland, Ohio					
16. Abstract The combustion characteristics of hydrazine strands were studied under both steady state and oscillatory conditions. A steady strand burner was used to measure steady strand burning rates, liquid temperature distributions and surface temperatures as a function of pressure in the pressure range of 0.32 to 42 atm. It was found that for subatmospheric pressures the burning rate varied as the square root of pressure; for pressures greater than atmospheric the burning rate varied linearly with pressure. A theoretical model of the strand combustion system was developed and matched to the steady burning rates by assuming a reaction order of one for subatmospheric pressures and a reaction order of two for pressures greater than atmospheric. The model was also found to be in good agreement with measurements of liquid temperature distributions and surface temperatures. With the confidence gained in the model from the steady results, predictions were made of oscillatory burning rates. An oscillatory version of the steady strand apparatus was developed to provide experimental data for comparison with the theoretical model. Theory and experiment were found to be in good agreement in the pressure range of 1 to 10 atm if the hydrazine decomposition reaction was assumed to be second order with an activation energy of about 40 kcal. The results show an increase in the response of the combustion process as interaction occurs with transient liquid phase effects, yielding a band of frequencies where the combustion process exerts sufficient amplifying power to provide a mechanism for driving combustion instability.					
17. Key Words (Suggested by Author(s)) Hydrazine fuel combustion Burning rate response Acoustic admittance			18. Distribution Statement Unclassified-Unlimited		
19. Security Classif. (of this report) Unclassified		20. Security Classif. (of this page) Unclassified		21. No. of Pages 137	22. Price* \$3.00

* For sale by the National Technical Information Service, Springfield, Virginia 22151

ACKNOWLEDGMENTS

The author would like to express his appreciation to his advisor, Professor G. M. Faeth, for his invaluable guidance and encouragement throughout the investigation.

The financial support of the National Aeronautics and Space Administration under Contract No. NGR 39-009-077, with Dr. R. J. Priem of the Lewis Research Center serving as contract monitor, is also gratefully acknowledged.

PRECEDING PAGE BLANK NOT FILMED

TABLE OF CONTENTS

	<u>Page</u>
ACKNOWLEDGMENTS	ii
LIST OF TABLES	vi
LIST OF FIGURES	vii
NOMENCLATURE.	x
I. INTRODUCTION	1
1.1 General Statement of the Problem.	1
1.2 Previous Related Studies.	3
1.2.1 Steady Hydrazine Combustion.	3
1.2.2 Combustion Instability	5
1.3 Specific Statement of the Problem	7
II. EXPERIMENTAL APPARATUS	9
2.1 Steady Strand Apparatus	9
2.1.1 General Description.	10
2.1.2 Test Procedure	12
2.2 Oscillatory Strand Combustion Apparatus	14
2.2.1 General Description.	14
2.2.2 Photographic System.	16
2.2.3 Pressure Supply System	18
2.2.4 Test Procedure	21
III. THEORETICAL CONSIDERATIONS	23
3.1 Existing Theories	23
3.2 General Model and Assumptions	25
3.3 Governing Equations	29
3.3.1 Dimensional Equations.	29
3.3.2 Nondimensional Equations	32
3.3.3 Perturbation Analysis.	36
3.4 Zero Order (Steady State) Problem	37
3.4.1 Equations.	37
3.4.2 Solution Method.	38

	<u>Page</u>
3.5 First Order Problem	40
3.5.1 Equations.	40
3.5.2 Solution Method.	42
IV. RESULTS AND DISCUSSION	44
4.1 Steady Strand Combustion.	44
4.1.1 Burning Rates.	46
4.1.2 Liquid Temperatures.	52
4.1.3 Additional Theoretical Results	54
4.2 Oscillatory Combustion.	62
4.2.1 Data Reduction	62
4.2.2 Effect of Pressure Amplitude	64
4.2.3 High Pressure Results.	67
4.2.4 Low Pressure Results	71
4.2.5 Additional Implications of the Theoretical Model.	74
4.2.5.1 Effect of Mean Pressure	74
4.2.5.2 Effect of Conditioning Temperature.	82
4.2.5.3 Acoustic Admittance	89
V. SUMMARY AND CONCLUSIONS.	96
5.1 Summary	96
5.2 Conclusions	98
5.2.1 Steady Strand Combustion	98
5.2.2 Oscillatory Strand Combustion.	99
BIBLIOGRAPHY.	100
APPENDIX A: CHECK OF THE ASSUMPTIONS OF THE ANALYSIS	104
A.1 Estimation of Radiation Effects During Strand Burning	105
A.2 Phase Equilibrium Assumption.	106
A.3 Constant Total Pressure Assumption.	106
APPENDIX B: FORM OF THE ZERO ORDER ENERGY EQUATION FOR LARGE η	108
APPENDIX C: SOLUTION METHOD FOR THE FIRST ORDER PROBLEM.	111
APPENDIX D: PHYSICAL PROPERTIES.	122

APPENDIX E: SURFACE MASS FRACTION USING THE INFINITE ACTIVATION ENERGY ASSUMPTION	126
APPENDIX F: DEVELOPMENT OF THE TOTALLY QUASI-STEADY ANALYSIS	129
APPENDIX G: DEVELOPMENT OF THE ACOUSTIC ADMITTANCE EXPRESSION	131
APPENDIX H: EXPERIMENTAL DATA.	134

LIST OF TABLES

<u>Table</u>	<u>Title</u>	<u>Page</u>
1	Properties Used in the Theoretical Model	45
2	Correlation Conditions and Parameters Used in the Theoretical Model.	51
3	Additional Correlation Condition and Parameters Used in the Theoretical Model	75
4	References for Physical Properties	124
5	Hydrazine Steady Strand Burning Rates.	135
6	Hydrazine Liquid Surface Temperatures.	136
7	Hydrazine Liquid Surface Oscillation Amplitude and Mean Burning Rate at a Mean Pressure of 1.54 atm and a Frequency of 1.32 Hz for Various Pressure Amplitudes . . .	136
8	Hydrazine Liquid Surface Oscillation Amplitude and Phase Angle at a Mean Pressure of 9.77 atm for Various Frequencies.	137
9	Hydrazine Liquid Surface Oscillation Amplitude and Phase Angle at a Mean Pressure of 1.18 atm for Various Frequencies.	137

LIST OF FIGURES

<u>Figure</u>	<u>Caption</u>	<u>Page</u>
1	Sketch of the Steady Strand Burner Apparatus	11
2	Sketch of the Oscillatory Strand Combustion Apparatus. . .	15
3	Photograph of the Oscillatory Strand Test Chamber.	17
4	Photograph of the Rotary Valve Arrangement	20
5	Sketch of the Theoretical Model.	26
6	Steady Strand Burning Rates as a Function of Pressure for Various Liquid Purities	47
7	Steady Strand Burning Rates as a Function of the Reciprocal of the Tube Diameter.	49
8	Theoretical and Experimental Steady Strand Burning Rates as a Function of Pressure.	50
9	Theoretical and Experimental Liquid Phase Temperature Distributions.	53
10	Theoretical and Experimental Liquid Surface Temperatures as a Function of Pressure.	55
11	Steady State Gas Phase Temperature and Reaction Rate Distributions for $n = 2$, $E = 1$	57
12	Steady State Gas Phase Temperature and Reaction Rate Distributions for $n = 2$, $E = 10$	58
13	Steady State Gas Phase Temperature and Reaction Rate Distributions for $n = 2$, $E = 30$	59
14	Steady State Gas Phase Temperature and Reaction Rate Distributions for $n = 1$, $E = 1$	60
15	Steady State Gas Phase Temperature and Reaction Rate Distributions for $n = 1$, $E = 10$	61
16	Typical Experimental Pressure and Liquid Surface Oscillations as a Function of Time	63
17	Amplitude of the Liquid Surface Oscillations as a Function of Pressure Amplitude	65

LIST OF FIGURES (CONTINUED)

<u>Figure</u>	<u>Caption</u>	<u>Page</u>
18	Mean Burning Rates as a Function of Pressure Amplitude . .	66
19	Theoretical and Experimental Magnitude of the Liquid Surface Oscillations as a Function of Frequency at a Mean Pressure of 9.77 atm.	68
20	Theoretical and Experimental Phase Angle of the Liquid Surface Oscillations as a Function of Frequency at a Mean Pressure of 9.77 atm.	70
21	Theoretical (n = 1) and Experimental Magnitude of the Liquid Surface Oscillations as a Function of Frequency at a Mean Pressure of 1.18 atm	72
22	Theoretical (n = 1) and Experimental Phase Angle of the Liquid Surface Oscillations as a Function of Frequency at a Mean Pressure of 1.18 atm	73
23	Theoretical (n = 2) and Experimental Magnitude of the Liquid Surface Oscillations as a Function of Frequency at a Mean Pressure of 1.18 atm	76
24	Theoretical (n = 2) and Experimental Phase Angle of the Liquid Surface Oscillations as a Function of Frequency at a Mean Pressure of 1.18 atm	77
25	Burning Rate Oscillation Amplitude and Phase Angle as a Function of Frequency for $P_{\circ}^* = 1$ atm, n = 2, E = 1. .	79
26	Burning Rate Oscillation Amplitude and Phase Angle as a Function of Frequency for $P_{\circ}^* = 10$ atm, n = 2, E = 1 .	80
27	Burning Rate Oscillation Amplitude and Phase Angle as a Function of Frequency for $P_{\circ}^* = 100$ atm, n = 2, E = 1. .	81
28	Burning Rate Oscillation Amplitude and Phase Angle as a Function of Frequency for $P_{\circ}^* = 1$ atm, n = 2, E = 10 .	83
29	Burning Rate Oscillation Amplitude and Phase Angle as a Function of Frequency for $P_{\circ}^* = 10$ atm, n = 2, E = 10. .	84
30	Burning Rate Oscillation Amplitude and Phase Angle as a Function of Frequency for $P_{\circ}^* = 100$ atm, n = 2, E = 10	85
31	Burning Rate Oscillation Amplitude and Phase Angle as a Function of Frequency for $P_{\circ}^* = 1$ atm, n = 2, E = 30. . . .	86

LIST OF FIGURES (CONTINUED)

<u>Figure</u>	<u>Caption</u>	<u>Page</u>
32	Burning Rate Oscillation Amplitude and Phase Angle as a Function of Frequency for $P_o^* = 10$ atm, $n = 2$, $E = 30$. . .	87
33	Burning Rate Oscillation Amplitude and Phase Angle as a Function of Frequency for $P_o^* = 100$ atm, $n = 2$, $E = 30$. . .	88
34	Burning Rate Oscillation Amplitude and Phase Angle as a Function of Frequency for $P_o^* = 1$ atm, $n = 2$, $E = 9.628$, $T_{\infty}^* = 350^\circ\text{K}$	90
35	Real Part of the Acoustic Admittance as a Function of Frequency for $n = 2$, $E = 1$ and Various Pressures	91
36	Real Part of the Acoustic Admittance as a Function of Frequency for $n = 2$, $E = 10$ and Various Pressures.	92
37	Real Part of the Acoustic Admittance as a Function of Frequency for $n = 2$, $E = 30$ and Various Pressures.	93

NOMENCLATURE

<u>Symbol</u>	<u>Description</u>
A	Defined in Equation (30)
A_b	Acoustic admittance
a	Constant in Clausius-Clapeyron Equation, see Equation (16)
B*	Pre-exponential factor
C	Constant, see Equations (55 and 56)
C_l	Specific heat of liquid
C_p	Specific heat of gas
D	Diffusion coefficient
E	Activation energy
h_i^o	Standard heat of formation of species i
i	$\sqrt{-1}$
K_1	Constant, see Equation (C.1)
L	Heat of vaporization
L_1	Constant in Clausius-Clapeyron Equation, see Equation (16)
M	Molecular weight
N	Total number of species
n	Reaction order
P	Pressure
q	Heat of combustion
R	Gas constant
r	Defined in Equation (21)
T	Temperature
$T_{-\infty}$	Temperature of cold end of liquid fuel

<u>Symbol</u>	<u>Description</u>
t	Time
v	Velocity
w	Reaction rate
x	Distance
x_s	Instantaneous position of liquid surface
Y	Mass fraction
α	Liquid diffusivity
β	Ratio of specific heats, see Equation (39)
γ	Specific heat ratio
δ	Temperature dependence of pre-exponential factor
δ_{\perp}	Defined by Equation (35)
ϵ	Amplitude of oscillatory pressure
η	Dimensionless distance, see Equation (20)
θ	Defined by Equation (22)
λ	Thermal conductivity
$\sqrt{\cdot}_i$	Defined by Equation (7)
$\sqrt{\cdot}'_i$	Stoichiometric coefficient of species i as reactant
$\sqrt{\cdot}''_i$	Stoichiometric coefficient of species i as product
ρ	Density
ϕ	Phase angle
ω	Nondimensional frequency

Subscripts

F	Fuel
f	Flame surface
H	Homogeneous solution

<u>Symbol</u>	<u>Description</u>
I	Imaginary quantity
i	Species i
l	Liquid
P	Particular solution
R	Real quantity
s	Liquid surface
s ⁻	Inner side of liquid surface
s ⁺	Outer side of liquid surface
o	Steady state quantities
1	First order quantities
∞	Far from liquid surface

Superscripts

*	Dimensional quantities
---	------------------------

SUMMARY

The major objective of the present study was to investigate the combustion characteristics of liquid hydrazine strands under both steady state and oscillatory conditions. A theoretical model of the combustion system was developed and compared with the experimental results.

The theoretical model of the system assumed one-dimensional flow and used global kinetic parameters to characterize the hydrazine decomposition flame. The properties of the liquid phase were assumed constant; however, a variable property gas phase solution was obtained through the use of a modified Howarth transformation. Conventional low pressure phase equilibrium was used to characterize the liquid surface. The equations resulting from the theoretical model were solved using a perturbation analysis with the amplitude of the imposed pressure oscillations taken as the perturbation parameter. Thus, in zero order, the model corresponds to steady strand combustion while the first order model takes into account the effects of a small amplitude, sinusoidal pressure disturbance.

The steady experimental results were obtained using a steady strand burner. With this apparatus, steady strand burning rates were obtained for mean pressures ranging from 0.32 up to 42 atm. Liquid temperature disturbances and surface temperatures were measured in the range of 1.0 to 20.5 atm.

For the unsteady measurements, an oscillatory version of the steady strand apparatus was developed. With this apparatus, the

burning rate response of hydrazine to imposed pressure oscillations was measured. The apparatus permitted the amplitude of the oscillating pressure to be varied independently of the frequency at a given mean pressure. Oscillatory burning rates were obtained in the mean pressure range of 1 to 10 atm with frequencies varying from 0.40 to 5.2 Hz and pressure amplitudes up to 35% of the mean pressure.

The experimental steady strand burning rates were found to be dependent on the liquid hydrazine purity. Adding water as an impurity to the fuel resulted in a reduction in the burning rate. However, for the highest purity fuels tested (98.6 and 99.4%) the burning rate of the two fuels was not appreciably different.

The diameter of the sample tube was found to have an effect upon the experimental burning rate. As tube size increased, the burning rate decreased due to the reduction in the effects of surface tension for the larger tubes. By plotting the strand burning rate as a function of the reciprocal of the tube diameter, linear plots were obtained allowing the determination of the fundamental strand burning rate (burning rate in an infinite diameter tube) by extrapolation.

For subatmospheric pressures the fundamental burning rate varied as the square root of pressure; for pressures greater than atmospheric, the fundamental burning rate varied linearly with pressure. The theory was matched to these results by assuming a first order decomposition reaction for subatmospheric pressures and a second order reaction for pressures greater than atmospheric.

The liquid temperature experimental results gave a good prediction of the theoretical model assuming constant liquid properties and by using a value of $1.26 \times 10^{-3} \text{ cm}^2/\text{sec}$ for the liquid thermal diffusivity of hydrazine. The liquid surface temperature results were also adequately predicted by the theoretical model, justifying the low pressure phase equilibrium assumption.

The steady strand results indicated that the theoretical model was in good agreement with all the available data on hydrazine strand combustion. Next, the theoretical model was compared to the experimental oscillatory burning rate measurements. It was found that the oscillatory measurements of both amplitude and phase angle of the liquid surface oscillations were in good agreement with the theoretical model if the decomposition reaction was assumed to be second order with an activation energy of about 40 kcal ($E=15$) for mean pressures in the range of 1-10 atm. Unlike the steady state where activation energy had little effect upon the predicted burning rate, for the oscillatory case activation energy had a pronounced effect upon both the amplitude and phase angle of the unsteady burning rate.

The theoretical results showed that for activation energies characteristic of hydrazine ($E=10-15$) an increase in the response of the combustion process occurred due to interaction with transient liquid phase effects. This yielded a band of frequencies where the combustion process exerted sufficient amplifying power to provide a mechanism for driving combustion instability. As pressure increased the amplifying power of the combustion process increased and this frequency band moved to higher frequencies.

CHAPTER I

INTRODUCTION

1.1 General Statement of the Problem

The problem of combustion instability has plagued liquid rocket engine designers for a number of years. Since this phenomenon severely reduces the efficiency and thrust of the engine and in extreme cases may even cause destruction of the rocket, there is much interest in gaining an understanding of the process. Briefly, combustion instability results from the coupling of the combustion processes with the fluid dynamic processes in a combustion chamber. As a result of this coupling, the combustion supplies oscillatory energy to sustain any oscillations of the fluid dynamic variables (pressure, velocity, etc.). If sufficient damping exists in the system, the energy will be dissipated more rapidly than it is supplied and the oscillations will decay. Thus, combustion instability can be prevented by either increasing the damping of the system or by decreasing the coupling of the combustion and fluid dynamic processes.

The main method of suppressing combustion instability has been to use acoustic liners, Helmholtz resonators and other damping devices in the combustion chamber. However, even with these damping devices one can never be sure a combustion chamber will be stable until test firings are made. The most desirable approach to the problem is to gain an understanding of the coupling between the combustion and fluid dynamics of the system and then to develop means of reducing this effect.

There have been basically two approaches to the theoretical description of the processes taking place in a combustion chamber. One method is the heuristic approach of Crocco [1, 2, 3] or the so-called time-lag theory. Crocco postulates the existence of a time-lag between the time when an element of fuel is injected into the combustion chamber and the time when it is gasified by combustion to final products. However, the time-lag can only be deduced from experimental rocket firings and no detailed description of the coupling between combustion and the gas dynamics is offered.

The other approach has been due to Priem [4, 5, 6] who numerically solves the gas dynamic equations for the combustion chamber. Two of the most important parameters of the analysis are the thermal energy and gas release rates of the combustion process. With Priem's approach, attention is focussed on the nonsteady burning rate response of an individual droplet to a fluctuation in the surrounding gaseous flow field (either a pressure or a velocity fluctuation or both). This burning rate response is then used as the source term in the gas dynamic equations.

The above discussion has indicated the importance of the burning rate response of a liquid to fluctuations in its environment. Thus the subject of the present investigation is the study of the burning rate response of a liquid to fluctuations in ambient conditions. For ease of interpretation of the results, only pressure fluctuations are considered. In addition, the pressure fluctuations are assumed small when compared to the mean pressure. The particular fuel chosen for study is hydrazine since the hydrazine

family of fuels comprise some of the most important fuels used in current space rocket applications.

In the next section a review is made of the available literature on steady hydrazine combustion. Emphasis is placed on hydrazine strand burning since this experimental technique is used in the present study. In the following section, the literature on liquid combustion instability, in particular the unsteady burning rate response of a liquid to fluctuations in its environment, is reviewed.

1.2 Previous Related Studies

1.2.1 Steady Hydrazine Combustion

Numerous studies have been conducted on steady state liquid hydrazine combustion as droplets and also as liquid strands. The literature on hydrazine droplet combustion has been reviewed in detail in Reference [7]. By considering the bulk of the data on hydrazine droplet combustion, References [7-11], Reference [7] concludes that a monopropellant gas phase model is more realistic than a bipropellant model for hydrazine.

The work on hydrazine strand combustion has been mainly concerned with the effect of pressure on hydrazine burning rates. With the strand burner technique, liquid hydrazine is placed in an open-ended test tube which is contained within a windowed pressure vessel. After ignition, the liquid surface moves down the tube as the fuel is consumed by the combustion process. The rate of propagation of the liquid surface (the strand burning rate) is then measured as a function of pressure.

Adams and Stocks [12] investigated the burning rate of liquid hydrazine strands in a nitrogen pressurized vessel over the pressure range of 1-45 atm. Tube diameters of 3 and 5 mm were used. Burning rates were measured by timing the movement of the liquid surface, between marks placed 3 cm apart on the tube surface, with a stopwatch. The results of Adams and Stocks [12] show considerable scatter. However, they conclude that for pressures up to about 10 atm the burning rate of liquid hydrazine is proportional to the square root of pressure. For higher pressures their data indicates that the burning rate is independent of pressure. They also found that above a certain pressure hydrazine failed to burn as a liquid strand. This upper extinction pressure was found to be a function of the tube diameter and also the concentration of the liquid hydrazine. The upper extinction pressure increased with increasing tube diameter and increasing liquid fuel concentration. In addition, the upper extinction pressure increased by substituting helium for the nitrogen pressurizing gas.

Gray and Kay [13] and Gray, et al., [14] extended the work of Adams and Stocks [12] to subatmospheric pressures. They found that a lower extinction pressure, below which the liquid failed to propagate down the tube, also exists for hydrazine.

The burning rate of liquid hydrazine was found to be proportional to the square root of pressure for pressures as low as 0.4 atm [13 and 14] in agreement with the results of Adams and Stocks [12]. The lower extinction pressure increased with increasing tube diameter and also increased with decreasing liquid purity. As

the lower extinction pressure was approached a slight bubbling of the liquid near the liquid surface was observed.

Antoine [15] studied the burning rate of liquid hydrazine strands in the pressure range of 1-19 atm. The tube diameter and liquid purity were found to have a significant effect on the burning rate. As tube diameter decreased and/or liquid purity decreased, the burning rate decreased significantly at a given pressure. For the 100% concentration liquid hydrazine burning in the largest diameter tube tested (12.7 mm), the burning rate varied linearly with pressure over the pressure range tested. The extinction pressures for hydrazine were not investigated by Antoine.

Thus, the previous studies on liquid hydrazine strand combustion all indicate that liquid phase purity and tube diameter have a significant effect on the burning rate. The results of Adams and Stocks [12], Gray and Kay [13] and Gray, et al., [14] indicate that the burning rate of hydrazine is proportional to the square root of pressure in the pressure range of 0.4-10.0 atm whereas the results of Antoine [15] indicate that for 100% N_2H_4 the burning rate is proportional to pressure in the pressure range of 1-10 atm for the 12.7 mm tube.

1.2.2 Combustion Instability

The literature on liquid propellant combustion instability is vast (for example, Reference [16] cites 778 references). Therefore, only the most important studies on liquid burning rate response to imposed ambient oscillations will be considered here.

Experimental studies on nonsteady liquid combustion are virtually non-existent. The approach used in the past has been to infer the burning rate response from the pressure-time curves from actual rocket engine firings. Of course, this approach depends on some theoretical model of the combustion-gas dynamic problem, and direct experimental verification of any unsteady combustion model is impossible with this technique.

Numerous unsteady liquid combustion theoretical models have been proposed. Two of the earliest models are quite similar. Williams [17] and Strahle [18, 19] considered longitudinal standing wave fluctuations acting on the leading edge of a burning droplet. Both assumed the classic Burke-Schumann thin diffusion flame existed in the interior of the leading edge boundary layer. Williams considered only a flat plate whereas Strahle studied both the stagnation point and flat plate flows.

Both of these studies found only rather flat response curves as a function of frequency and, moreover, the peak that does exist occurs at such a large frequency (1000-10,000 Hz) that no influence on instability is expected. However, the fallacy with these treatments can be traced to the assumption of constant liquid temperature with time. It can be shown that the characteristic thermal wave time in the liquid phase is at least an order of magnitude greater than the characteristic thermal wave time in the gas phase. [20] Thus, on this basis, the gas phase is more logically considered quasi-steady compared to the liquid phase, especially at low frequencies. In other words, the assumption of constant liquid temperature cannot be true even at low frequencies.

Heidmann and Wieber [21] assumed that the gas phase burning rate of the fuel was equal to the liquid fuel vaporization rate at each instant of time. For low frequencies this is a valid assumption. However, as in the investigations of Williams [17] and Strahle [18, 19], the thermal wave time effects are neglected and the droplet temperature, at any instant of time, is considered uniform but varying with time.

T'ien and Sirignano [22] recognized the importance of the liquid thermal wave time. They considered a fuel evaporating from a flat plate with a reacting gaseous boundary layer and a longitudinally oscillating external flow. The gas phase was considered quasi-steady compared with the liquid phase which is correct in the limit of low frequency oscillations. They found peaks in the response function which are directly related to the effects of thermal lag in the liquid phase. However, it is questionable that this analysis indicates the true combustion gas dynamic coupling mechanism since the peaks are not of sufficient magnitude to provide instability in an actual rocket.

1.3 Specific Statement of the Problem

As indicated by the preceding discussion, although a number of theories of the unsteady combustion of liquid fuels have been developed, the direct experimental verification of any of them has not been accomplished up to the present time. In addition, all of the theoretical models consider a bipropellant gas phase combustion process. Some of the most important fuels used in current space rocket applications are liquid hydrazine and its derivatives. Earlier

work on the combustion of hydrazine indicates that a monopropellant gas phase model is more realistic for the hydrazine fuels. [7] However, discrepancies exist concerning the reported dependence of the steady burning rate of hydrazine on pressure. [12-15]

Thus, the specific objectives of the present study were:

1. Study the steady strand combustion characteristics of hydrazine both theoretically and experimentally.
 - a. Experimentally determine the steady strand burning rate as a function of pressure, liquid concentration and tube diameter.
 - b. Experimentally measure the liquid temperature distribution and surface temperature as a function of pressure.
 - c. Develop a theoretical model of the system and compare directly with the experimental results.
2. Study the oscillatory combustion characteristics of hydrazine both theoretically and experimentally.
 - a. Experimentally measure the oscillatory burning rate (both magnitude and phase angle with respect to to the imposed pressure oscillations) of hydrazine as a function of mean pressure and the frequency and amplitude of the imposed pressure oscillations.
 - b. Develop a theoretical model of the oscillatory system and directly compare the theoretical predictions with the experimental results.

CHAPTER II

EXPERIMENTAL APPARATUS

As indicated in the Introduction, a major objective of the present study was to experimentally measure unsteady hydrazine burning rates. However, before studying the unsteady combustion characteristics of hydrazine, the steady state characteristics were studied thoroughly.

In this chapter the apparatus used to obtain the experimental data are described. First, the steady strand combustion apparatus is discussed followed by a description of the oscillatory combustion apparatus. Since the basic configurations of the two apparatus were the same, many of the components used in the apparatus, such as the ignitor, pressure gages and instrumentation, were similar. These components are described in detail in the section on the steady strand apparatus.

2.1 Steady Strand Apparatus

The liquid strand combustion apparatus was used to study the steady state combustion characteristics of hydrazine. With this technique the burning rate of the fuel is determined by measuring the constant rate of regression of the liquid surface as the fuel is consumed by the combustion process. In addition to measuring burning rates, liquid temperatures were measured using a thermocouple. In the next section the steady strand burner is described in detail followed by a description of the test procedure.

2.1.1 General Description

A sketch of the steady strand apparatus is shown in Figure 1. The pressure vessel used for the tests had an inside diameter of 6.4 cm with an inside length of 28 cm and was rated to a pressure of 400 atm. The windows of the vessel provided a 2.5 cm diameter viewing space. The ignitor coil used to ignite the fuel sample was made of spiral wound 24 gage nichrome wire about 30 cm in length. The voltage applied to the wire varied from between 55 to 65 volts. A Heise pressure gage with a range of 0-750 psia was used to measure the total pressure in the test chamber.

Three sizes of pyrex sample tubes were used--4, 8 and 12 mm I.D. each with a wall thickness of 1 mm. The thermocouple was located 4 cm from the lower edge of the ignitor coil and 3 cm from the bottom of the tube to insure that the combustion wave was steady when the temperature measurements were made.

The optical system consisted of a background light and high speed motion picture camera. A PEK Labs. Model No. 911 mercury arc lamp was used to provide the back light to the liquid column. The shadowgraphs were taken with a Photosonics Model No. 16 mm-1b 16 mm camera using Kodak Plus X Reversal film operating at speeds up to 100 frames per second. The distance measurements from the film records were obtained using a Vanguard Motion Analyzer. The Vanguard provided a gain of about 25:1 which was adequate for accurate resolution of the film records.

The thermocouples used to record the liquid temperatures were constructed with 0.0003 inch O.D. platinum-platinum 10% rhodium butt welded wire. The procedure used to construct the thermocouples is

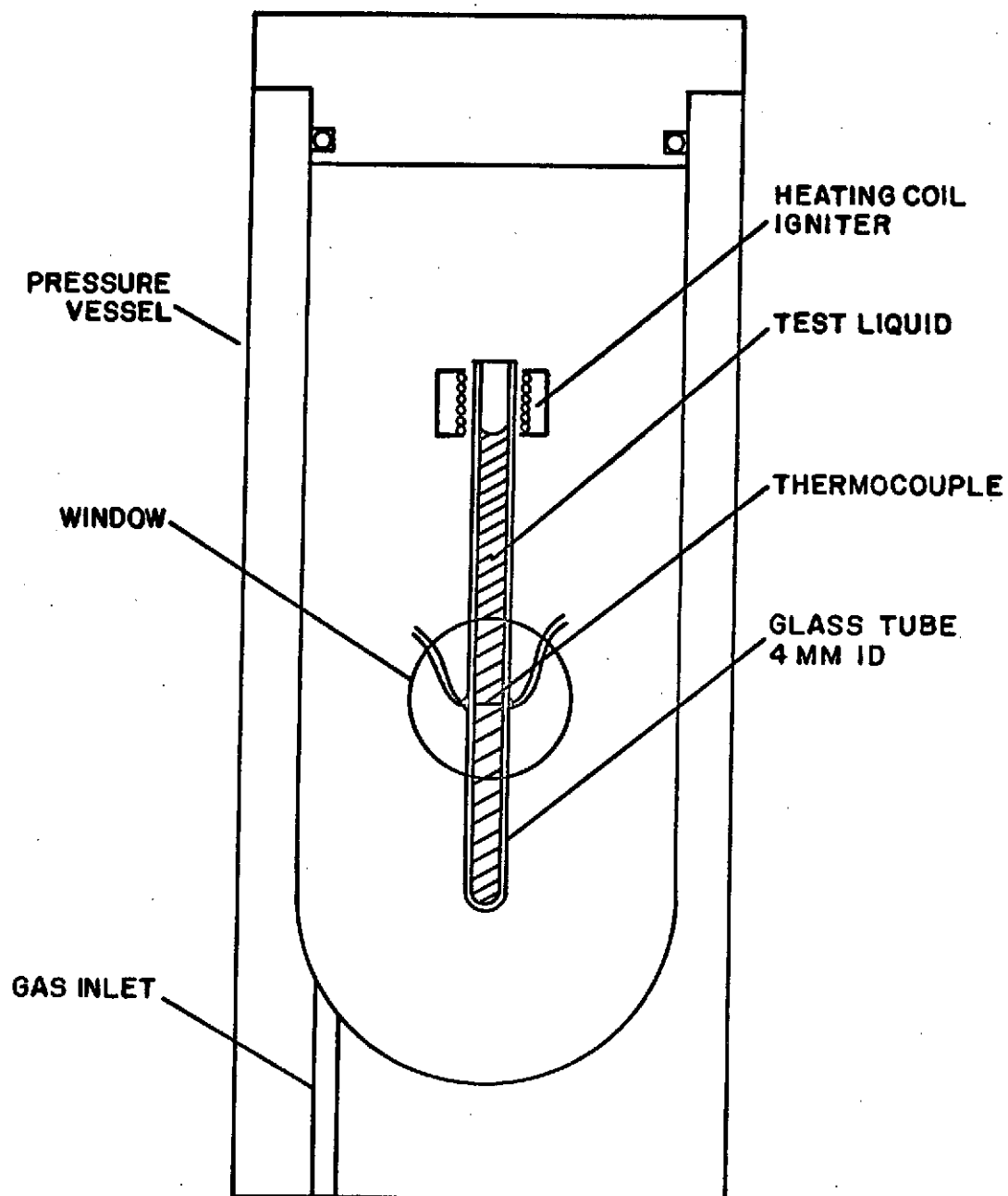


Figure 1 Sketch of the Steady Strand Burner Apparatus

described in Reference [23]. The thermocouples were stretched horizontally (to minimize conduction errors) through holes burned in the glass tube and sealed in place with epoxy. In order to maintain the reference junction of the thermocouple at a fixed temperature, the thermocouple leads were carried outside of the test chamber such that the reference temperature was maintained at room temperature.

The thermocouple output was recorded on a CEC Type 5-124 oscillograph having a flat frequency response to 2000 Hz. The film and temperature records were synchronized by a switch closure which deflected a galvanometer on the oscillograph and started a light streak on the film. A 100 Hz timing signal was placed on the oscillograph using its internal timing generator and also on the film record using a 100 Hz Wollensak pulse generator.

Hydrazine (95+% purity) obtained from the Eastman Organic Chemicals Company was used in the bulk of the testing. A gas chromatographic analysis performed on a sample of this fuel by Bell Aerospace Company indicated that it was composed of 98.5% hydrazine, 1.3% water and 0.1 trace impurities. Some limited testing was also done using hydrazine of 99.4% obtained from the Matheson, Coleman and Bell Corporation.

2.1.2 Test Procedure

The general experimental procedure was similar to that employed in References [24-26]. The liquid fuel was placed in a glass tube contained within a windowed chamber. After pressurizing the chamber with nitrogen to the desired test pressure, the fuel

was ignited with a heater coil. Following ignition, the liquid burned down the tube with a constant rate, after a short development period for the combustion wave. As the liquid surface propagated past the window in the chamber, the rate of regression of the liquid column as well as the position of the thermocouple in the liquid phase was determined from motion picture shadowgraphs taken through the windows of the chamber. Thus the test data consisted of a complete liquid phase temperature record as well as the burning rate of the fuel.

Prior to testing on any given day with the steady strand combustion apparatus, the thermocouple and optical systems were calibrated. The oscillograph was calibrated by applying a known voltage to the input of the galvanometer and noting the output deflection of the light beam on the trace. The optical system was calibrated by positioning a wire of known diameter (measured with a micrometer) at the thermocouple location in the viewing space of the camera and photographing it.

After calibration, the following steps were followed during a typical experimental run. First the tube and test chamber windows were cleaned. The tube was then filled with fuel and positioned in the test chamber. The camera was focussed and the chamber pressurized with nitrogen to the desired test pressure. The ignitor was turned on and then off following ignition; the oscillograph and camera were turned on. As the liquid surface came into the viewing space of the camera, the synchronization switch was activated to synchronize the film and temperature records. Following

completion of the test all systems were turned off, and the chamber was flushed with nitrogen to remove the combustion product gases.

2.2 Oscillatory Strand Combustion Apparatus

In order to study the unsteady combustion of hydrazine an oscillatory version of the steady strand apparatus was developed. As noted previously, in the steady strand combustion case the liquid surface regresses at a constant rate down the tube. However, under unsteady conditions the surface regression rate is no longer steady and, in particular, under oscillatory conditions the surface regression rate oscillates about some mean burning rate. The next four sections give a detailed description of the oscillatory apparatus and its operation.

2.2.1 General Description

The experimental apparatus was required to have the capability of varying the mean pressure and the amplitude and frequency of the pressure oscillations and measuring the response of a burning liquid to these parameters. Figure 2 is a sketch of the oscillatory combustion apparatus with the above capabilities. The major components of this apparatus are the glass tube filled with liquid fuel, the camera-lens optical system used to measure the fluctuations of the burning liquid surface in response to the imposed pressure oscillations, and the rotary valve arrangement used to provide the oscillating pressure variations.

In order to minimize the total flow rate of air required to produce a given pressure oscillation, the chamber volume was kept to a

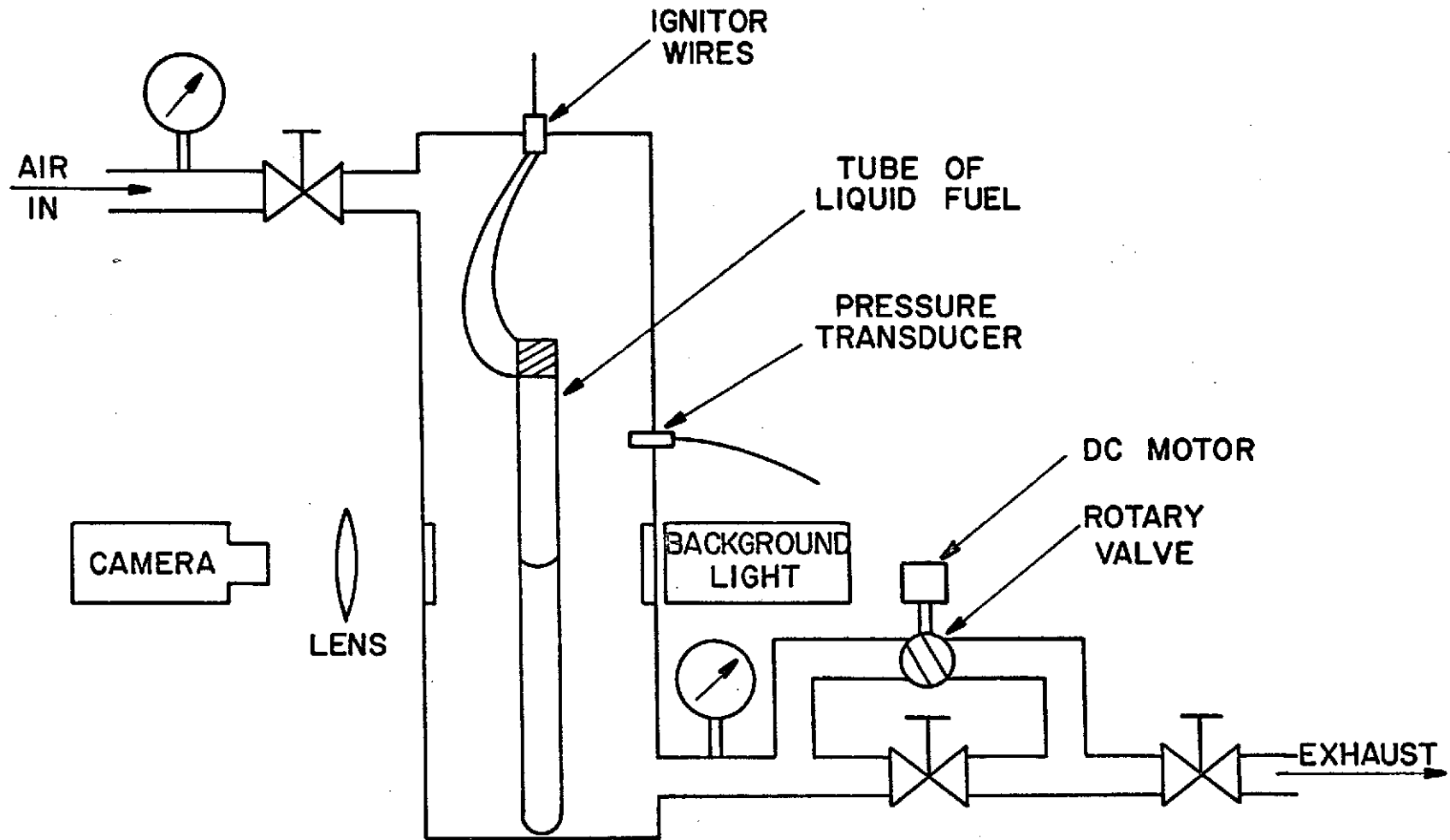


Figure 2 Sketch of the Oscillatory Strand Combustion Apparatus

minimum. The test chamber used in the oscillatory experiments had an inside diameter of 2.6 cm with an inside length of 17 cm and was leak checked to a pressure of 15 atm. The windows in the chamber had a 2.5 cm viewing space.

A photograph of the test chamber is shown in Figure 3. Also shown in the photograph are the camera and lens used to photograph the liquid surface. These items are discussed in detail in the next section.

The ignitor coil used to ignite the fuel sample was of similar construction to that used in the steady strand burner. The static pressure gages sketched in Figure 2 were 0-300 psia Heise gages.

In contrast to the steady strand experiments, only one size sample tube was used in the oscillatory tests. The tube size used was 8 mm I.D. with a tube wall thickness of about 1 mm. As in the steady strand work, the oscillatory burning rate measurements were made at a position about 4 cm from the lower edge of the ignitor coil and about 3 cm from the bottom edge to insure that end effects were minimal. The 98.6% purity hydrazine obtained from Eastman Organic Chemicals Company was used throughout the oscillatory testing.

2.2.2 Photographic System

Quasi-steady analysis indicated that typical liquid surface oscillation amplitudes were on the order of 0.01 mm. In order to optically resolve such small distances, the camera-lens system sketched on Figure 2 and shown in the photograph in Figure 3 was used

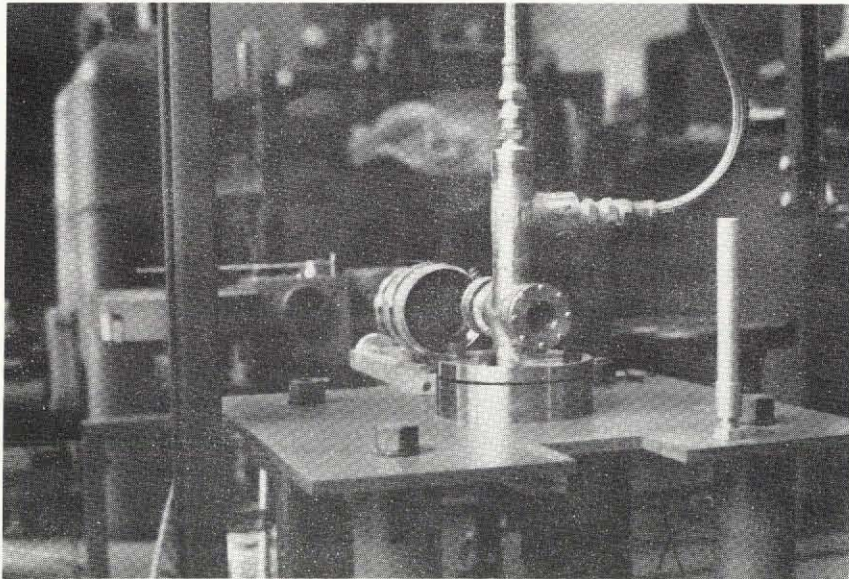


Figure 3 Photograph of the Oscillatory Strand Test Chamber

in conjunction with a Vanguard motion analyzer. The camera was a 35 mm Dumont Type 2582 strip camera and the lens had a focal length of 150 mm and was 6 mm in diameter. The camera was modified by removing its lens and replacing it with an 0.02 inch slot.

Both the lens and camera were mounted on movable bases so that the overall gain of the camera-lens system could be varied. Primary gains as high as 5:1 were obtained with this system. This gain coupled with the gain of about 25:1 of the Vanguard Motion Analyzer provided overall gains of 125:1 which was adequate for accurate resolution of the film records.

Kodak Plus-X Pan film was used throughout the testing. The camera speed was varied depending on the test conditions from about 133 to 400 inches per minute. Timing marks were placed on the films using an Adtrol timing pulse generator.

The background light was supplied by a mercury arc lamp identical to the one used in the steady strand work. The background light was dispersed by passing it through a ground glass filter. The intensity of the light was reduced by removing the focussing mirror from the lamp and also by passing the light through a blue filter.

2.2.3 Pressure Supply System

The oscillating pressure in the test chamber was established using the rotary valve arrangement shown in Figure 2. This method is similar to the system described in Reference [27] for establishing an oscillating propane gas flame. With this technique an oscillating pressure was set up in the test chamber by an oscillating air stream. A stream of air was passed through a needle valve and ball valve

mounted in parallel. The amplitude of the oscillatory pressure was varied independently of the frequency by varying the relative amounts of air passing through the two valves. The frequency of the oscillating pressure was varied by changing the speed of the DC motor used to rotate the ball valve. The mean pressure in the chamber was varied by the setting of the needle valve downstream from the ball valve. A photograph of the rotary valve arrangement and DC motor are shown in Figure 4. The speed of the DC motor was reduced about 6:1 with the pulley-V belt system shown in Figure 4.

Two configurations for the rotary valve system were tested. The first configuration tested had the rotary valve system upstream of the test chamber. However, by placing the rotary valve system downstream of the test chamber, as sketched in Figure 2, a more nearly sinusoidal pressure trace was obtained.

The pressure in the chamber was recorded using a Kistler Type 603A pressure transducer with the output displayed on both an oscilloscope and an oscillograph for retention. The output from the transducer was fed through a Kistler Model 504 Electrostatic Charge Amplifier and then to the oscilloscope. From the charge amplifier the signal was fed through a CEC Type 1-165 DC amplifier to the CEC Type 5-124 oscillograph. The gain of the pressure recording system with the oscillograph varied from about 0.8 psi/inch up to about 3 psi/inch.

The incoming air stream was supplied by a 350 psi shop oil-free compressor. Three-eighths inch stainless steel tubing was used for all the piping in the pressure supply system.

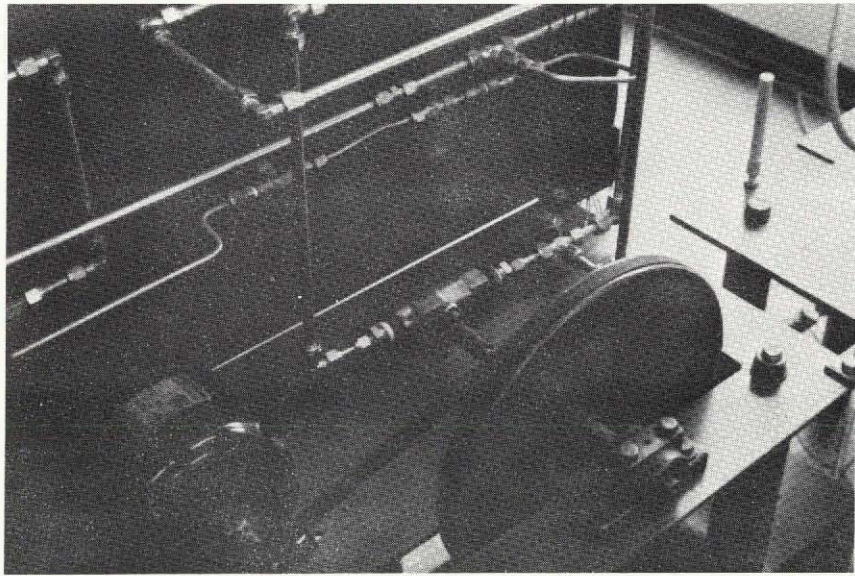


Figure 4 Photograph of the Rotary Valve Arrangement

Any phase shift between the imposed pressure oscillations and the resulting burning rate oscillations were determined from the films and the pressure trace registered on the oscillograph. The film and pressure records were synchronized by a switch closure which deflected a galvanometer on the pressure record and started a light streak on the film. Since the camera had no internal lamp, the light streak was supplied by an external neon lamp. Fiber optics were used to pipe the light from the neon lamp through the camera housing to the film. Timing marks were placed on the pressure record using the internal timing generator of the oscillograph and on the film records by an Adrol timing generator.

2.2.4 Test Procedure

The Kistler pressure transducer was calibrated using a dead weight tester and the calibration was checked each day of testing with a mercury manometer. The optical system was calibrated at the beginning of each day of testing and also after each adjustment of the gain by photographing the resulting movement of the liquid surface when adding a known volume of liquid from a Hamilton Type 1001-N micro-syringe. For the optical calibration, air was passed through the system at about the total flow rate used in testing so any effects of the air flow could be taken into account.

After the daily calibrations, the windows and lens were thoroughly cleaned. The sample tube was filled with fuel and positioned in the test chamber. The test condition in the chamber was set by the pressure supply system. The fuel was then ignited with the heater coil. Both the camera and oscillograph were turned

on; the switch was activated which started the light streak on the film and deflected the galvanometer on the pressure trace. After completion of the test, the camera and oscillograph were turned off. After flushing the combustion product gases from the chamber, the tube was removed and cleaned, and the windows and lens were cleaned in preparation for the next test.

CHAPTER III

THEORETICAL CONSIDERATIONS

As indicated in the Introduction, this study was concerned with the influence of pressure transients on the combustion of a liquid monopropellant fuel. The combustion system which the theoretical model must describe consists of a fuel evaporating from a liquid surface and then subsequently undergoing exothermic chemical decomposition in the gas phase. A portion of the heat evolved in the decomposition process flows back to the liquid surface providing the energy for further evaporation of the liquid; the remainder of the energy released is convected downstream by the gas flow. The main thrust of this study was to gain an understanding of the coupling between an oscillatory pressure wave and the fuel burning rate.

In this chapter the theoretical model of the monopropellant combustion process is described. After reviewing some related solid propellant theories, the model and assumptions are discussed, followed by the development of the equations describing the system. These equations are placed in dimensionless form and a perturbation solution sought with the amplitude of the oscillating pressure used as the small perturbation parameter.

3.1 Existing Theories

Since the process is assumed to be one dimensional, some insight into the modelling of the experiment can be gained by studying solid propellant combustion instability theories. In particular,

neglecting condensed phase reactions, solid propellant models are applicable to the present problem with modified boundary conditions at the two phase interface and slight modifications of the gas phase analysis. However, even with the one dimensional assumption the equations describing the complete unsteady process are extremely complex since they must account for the interaction between the time dependent chemical kinetics and gas dynamics. Although the present theoretical model is of the one-dimensional experiment, the results should lead to a better understanding of liquid response and thus to improved droplet response models.

In contrast to liquid propellant instability studies, solid propellant investigators have recognized the importance of the condensed phase characteristic thermal wave time for many years. Hart and McClure [28] discuss the relevant characteristic times for the various time dependent processes associated with unsteady solid propellant combustion. Based on this study, the various theoretical models [29-31] have all assumed a quasi-steady gas phase and completely unsteady condensed phase. An exception to this is the recent study of T'ien [32] who relaxed the quasi-steady gas phase assumption and numerically obtained solutions for an unsteady gas phase as well as an unsteady liquid phase.

However, even with the quasi-steady gas phase assumption, analytical solutions cannot be obtained unless further simplifying assumptions are made. The need for further simplification arises because of the highly nonlinear chemical kinetic terms appearing in the quasi-steady gas phase equations. The form of these simplifying

assumptions is where the various theories differ. For example, Krier, et al., [29] assume a zero activation energy for the global form of the kinetic term whereas Friedly and Petersen [30] effectively limit their solution to infinite activation energies (infinitely thin flames) by using the Zel'dovich [33] flame theory. Denison and Baum [31] use the results of adiabatic laminar flame theory to formulate the nonadiabatic solid combustion problem in analytically tractable form. Reference [34] offers a more complete discussion of the various solid combustion theories.

The most rigorous approach to the solid propellant combustion problem is that due to T'ien [32] who models the gaseous reaction with global kinetic parameters and numerically integrates the steady state gas phase equations. An approach similar to that of T'ien was used in the present investigation. The major differences between the present analysis and that of T'ien involve phase equilibrium through the Clausius-Clapeyron equation and variable gas phase properties in the present case as opposed to an Arrhenius surface gasification rate and constant gas phase properties for T'ien's analysis. In addition, T'ien numerically integrated his equations from the surface to some fictitious flame length. The present solution method avoids the introduction of a flame length by using asymptotic analysis to generate starting values for large distances from the surface and numerically integrating to the surface.

3.2 General Model and Assumptions

A sketch of the theoretical model is shown on Figure 5. The coordinate system chosen is inertial with respect to the origin.

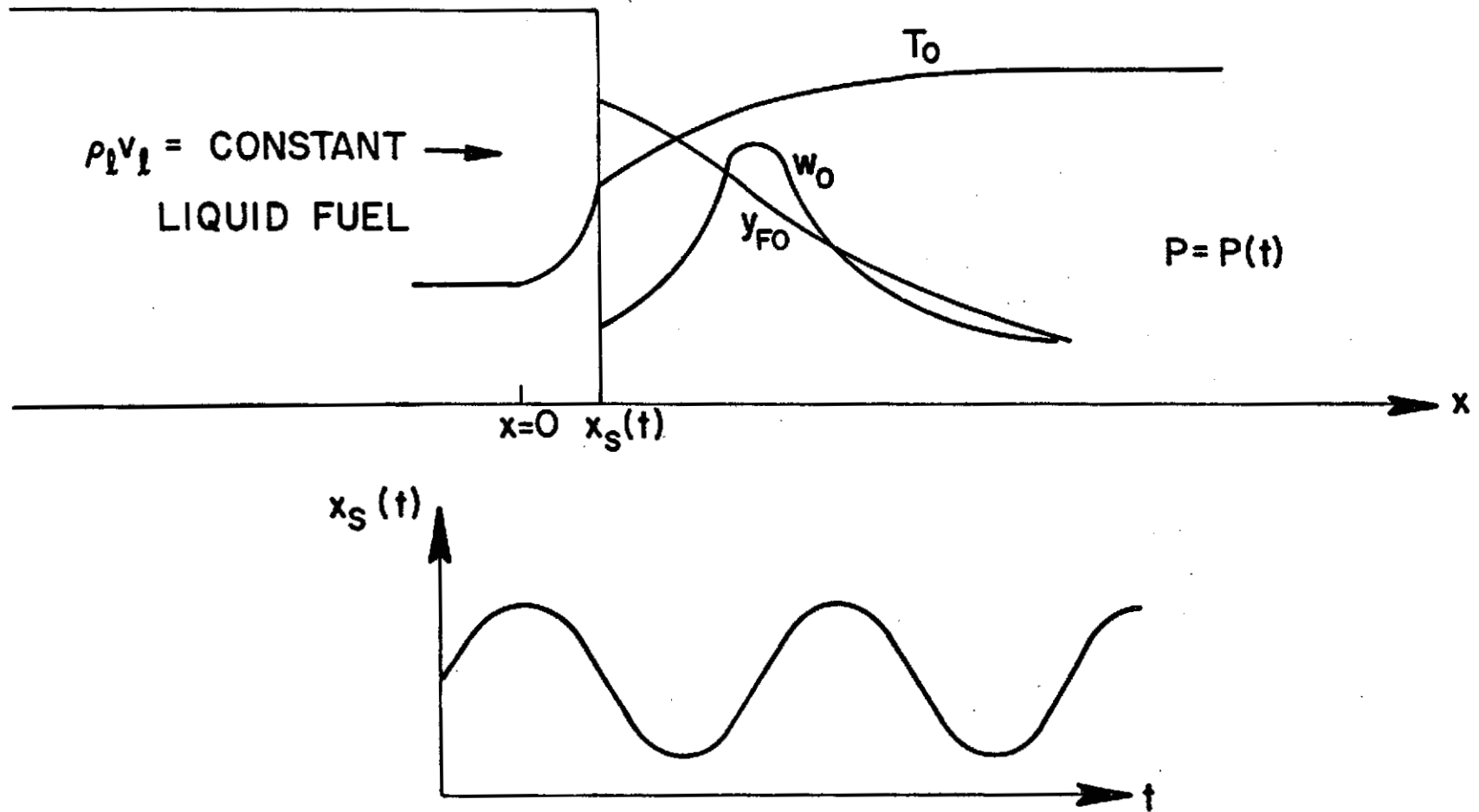


Figure 5 Sketch of the Theoretical Model

which is located at the mean position of the burning surface. [35, 36] Assuming imposed sinusoidal pressure oscillations, the instantaneous position of the liquid surface, x_s , varies as shown in Figure 5 to first order in pressure amplitude. The general appearance of the steady state temperature, fuel mass fraction and gas phase reaction rate profiles are also sketched on Figure 5.

For generality, the gas phase transient effects have been included in the analysis, similar to the approach used by T'ien for solid propellants. [32] The effects of variable properties are also included through the introduction of a modified Howarth transformation.

The major assumptions used in the analysis are as follows:

1. The flow is one-dimensional with a Mach number much less than unity and all body forces are negligible.
2. The flame is premixed and laminar. A one-step, irreversible chemical reaction takes place in the gas phase and any time lags associated with the chemical reaction itself are negligible.
3. Radiation heat transfer is negligible. An estimation of the radiation contribution indicates that it accounts for less than 1% of the total energy required for the vaporization of hydrazine under steady state conditions (see Appendix A). This is primarily due to the fact that hydrazine has a low adiabatic flame temperature.
4. With regard to thermodynamic properties, all gas phase diffusion coefficients are equal, all molecular

weights are equal and constant, all gas phase specific heats are equal and constant, the gas phase mixture thermal conductivity varies linearly with temperature but is independent of composition, and the liquid is composed of a single chemical substance having constant properties.

5. Since the pressure levels are low, the combustion products are taken to be insoluble in the liquid phase. Chemical reaction is also neglected in the liquid phase.
6. Based on the findings of the steady strand portion of the study, the Lewis number is assumed to be unity.
7. The gas phase is taken to be an ideal gas and at the liquid surface fuel mass fraction is related to the surface temperature through the Clausius-Clapeyron equation. The justification of the use of the Clausius-Clapeyron equation is presented in Appendix A.
8. Since the Mach number is much less than unity, the inertial and viscous terms in the momentum equation are neglected.
9. The complete unsteady gas phase equations are used but the wavelength of any periodic pressure disturbance is assumed to be long compared to the distance from the outer edge of the reaction zone to the liquid surface. Estimation indicates that this assumption is valid for frequencies up to about 50,000 Hz (see

Appendix A). Assumptions 8 and 9 indicate that pressure is only a function of time.

Thus, the theoretical model includes the effects of time dependent heat and mass transfer in both the liquid and gas phases. Variable property effects are also included in the gas phase and global kinetic parameters are used to characterize the hydrazine decomposition flame.

3.3 Governing Equations

3.3.1 Dimensional Equations

With the above assumptions, the equations of overall continuity, species conservation and energy in the gas phase and overall continuity and energy in the liquid phase were obtained from the general equations given by Williams [37].

The equations are as follows:

$$\text{Gas Phase, } x_s^*(t^*) < x^* < \infty$$

Conservation of Mass

$$\frac{\partial \rho^*}{\partial t^*} + \frac{\partial \rho^* v^*}{\partial x^*} = 0 \quad (1)$$

Conservation of Species

$$\rho^* \frac{\partial Y_i}{\partial t^*} + \rho^* v^* \frac{\partial Y_i}{\partial x^*} - \frac{\partial}{\partial x^*} \left[\rho^* D \frac{\partial Y_i}{\partial x^*} \right] = \nu_i w_F^* \quad (2)$$

Conservation of Energy

$$\rho^* C_p \frac{\partial T^*}{\partial t^*} + \rho^* v^* C_p \frac{\partial T^*}{\partial x^*} - \frac{\partial}{\partial x^*} \left[\lambda^* \frac{\partial T^*}{\partial x^*} \right] - \frac{\partial P^*}{\partial t^*} = q^* w_F^* \quad (3)$$

Since the gas is ideal

$$P^* = \rho^*RT^*/M \quad (4)$$

In Equations (2 and 3) the following definitions have been used:

$$w_F^* = B^*T^{*\delta} \left[\frac{P^*}{RT^*} \right]^n \left[\frac{Y_F}{M} \right]^n \exp \left[\frac{-E^*}{RT^*} \right] \quad (5)$$

$$q^* = - \sum_{i=1}^N h_i^o \frac{\sqrt{i}''}{\sqrt{i}'} \quad (6)$$

$$\sqrt{i} = \frac{(\sqrt{i}'' - \sqrt{i}')}{\sqrt{i}'} \quad (7)$$

Here w_F^* is the rate of reaction of the fuel with a pre-exponential factor of $B^*T^{*\delta}$ and an activation energy of E^* , q^* is the heat of combustion and \sqrt{i} is related to the stoichiometric coefficients.

Liquid Phase, $-\infty < x^* < x_s^*(t^*)$

Conservation of Mass

$$v_\ell^* = \text{constant} \quad (8)$$

Conservation of Energy

$$\rho_\ell^* C_\ell \frac{\partial T^*}{\partial t^*} + \rho_\ell^* v_\ell^* C_\ell \frac{\partial T^*}{\partial x^*} - \lambda_\ell^* \frac{\partial^2 T^*}{\partial x^{*2}} = 0 \quad (9)$$

Since only oscillatory solutions are required, the initial conditions are irrelevant. The boundary conditions applicable to the present problem can be summarized as follows. At the cold end of the liquid propellant, the temperature must be constant with respect to both x^* and t^* .

$$x^* \rightarrow -\infty$$

$$T^* \rightarrow T_{-\infty}^* \quad (\text{a constant}) \quad (10)$$

At the liquid surface, $x_s^*(t^*)$, six conditions must be satisfied.

The first two are obvious and are mentioned only for completeness.

That is, the temperature and pressure must be continuous across the surface.

$$T_{s-}^* = T_{s+}^* \quad (11)$$

$$P_{s-}^* = P_{s+}^* \quad (12)$$

Conservation of mass applied across the moving surface reduces to:

$$\rho_{\ell}^*(v_{\ell}^* - \dot{x}_s^*) = \rho^*(v^* - \dot{x}_s^*) \quad (13)$$

and conservation of energy at the surface yields:

$$\lambda_{\ell}^* \left[\frac{\partial T^*}{\partial x^*} \right]_{s-} = \left[\lambda^* \frac{\partial T^*}{\partial x^*} \right]_{s+} - \rho_{\ell}^*(v_{\ell}^* - \dot{x}_s^*) [(C_p - C_{\ell})T_s^* + L^*] \quad (14)$$

Since the products of combustion are assumed to be insoluble in the liquid phase, the gradient of the fuel mass fraction is related to the fuel mass fraction itself at the liquid surface as follows:

$$\left[\rho^* D \frac{\partial Y_F}{\partial x^*} \right]_{s+} = \rho_{\ell}^*(v_{\ell}^* - \dot{x}_s^*) (Y_{F,s} - 1) \quad (15)$$

The Clausius-Clapeyron equation relates the fuel mass fraction at the surface to the surface temperature

$$Y_{F,s} = \frac{a^*}{P^*} \exp \left[\frac{-L_1^*}{RT_{s+}} \right] \quad (16)$$

where L^* is the heat of vaporization of the fuel and a^* is a constant with the dimensions of pressure. The remaining boundary conditions relate the variation of fuel mass fraction and temperature far from the liquid surface. Far from the surface, the gas phase chemical reaction must go to completion since eventually all the fuel will react. Thus

$$\begin{aligned} x^* &\rightarrow \infty \\ Y_F &\rightarrow 0 \end{aligned} \quad (17)$$

for all time. In addition, the temperature must become independent of x^* since the only energy source, the chemical reaction, has gone to completion and heat conduction will smooth out any temperature variations with respect to distance. However, the temperature will still vary with time since the pressure is a function of time.

Therefore:

$$\begin{aligned} x^* &\rightarrow \infty \\ T^*(x^*, t^*) &\rightarrow T_{\infty}^*(t^*) \end{aligned} \quad (18)$$

where $T_{\infty}^*(t^*)$ is a known function.

3.3.2 Nondimensional Equations

Equations (1-18) are placed in dimensionless form by introducing the following variables.

$$\begin{aligned} \rho &= \frac{\rho^*}{\rho_{\infty 0}^*} & T &= \frac{T^*}{T_{\infty 0}^*} & v &= \frac{v^*}{v_{\infty 0}^*} \\ P &= \frac{P^*}{P_{\infty 0}^*} & \lambda &= \frac{\lambda^*}{\lambda_{\infty 0}^*} & t &= \frac{t^* \rho_{\infty 0}^* C_p v_{\infty 0}^{*2}}{\lambda_{\infty 0}^*} \end{aligned}$$

$$x = \frac{x^* \rho_{\infty 0}^* C_{P \infty 0} v_{\infty 0}^*}{\lambda_{\infty 0}^*} \quad (19)$$

The subscript $\infty 0$ signifies a zero order (steady state) quantity evaluated at infinity.

Treatment of variable gas phase properties is accomplished by the Howarth Transformation appropriate to the present coordinate system by defining

$$\eta = \frac{C_{P \infty 0} v_{\infty 0}^*}{\lambda_{\infty 0}^*} \int_{x_s^*(t^*)}^{x^*} \rho^* dx^* \quad (20)$$

and by defining a modified mass flux as

$$r = \rho v + \frac{\partial}{\partial t} \int_{x_s(t)}^x \rho dx \quad (21)$$

The Shvab-Zeldovich variable θ , is also introduced as a new dependent variable.

$$\theta = qY_F + T \quad (22)$$

Substituting Equations (19-22) into Equations (1-4) then yields:

Gas Phase, $0 < \eta < \infty$

$$\frac{\partial r}{\partial \eta} = 0 \quad (23)$$

$$\frac{\partial \theta}{\partial t} + r \frac{\partial \theta}{\partial \eta} - P \frac{\partial^2 \theta}{\partial \eta^2} - \left[\frac{\gamma-1}{\gamma} \right] \frac{1}{\rho} \frac{\partial P}{\partial t} = 0 \quad (24)$$

$$\frac{\partial T}{\partial t} + r \frac{\partial T}{\partial \eta} - P \frac{\partial^2 T}{\partial \eta^2} - \left[\frac{\gamma-1}{\gamma} \right] \frac{1}{\rho} \frac{\partial P}{\partial t} = qw \quad (25)$$

$$P = \rho T$$

In deriving Equations (24 and 25) use has been made of the fact that $\sqrt{F} = -1$. The dimensionless reaction rate is defined as

$$w = \frac{A}{q^n} T^{1+\delta-n} P^{n-1} (\theta-T)^n \exp \left[\frac{-E}{T} \right] \quad (27)$$

where E is the dimensionless activation energy,

$$E = \frac{E^*}{RT_{\infty 0}^*} \quad (28)$$

q is the dimensionless heat of combustion

$$q = \frac{q^*}{C_p T_{\infty 0}^*} \quad (29)$$

and A is related to the pre-exponential factor and zero order mass flux

$$A = \frac{B^* T_{\infty 0}^{*\delta} \lambda_{\infty 0}^*}{\rho_{\infty 0}^2 v_{\infty 0}^2 C_p} \left[\frac{P_o^*}{MRT_{\infty 0}^*} \right]^n \quad (30)$$

Also, noting that

$$\frac{\lambda^*}{\lambda_{\infty 0}^*} = \frac{T^*}{T_{\infty 0}^*} \quad (31)$$

and through the use of the ideal gas equation of state, it follows that

$$\rho \lambda = P \quad (32)$$

The dimensionless liquid phase continuity and energy equations are

$$\text{Liquid Phase, } -\infty < \eta < 0$$

$$r = r(t) \quad (33)$$

$$\frac{\partial T}{\partial t} + r \frac{\partial T}{\partial \eta} - \delta_1 \frac{\partial^2 T}{\partial \eta^2} = 0 \quad (34)$$

The dimensionless parameter δ_1 is a constant defined as

$$\delta_1 = \frac{\rho_l \lambda_l C_p}{C_l} \quad (35)$$

The nondimensional boundary conditions are as follows. At the cold end of the fuel,

$$\begin{aligned} \eta &\rightarrow -\infty \\ T(\eta, t) &\rightarrow T_{-\infty} \end{aligned} \quad (36)$$

At the liquid surface, the conservation of mass yields

$$\begin{aligned} \eta &= 0 \\ r(t) &= \rho(o) [v(o) - \dot{x}_s] = \rho_l (v_l - \dot{x}_s) \end{aligned} \quad (37)$$

The conservation of energy across the surface becomes

$$\rho_l \lambda_l \left[\frac{\partial T}{\partial \eta} \right]_{\eta=0^-} = P \left[\frac{\partial T}{\partial \eta} \right]_{\eta=0^+} - r [T(o)(1-\beta) + L] \quad (38)$$

where β is the ratio of liquid to gas specific heats

$$\beta = \frac{C_l}{C_p} \quad (39)$$

and L is the nondimensional heat of vaporization

$$L = \frac{L^*}{C_p T_{\infty}^*} \quad (40)$$

The insolubility condition requires that

$$P \left[\frac{\partial \theta}{\partial \eta} \right]_{\eta=0+} = r[\theta(0) - T(0) - q] + P \left[\frac{\partial T}{\partial \eta} \right]_{\eta=0+} \quad (41)$$

The Clausius-Clapeyron equation after nondimensionalization is

$$\theta(0) = \frac{aq}{P} \exp \left[\frac{-L_1}{T(0)} \right] + T(0) \quad (42)$$

where

$$a = \frac{a^*}{p_o^*} \quad L_1 = \frac{L_1^*}{RT_{\infty o}^*} \quad (43)$$

The dimensionless conditions far from the surface reduce to

$$\eta \rightarrow \infty$$

$$\theta(\eta, t) \rightarrow T(\eta, t) \rightarrow T(t) \quad (44)$$

where $T(t)$ is a specified function.

3.3.3 Perturbation Analysis

To solve the system of partial differential equations, Equations (23-25 and 34), with the given boundary conditions, it is assumed that all amplitudes of oscillation are small. This assumption allows the use of a perturbation analysis. For oscillatory solutions, the dependent variables can be expressed as a function of a perturbation parameter ϵ , where ϵ is assumed to be small

$$\begin{aligned} P(t) &= 1 + \epsilon e^{i\omega t} \\ T(\eta, t) &= T_o(\eta) + \epsilon T_1(\eta) e^{i\omega t} \\ \theta(\eta, t) &= \theta_o(\eta) + \epsilon \theta_1(\eta) e^{i\omega t} \\ r(t) &= r_o + \epsilon r_1 e^{i\omega t} \\ x_s(t) &= 0 + \epsilon x_{s1} e^{i\omega t} \end{aligned} \quad (45)$$

In these equations ε represents the normalized amplitude of the imposed pressure oscillations. Substituting Equation (45) into Equations (23-25, and 34) and the boundary conditions, the resulting equations are separated in terms of like powers of $\varepsilon e^{i\omega t}$.

3.4 Zero Order (Steady State) Problem

3.4.1 Equations

For the zero order problem, the gas phase can be solved independently of the liquid phase. The problem reduces to the following:

Gas Phase, $0 < \eta < \infty$

$$\frac{d^2 T_o}{d\eta^2} - \frac{dT_o}{d\eta} + q^{1-n} A T_o^{1+\delta-n} (1-T_o)^n \exp\left[\frac{-E}{T_o}\right] = 0 \quad (46)$$

with the boundary conditions

$$\begin{aligned} \eta \rightarrow \infty \\ T_o \rightarrow 1 \end{aligned} \quad (47)$$

and at $\eta = 0$.

$$\left[\frac{dT_o}{d\eta} \right]_{\eta=0+} = q + T_o(0) - 1 \quad (48)$$

$$T_o(0) = 1 - aq \exp\left[\frac{-L_1}{T_o(0)}\right] \quad (49)$$

In Equations (46-49) use has been made of the conservation of mass requirement that

$$r_o = \text{constant} = \rho_{\infty o} v_{\infty o} = 1 \quad (50)$$

and also that

$$\theta_o(\eta) = 1 \quad (51)$$

from Equations (24) and (45).

In Equation (46), the quantity A is unknown since it is related to the burning rate $\rho_{\infty o}^* v_{\infty o}^*$ which is unknown. The three boundary conditions permit a unique value of A to be determined.

The liquid phase solution is required for the complete specification of the first order problem. To zero order in ϵ , the equation and boundary conditions are:

Liquid Phase, $-\infty < \eta < 0$

$$\delta_1 \frac{d^2 T_o}{d\eta^2} - \frac{dT_o}{d\eta} = 0 \quad (52)$$

$$\eta \rightarrow -\infty \quad T_o \rightarrow T_{-\infty} \quad \eta = 0 \quad T_o = T_o(0) \quad (53)$$

The solution of Equation (52) subject to the boundary conditions of Equation (53) is

$$T_o = T_{-\infty} + [T_o(0) - T_{-\infty}] \exp(\eta/\delta_1) \quad (54)$$

3.4.2 Solution Method

The zero order problem is given by Equations (46-49). Equation (46) is highly nonlinear and must be solved numerically. Since the domain of interest is half-infinite, one obviously can not integrate to infinity numerically. One approach to this problem is to integrate from $\eta = 0$ to some finite η , the outer flame edge, where T_o is within some small percentage of its true value at

infinity, i.e., unity. This was the approach used in Reference [32]. A more rigorous approach is to consider the asymptotic form of Equation (46) for large η . The form of the solution for T_o for large η depends on the reaction order n , and further considerations are limited to first and second order reactions. It is shown in Appendix B that with $n = 2$, by balancing convection and reaction, $T_o(\eta)$ must be of the form

$$T_o = 1 - \left[\frac{A}{q} \exp(-E)\eta - C \right]^{-1} \quad (55)$$

for large η where C is an unknown constant. For $n = 1$, $T_o(\eta)$ must be of the form

$$T_o = 1 - C \exp \left[\frac{1 - \sqrt{1+4A \exp(-E)}}{2} \eta \right] \quad (56)$$

for large η where again C is an unknown constant.

With the asymptotic form of T_o for large η , Equation (46) can be solved numerically without specifying an arbitrary outer flame edge. Equation (55) or Equation (56) is used to generate starting values for the numerical solution for some large, but finite, η with an assumed value of C . With these starting values, Equation (46) is integrated numerically to $\eta = 0$ with an assumed A . At $\eta = 0$ the boundary conditions, Equations (48-49), must be satisfied and thus A and C are determined uniquely. However, since Equation (46) is nonlinear, a double iteration technique must be used and Equation (46) solved at each step of the iteration in A and C until Equations (48-49) are satisfied. With this solution technique, the outer boundary condition, Equation (47), is only satisfied at the true mathematical infinity.

3.5 First Order Problem

3.5.1 Equations

To first order in ϵ the equation and boundary conditions for the liquid phase are:

$$\delta_1 \frac{d^2 T_1}{d\eta^2} - \frac{dT_1}{d\eta} - i\omega T_1 = r_1 \frac{dT_o}{d\eta} \quad (57)$$

$$\eta \rightarrow -\infty \quad T_1 \rightarrow 0 \quad \eta = 0 \quad T_1 = T_1(0) \quad (58)$$

The solution of the first order system is

$$T_1 = \left\{ T_1(0) + \frac{r_1}{\delta_1 i\omega} [T_o(0) - T_{-\infty}] \right\} \exp \left[\frac{1 + \sqrt{1 + 4i\omega\delta_1}}{2\delta_1} \eta \right] \\ - \frac{r_1}{\delta_1 i\omega} [T_o(0) - T_{-\infty}] \exp(\eta/\delta_1) \quad (59)$$

The first order gas phase equations reduce to the following.

Gas Phase, $0 < \eta < \infty$

$$r_1 = \text{constant} \quad (60)$$

$$\frac{d^2 \theta_1}{d\eta^2} - \frac{d\theta_1}{d\eta} - i\omega \theta_1 = - \left[\frac{\gamma-1}{\gamma} \right] i\omega T_o \quad (61)$$

$$\frac{d^2 T_1}{d\eta^2} - \frac{dT_1}{d\eta} + T_1 \left\{ qw_o \left[\left(\frac{1+\delta-n}{T_o} \right) - \frac{n}{1-T_o} + \frac{E}{T_o^2} \right] - i\omega \right\} + \frac{nqw_o}{1-T_o} \theta_1 \\ = r_1 \frac{dT_o}{d\eta} - \frac{d^2 T_o}{d\eta^2} - \left[\frac{\gamma-1}{\gamma} \right] i\omega T_o - (n-1)qw_o \quad (62)$$

In Equation (62) w_o is defined by the following expression:

$$w_o = \frac{A}{q^n} T_o^{1+\delta-n} (1-T_o)^n \exp \left[\frac{-E}{T_o} \right] \quad (63)$$

Using Equation (59) the conservation of energy boundary condition to first order in ε becomes

$$\eta = 0$$

$$\begin{aligned} \left[\frac{dT_1}{d\eta} \right]_{\eta=0+} &= r_1 \left\{ \frac{\rho_\ell \lambda_\ell}{2\delta_1^2 i\omega} [T_o(0) - T_\infty] [\sqrt{1+4i\omega\delta_1} - 1] + T_o(0)(1-\beta) + L \right\} \\ &+ T_1(0) [1-\beta + \frac{\rho_\ell \lambda_\ell}{2\delta_1} (1 + \sqrt{1+4i\omega\delta_1})] - \left[\frac{dT_o}{d\eta} \right]_{\eta=0+} \end{aligned} \quad (64)$$

The Clausius-Clapeyron equation reduces to

$$\theta_1(0) = aq \frac{L_1 T_1(0)}{T_o^2(0)} \exp\left[\frac{-L_1}{T_o(0)}\right] + T_o(0) + T_1(0) - 1 \quad (65)$$

and the insolubility condition requires that

$$\left[\frac{d\theta_1}{d\eta} \right]_{\eta=0+} = r_1 [1 - T_o(0) - q] + \theta_1(0) - T_1(0) + \left[\frac{dT_1}{d\eta} \right]_{\eta=0+} + \left[\frac{dT_o}{d\eta} \right]_{\eta=0+} \quad (66)$$

The outer boundary conditions from Equation (44) are

$$\eta \rightarrow \infty$$

$$\theta_1(\eta) \rightarrow T_1(\eta) \rightarrow \text{a constant} \quad (67)$$

The constant in Equation (67) can be determined by solving Equation (61) for large η . It is easily verified that as $\eta \rightarrow \infty$,

$$\theta_1(\eta) \rightarrow T_1(\eta) \rightarrow \frac{\gamma-1}{\gamma} \quad (68)$$

which is the form for isentropic flow.

3.5.2 Solution Method

The first order problem involves the solution of two linear second order ordinary differential equations, Equations (61 and 62), involving an unknown constant, r_1 . Five boundary conditions, Equations (64-67) are imposed on the solution permitting a unique value of r_1 to be determined.

The solution method to the first order problem is discussed in detail in Appendix C. Briefly, the method consists of exploiting the linearity of the system to separate the problem into the numerical solution of five second order ordinary differential equations. As in the case of the zero order problem, the equations are integrated to $\eta = 0$ using asymptotic analysis to generate starting values for the numerical routine at large η .

For the first order problem the constant, r_1 , is related to the unsteady burning rate in response to the imposed pressure oscillations of amplitude ϵ . However, r_1 , is not measured directly in the experimental portion of this study. The amplitude and phase angle of the liquid surface oscillations, x_{s1}^* , are measured experimentally. However, x_{s1} and r_1 are uniquely related as developed in the following.

From the conservation of mass at the liquid surface, Equation (37), and Equation (45) it follows that

$$x_{s1} = r_1 / (\rho_l i \omega) \quad (69)$$

Since ρ_l is a given thermodynamic property, x_{s1} is directly related to r_1 . Moreover, x_{s1} is a complex number with both amplitude and

phase parameters. Both of these parameters can be directly compared with the measured amplitude of the liquid surface oscillations and the phase angle of these oscillations with respect to the pressure oscillations.

CHAPTER IV

RESULTS AND DISCUSSION

In this chapter the results of this investigation are described and discussed. In the first part of the chapter the findings of the steady strand experimental study are presented and compared with the theoretical predictions. The latter part of the chapter deals with the experimental and theoretical results of the oscillatory combustion case.

The theoretical model is described in detail in Chapter III. Since the experimental study was conducted with liquid hydrazine as the fuel, the properties used in the theoretical model are those applicable to hydrazine. These properties are listed in Table 1. The specific correlations and sources of data for these properties are given in Appendix D.

4.1 Steady Strand Combustion

This section deals with the steady strand results. As discussed in Chapter II, the steady strand experimental data consisted of a complete liquid temperature record displayed on an oscillograph, a film record of the liquid surface motion and the position of the thermocouple relative to the liquid surface as a function of time. From this data both steady strand burning rates and liquid phase temperature distributions were obtained.

Table 1

Properties Used in the Theoretical Model

Property	Value
T_{∞}^* (K)	298
δ	0
q^* (cal/gm)	1180
L^* (cal/gm)	410
L_1^* (cal/gm)	9750
$\ln a^*$ (atm)	12.601
γ	1.126
ρ_{λ}^* (gm/cm ³)	1.0
C_{λ} (cal/gm-°K)	0.74
C_p (cal/gm-°K)	0.74
$\lambda_{\infty 0}^*$ (cal/cm-sec-°K)	4.2×10^{-4}
$T_{\infty 0}^*$ (K)	1345

4.1.1 Burning Rates

As discussed in the Introduction previous investigators found that the purity of the liquid fuel had a significant effect upon hydrazine strand burning rates. [12-15] In order to clarify this point, a number of tests were conducted with hydrazine of varying liquid purities. These results are summarized in Figure 6.

The burning rates presented in Figure 6 were obtained using a 12 mm I.D. tube. While the differences between the 99.6 and 98.4% purity hydrazine were small, adding distilled water to the hydrazine as an impurity (95.6, 92.6% purity) resulted in a significant reduction in the burning rate in agreement with previous investigators. [12-15] However, Antoine [15] found that hydrazine exhibited abrupt increases in its burning rate for a small change in pressure. The present measurements did not detect any such discontinuous behavior. The 98.6% purity hydrazine was used in the remainder of the testing due to its greater availability.

Experimental steady strand burning rate measurements were terminated at the upper extinction pressure. Above this pressure, the fuel failed to sustain combustion following ignition. The upper extinction pressure increased slightly as the purity of the fuel increased. The upper extinction pressure also increased as the diameter of the sample tube increased.

Gray and Kay [13] also found lower extinction pressures for hydrazine. The lower extinction pressure was not investigated in the present study. It was observed, however, that slight bubbling of the liquid occurred at the lower pressures tested. Gray, et al.,

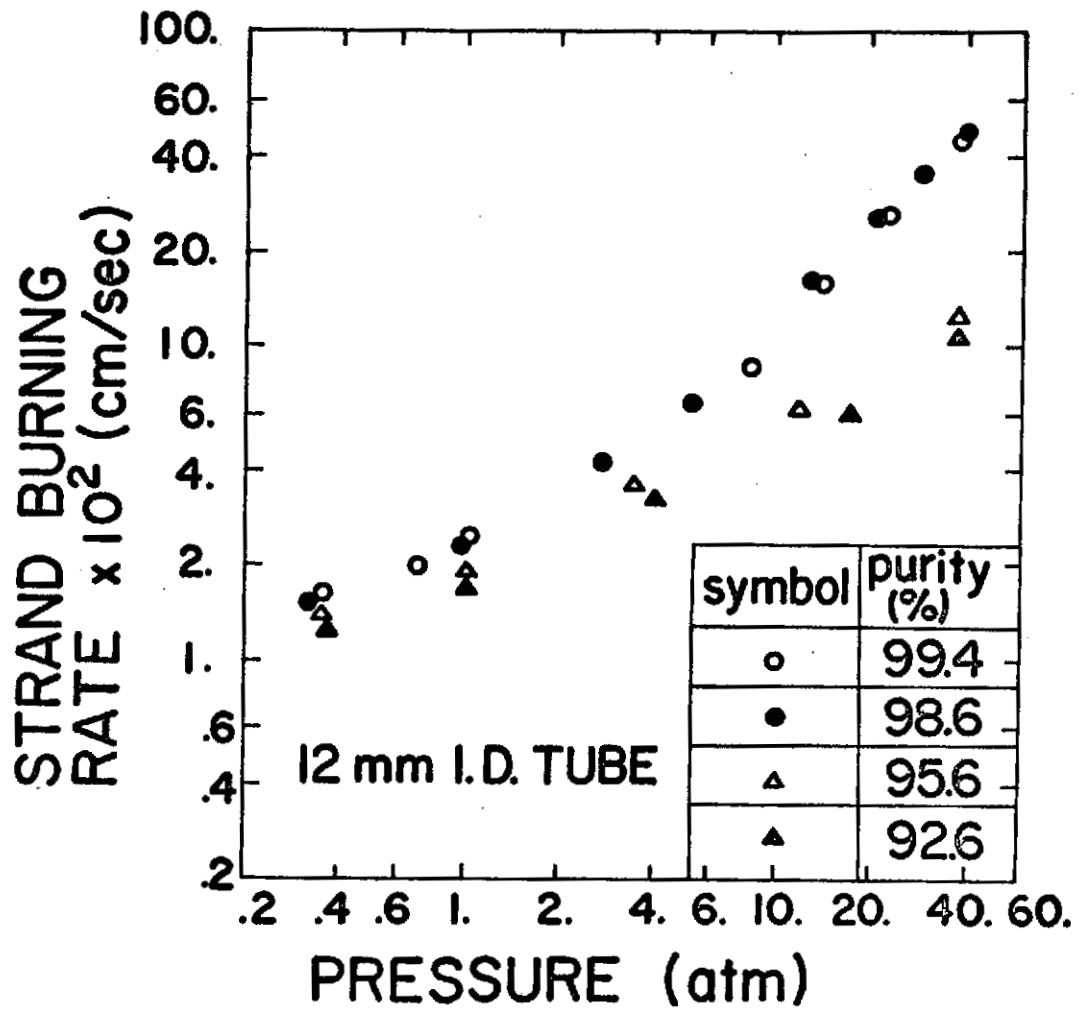


Figure 6 Steady Strand Burning Rates as a Function of Pressure for Various Liquid Purities

[14] indicate that bubbling of the liquid is an indication that the lower extinction pressure is being approached.

It is well known that steady strand burning rates are dependent upon sample tube diameter due to surface tension effects providing more liquid surface area for the combustion process. This effect is shown in Figure 7 at various pressures. By plotting the data as a function of reciprocal tube diameter, linear fits were obtained, allowing a determination of the correct fundamental burning rate (burning rate in an infinite diameter tube) by extrapolation.

Figure 8 is a plot of the fundamental burning rate as a function of pressure. Also shown on the plot are the theoretical predictions for various reaction orders and dimensionless activation energies. In order to obtain the theoretical curves shown on Figure 8 the theory was matched to the experimental results at atmospheric pressure assuming a first order reaction and at 6.7 atm assuming a second order reaction. This matching was required since the gas phase global kinetic constants are not known for liquid hydrazine strand combustion. Table 2 lists the correlation conditions and resulting dimensional pre-exponential factors used in Figure 8. These pre-exponential factors were used in the remainder of this study, except as noted later.

The results shown in Figure 8 indicate that the gas phase reaction for hydrazine strand combustion is first order at low pressures switching to second order at high pressures. These results are in agreement with the earlier work of both Gray [13, 14]

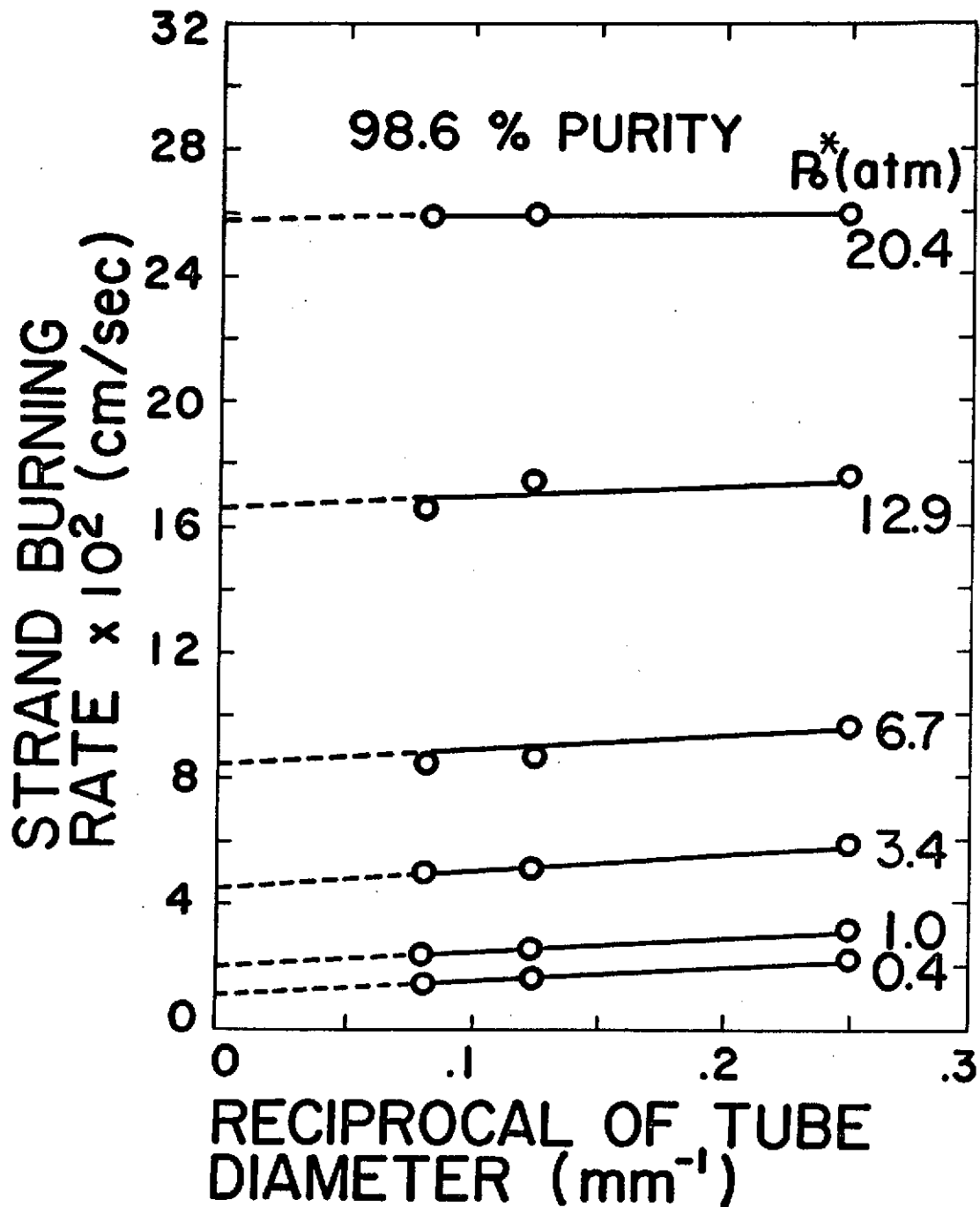


Figure 7 Steady Strand Burning Rates as a Function of the Reciprocal of the Tube Diameter

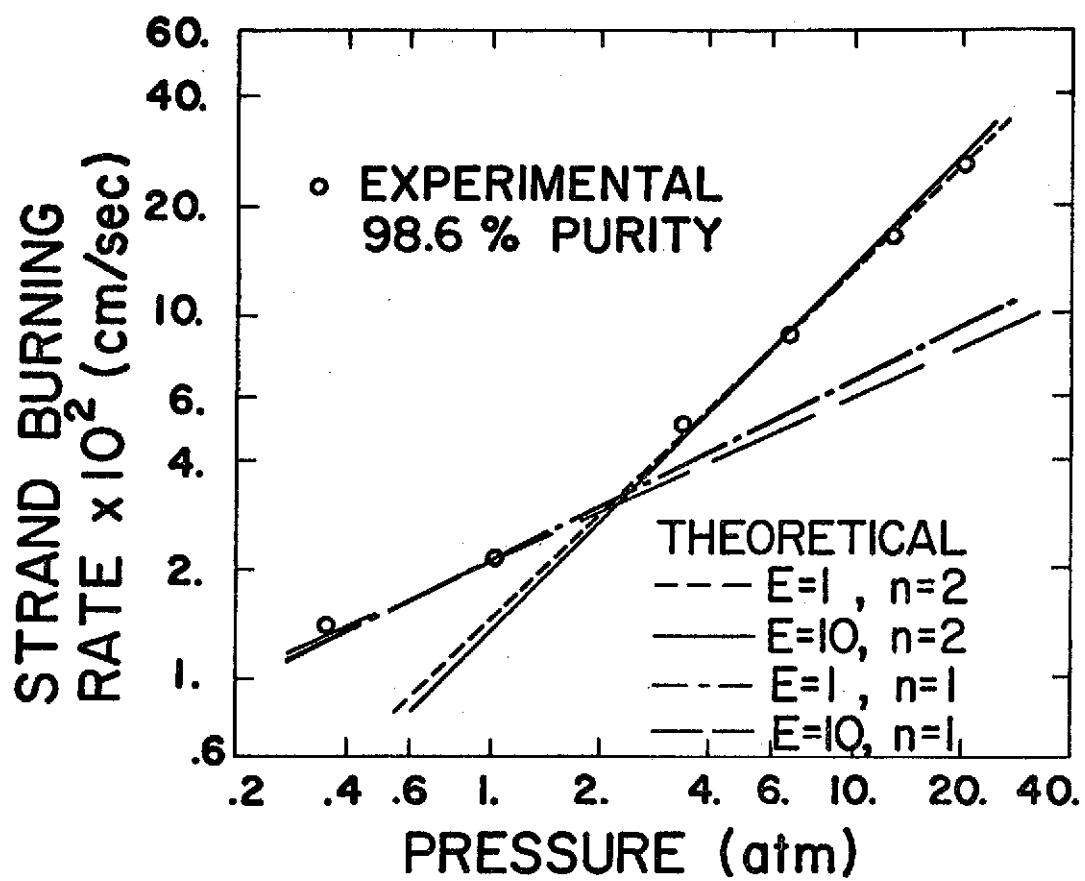


Figure 8 Theoretical and Experimental Steady Strand Burning Rates as a Function of Pressure

Table 2

Correlation Conditions and Parameters Used in the Theoretical Model

E	n = 1		n = 2	
	Correlation Condition $P_o^* = 1.0 \text{ atm}; v_{\lambda}^* = 0.021 \text{ cm/sec}$		Correlation Condition $P_o^* = 6.7 \text{ atm}; v_{\lambda}^* = 0.084 \text{ cm/sec}$	
	E^* (kcal/mole)	B^* (sec^{-1})	B^* ($\text{cm}^3/\text{gm-sec}$)	
1	2.673	3.473×10^4	7.608×10^7	
10	26.73	7.468×10^9	8.385×10^{13}	
15	40.08	--	3.749×10^{16}	
30	80.16	--	8.446×10^{23}	

and Antoine [15]. Gray found that for subatmospheric pressures the hydrazine strand burning rate was proportional to the square root of pressure, which is indicative of a first order reaction; Antoine found that for pure hydrazine the strand burning rate was proportional to pressure for pressures in the range 1-19 atm, which is indicative of a second order reaction. However, the results are not in agreement with those of Adams and Stocks [12] who found that the burning rate was proportional to the square root of pressure up to about 10 atm.

As is evident in Figure 8 the gas phase activation energy has little effect upon the theoretical strand burning rate. This result is in agreement with earlier droplet decomposition flame studies which also found that activation energy had little effect on steady burning rates. [7]

4.1.2 Liquid Temperatures

As discussed in Chapter II, liquid temperatures of burning strands of hydrazine were obtained by stretching a thermocouple horizontally across the tube and recording its output as the liquid surface propagated down the tube due to combustion. In this manner not only liquid temperature distributions but also liquid surface temperatures were obtained.

Figure 9 compares theoretical and experimental liquid temperatures at two pressures, 20.4 atm and 1.0 atm, as a function of distance from the liquid surface. The temperature readings at positive distances result from a liquid film formed around the thermocouple as it leaves the surface (due to surface tension) and should be disregarded. [38]

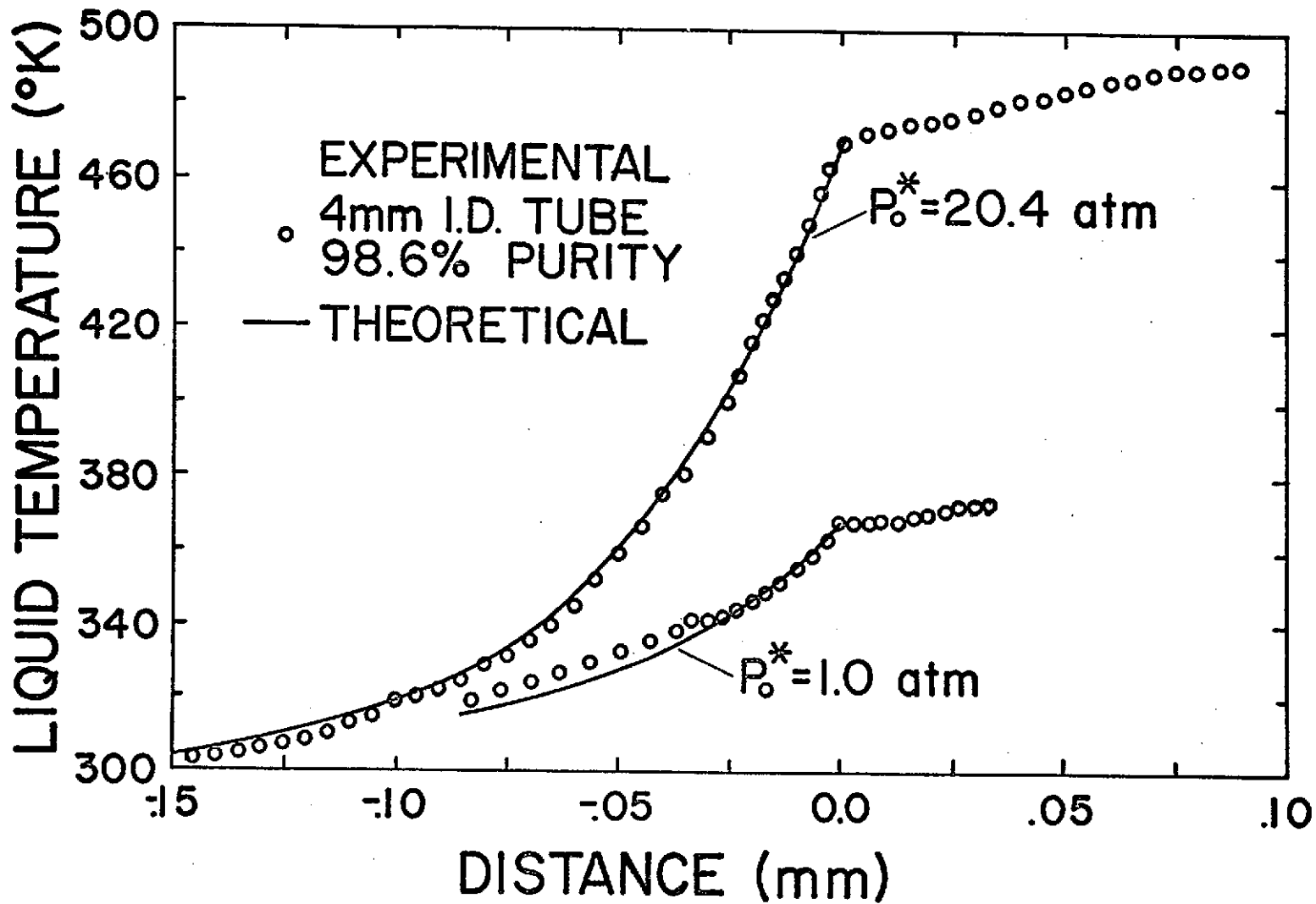


Figure 9 Theoretical and Experimental Liquid Phase Temperature Distributions

As is evident from Figure 9, the theoretical and experimental results agree quite well. The results at other pressures were similar to those shown in Figure 9, justifying the use of constant liquid phase properties. The value of the liquid thermal diffusivity used to compute the theoretical curves was $1.26 \times 10^{-3} \text{ cm}^2/\text{sec}$, which is a reasonable value for a liquid such as hydrazine.

The experimental values of the liquid surface temperatures were obtained in two ways. With the first method the surface temperature was taken as the temperature recorded by the thermocouple at the instant of time when the thermocouple was just tangent to the liquid surface (as obtained from the film record). With the second method the liquid surface temperature was taken as the temperature where the sharp "knee" appeared in the thermocouple output as shown on Figure 9. The two methods yielded surface temperatures differing by less than 1%.

The liquid surface temperature results are shown in Figure 10 as a function of pressure. Two theoretical curves are also shown on Figure 10. The present unity Lewis number theoretical analysis agrees well with the data, justifying the assumption of conventional phase equilibrium at the surface. An infinite activation energy analysis is also seen to yield essentially the same results. The theoretical development using the infinite activation energy assumption is presented in Appendix E.

4.1.3 Additional Theoretical Results

Solution of the steady gas phase problem gives not only the nondimensional eigenvalue, A , and the liquid surface temperature

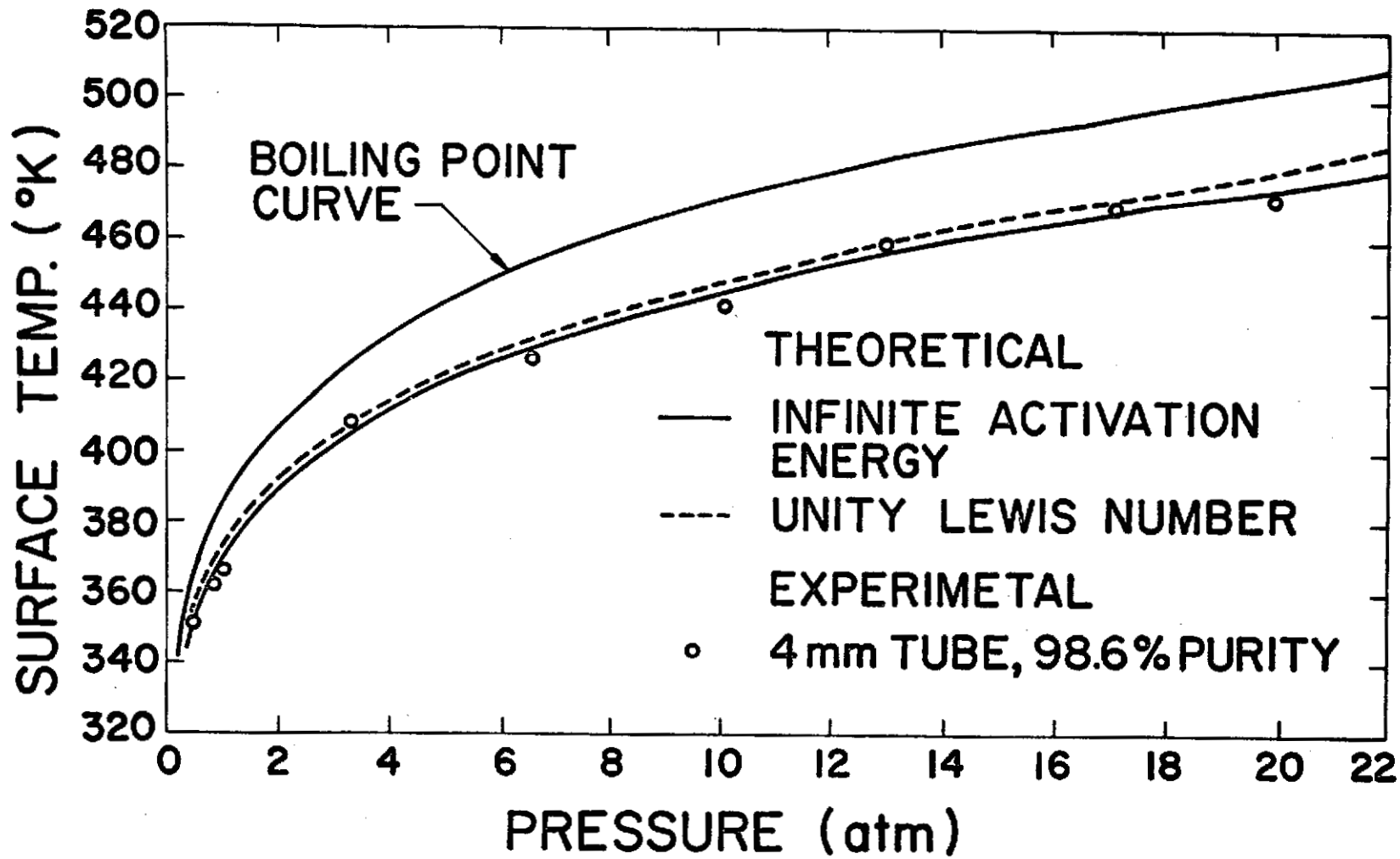


Figure 10 Theoretical and Experimental Liquid Surface Temperatures as a Function of Pressure

but also the complete gas phase temperature and reaction rate profiles at a given pressure (for an assumed reaction order and activation energy). In this section the theoretical gas phase temperature and reaction rate profiles are described.

Figures 11-13 show the gas phase temperature and reaction rate profiles for a second order reaction with nondimensional activation energies of 1, 10 and 30, respectively. The nondimensional reaction rate, w_{FO} , is defined as

$$w_{FO} = AT_o^{\delta-n} (1 - T_o)^n \exp \left(\frac{-E}{T_o} \right) / q^n \quad (70)$$

As the activation energy increases, Figures 11-13 indicate that the region where gas phase reaction effects are important becomes narrower and the reaction rate profiles become more sharply spiked. In addition the temperature reaches its limiting value closer to the liquid surface for a higher activation energy.

The qualitative aspects of the first order profiles are similar to those of a second order reaction. First order profiles are shown in Figures 14-15 for nondimensional activation energies of 1 and 10, respectively.

The effect of pressure on the nondimensional profiles for both a first and second order reaction was slight. Increasing pressure tended to cause the reaction rate profile to peak slightly closer to the surface with the result that the temperature more rapidly approached its limiting value.

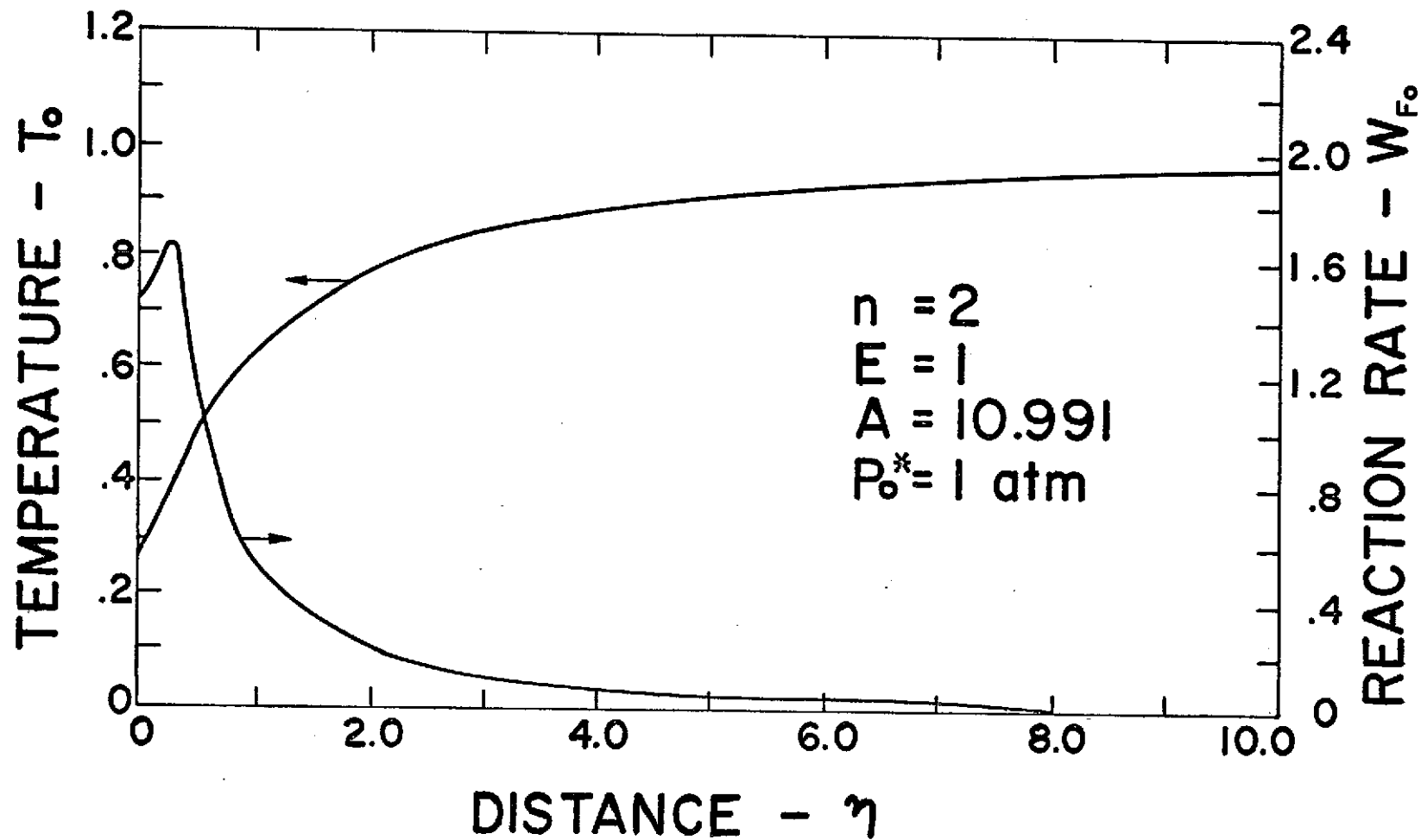


Figure 11 Steady State Gas Phase Temperature and Reaction Rate Distributions for $n = 2$, $E = 1$

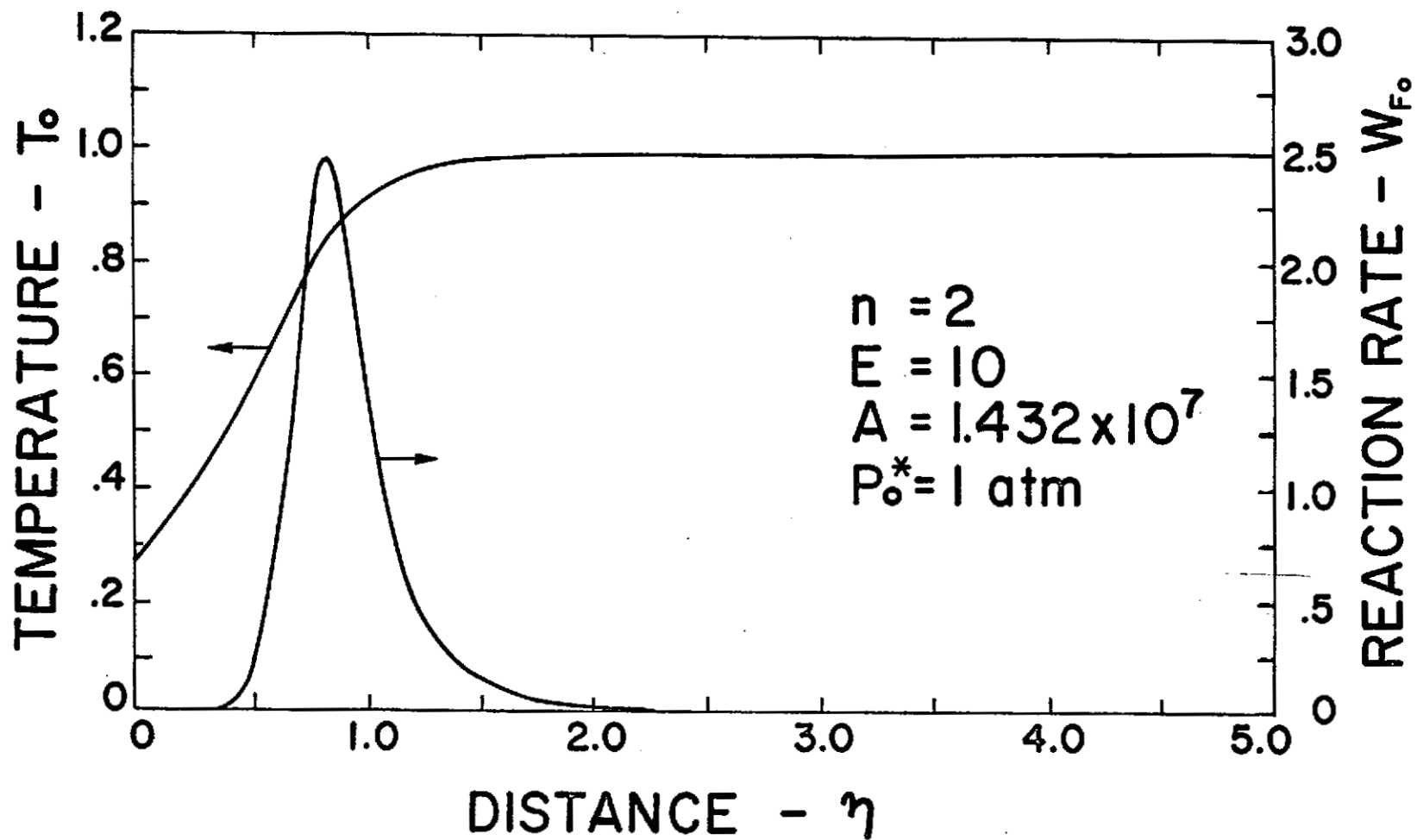


Figure 12 Steady State Gas Phase Temperature and Reaction Rate Distributions for $n = 2$, $E = 10$

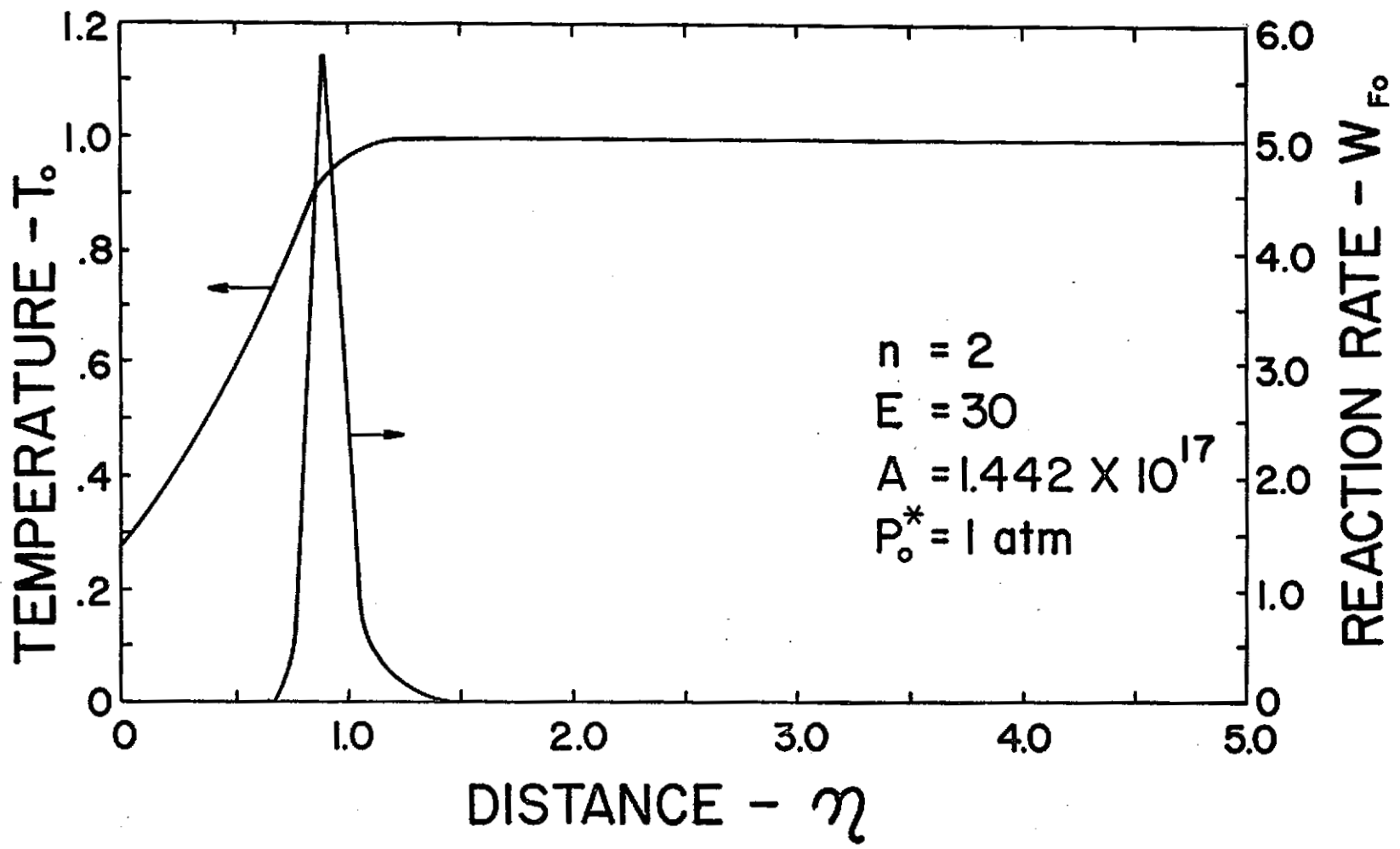


Figure 13 Steady State Gas Phase Temperature and Reaction Rate Distributions for $n = 2$, $E = 30$

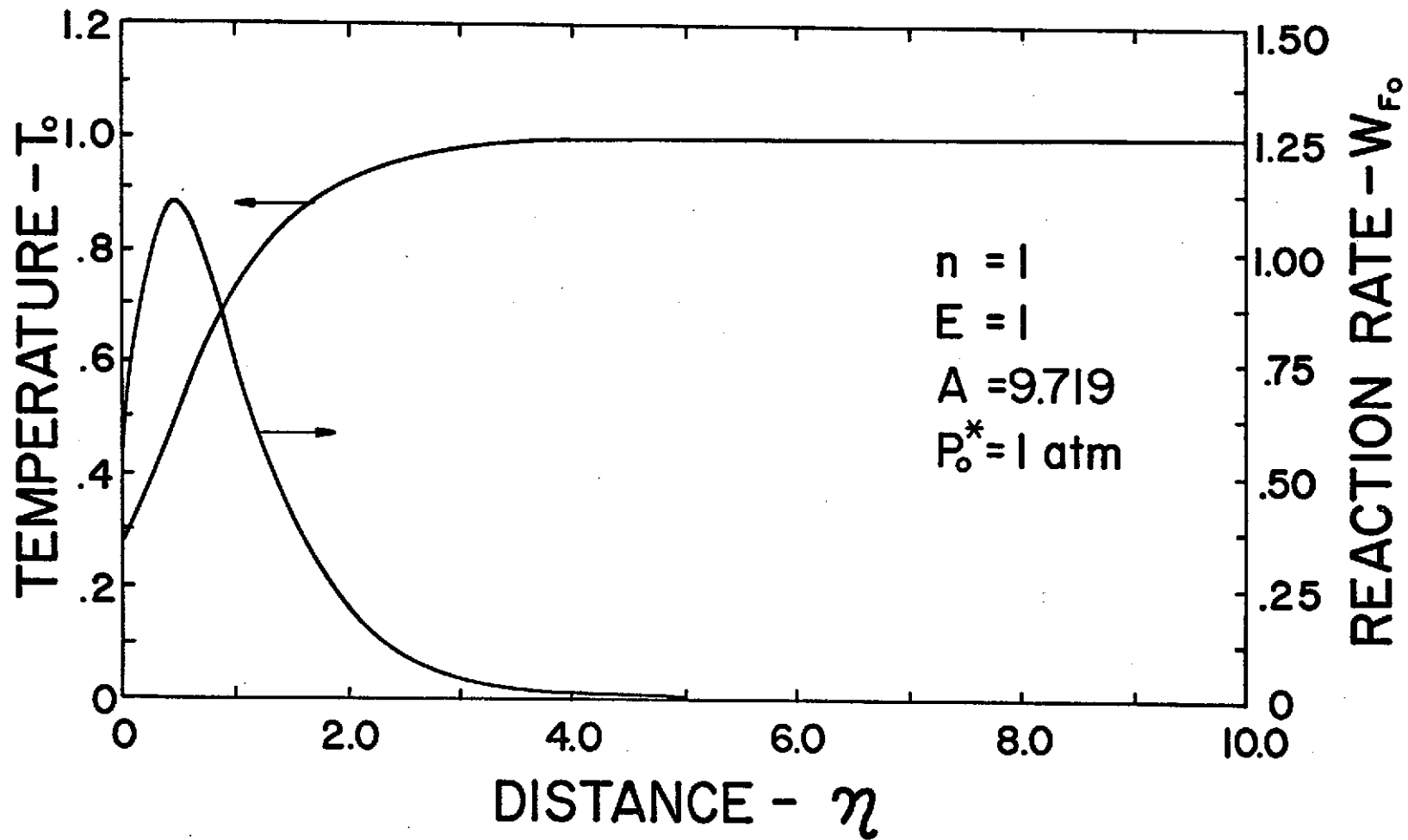


Figure 14 Steady State Gas Phase Temperature and Reaction Rate Distributions for $n = 1$, $E = 1$

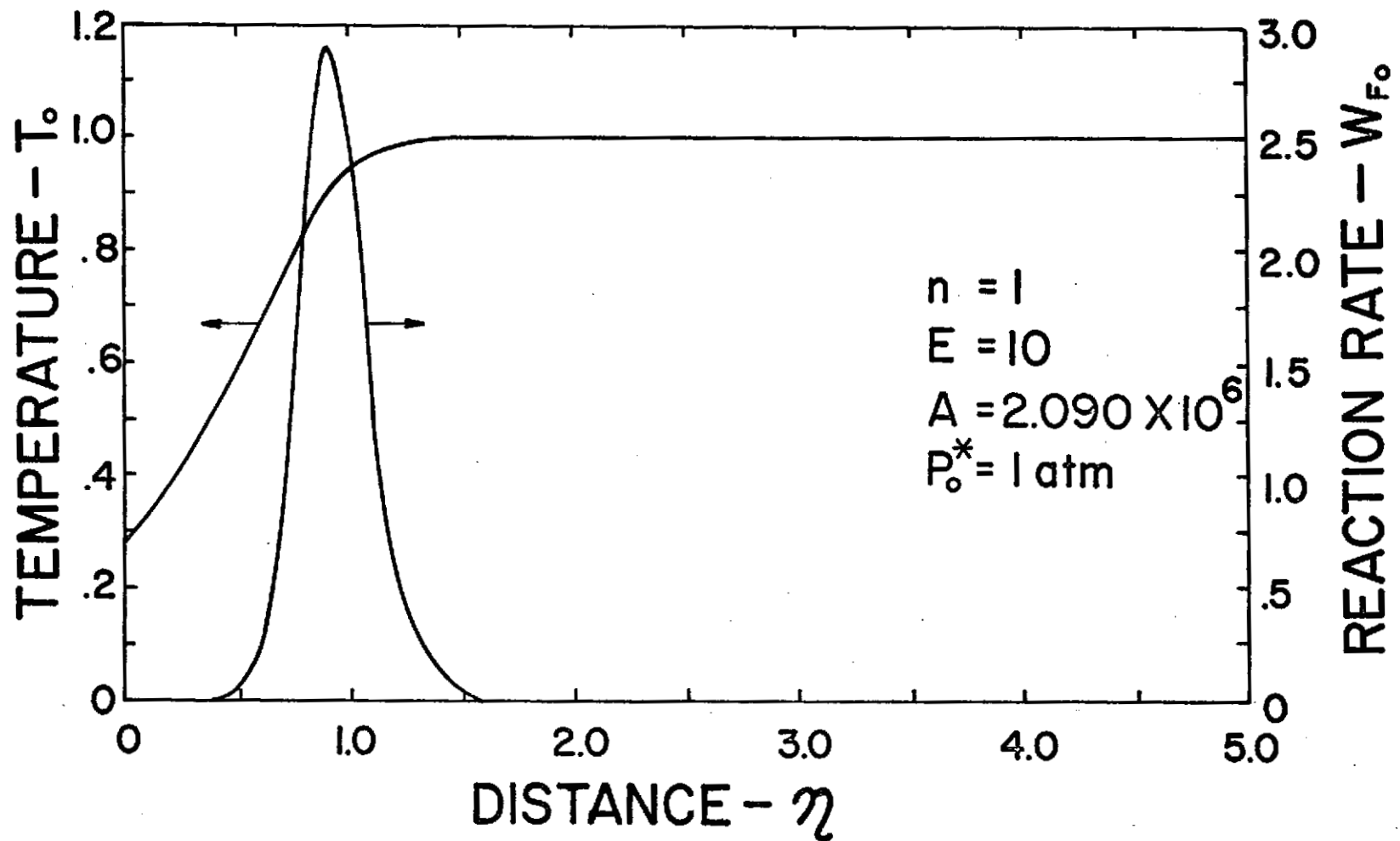


Figure 15 Steady State Gas Phase Temperature and Reaction Rate Distributions for $n = 1$, $E = 10$

4.2 Oscillatory Combustion

The results described in the previous section of this chapter indicate that the steady combustion portion of the theoretical model is in good agreement with available experimental measurements of the burning rates, liquid temperature distributions and surface temperatures of hydrazine strands. In this section experimental oscillatory strand burning rates are compared with the theoretical model.

4.2.1 Data Reduction

The data from the oscillatory version of the strand combustion apparatus consisted of an oscillograph record of the pressure in the test chamber and a film record of the liquid surface motion, both as a function of time. Typical experimental data from the oscillatory combustion apparatus are shown in Figure 16.

In Figure 16 the pressure record taken from the oscillograph trace and the liquid surface motion data taken from the film record are drawn to the same time scale. These results allow the determination of the amplitude and also the phase angle of the surface oscillations.

As shown in Figure 16 the phase angle of the surface oscillation with respect to the pressure oscillations was determined by measuring the distance between the peaks of the two curves. The amplitude of the oscillations was measured as half the distance between the maximum and minimum in the surface oscillations for one cycle. Some repeatability tests were conducted; the maximum difference between two sets of data taken at the same test condition was less than 25%. For those conditions where more than one set of

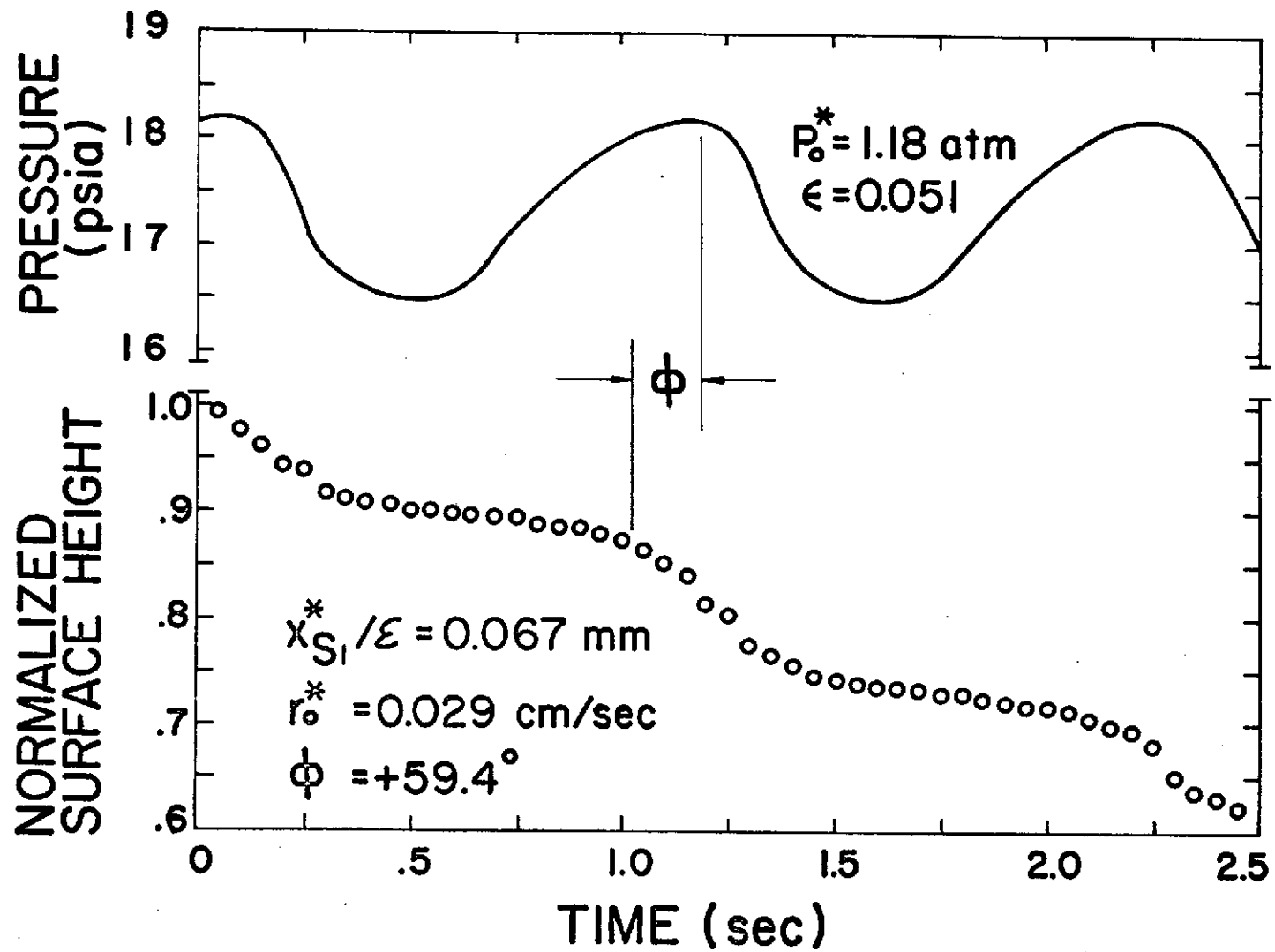


Figure 16 Typical Experimental Pressure and Liquid Surface Oscillations as a Function of Time

data was taken, the experimental points shown in the following figures are the average of the separate tests.

4.2.2 Effect of Pressure Amplitude

The theoretical model described in Chapter III assumed that the amplitude of the pressure oscillations was small enough so that only linear effects needed to be considered in the perturbation analysis. In order to check experimentally where this assumption breaks down, a series of tests were conducted with constant mean pressure and frequency of the imposed pressure oscillations but varying pressure amplitude. For these tests the mean pressure was held constant at 1.54 atm and the frequency was fixed at 1.32 Hz.

In Figure 17 the amplitude of the liquid surface oscillations divided by the normalized pressure amplitude, ϵ , is plotted as a function of pressure amplitude. The linear analysis assumes that the data plotted in this manner should be constant. It is evident from Figure 17 that the data begin to deviate significantly from this constant relation for pressure amplitudes above about 0.25.

In Figure 18 the mean burning rates for the same tests as shown in Figure 17 are plotted as a function of normalized pressure amplitude. Again the linear theory assumes that the mean burning rate is the same for all pressure amplitudes. As before, significant deviations from linearity appear to arise for pressure amplitudes above about 0.25.

Thus, both sets of experimental results indicate that nonlinearities in the combustion system are important for pressure amplitudes above about 0.25. To insure the validity of the linear

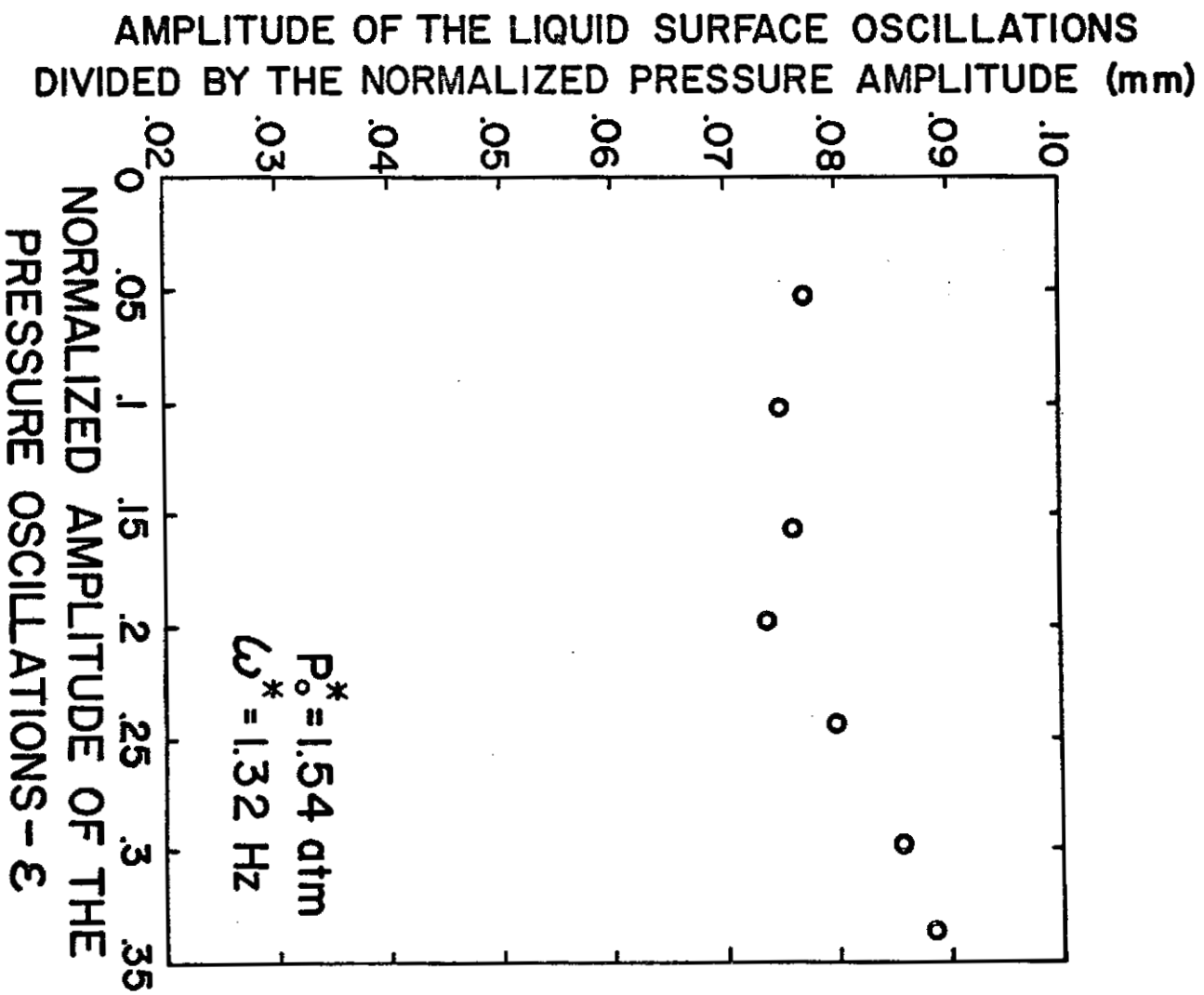


Figure 17 Amplitude of the Liquid Surface Oscillations as a Function of Pressure Amplitude

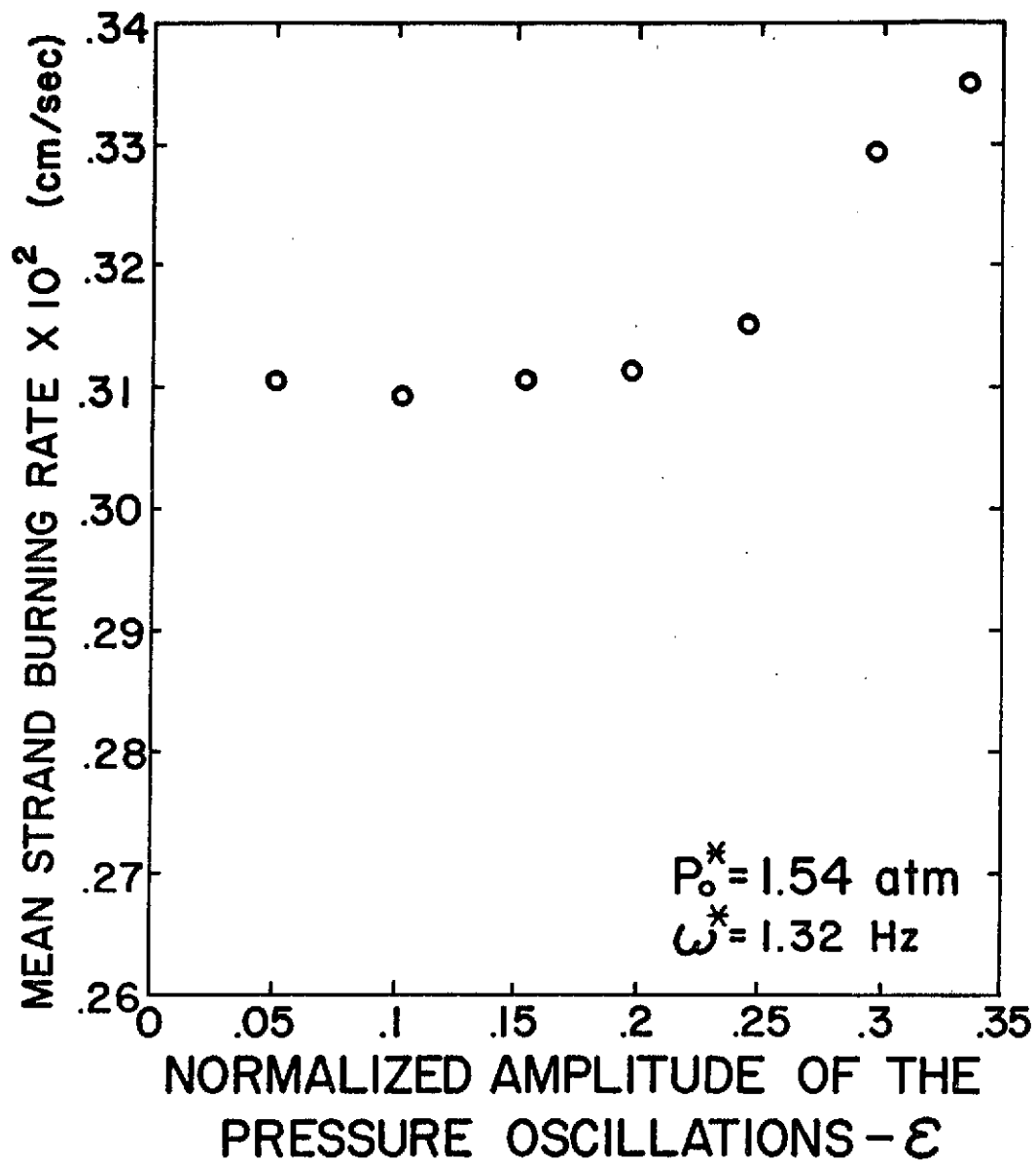


Figure 18 Mean Burning Rates as a Function of Pressure Amplitude

theory all additional experimental data was taken with pressure amplitudes less than 0.15.

4.2.3 High Pressure Results

The main thrust of the present work was to determine the effect of frequency upon the oscillatory burning rate of hydrazine. Two sets of data were taken with variable frequency; the first set was taken at a mean pressure of 9.77 atm and the second set at a mean pressure of 1.18 atm. This section describes the results at 9.77 atm while the next section describes the results at 1.18 atm.

One of the important parameters obtained from the theoretical model is r_1 , the nondimensional mass burning rate. However, x_{s1}^* , the dimensional amplitude and phase angle of the liquid surface oscillations are the quantities that are measured experimentally. As described in Section 3.5.2, r and x_{s1} are related by Equation (69).

Figure 19 is a plot of the surface oscillation amplitude as a function of frequency at a mean pressure of 9.77 atm. In addition to the curves obtained from the theoretical model, the curve obtained from a totally quasi-steady analysis (neglecting both liquid and gas phase transient effects) is also shown on Figure 19. The totally quasi-steady analysis is developed in Appendix E.

The transient analysis indicates a larger amplitude of surface oscillation than the totally quasi-steady analysis for the range of frequencies shown on Figure 19. However, at lower frequencies the two models approach one another as they must. Note that the gas phase activation energy has a pronounced effect upon the predicted

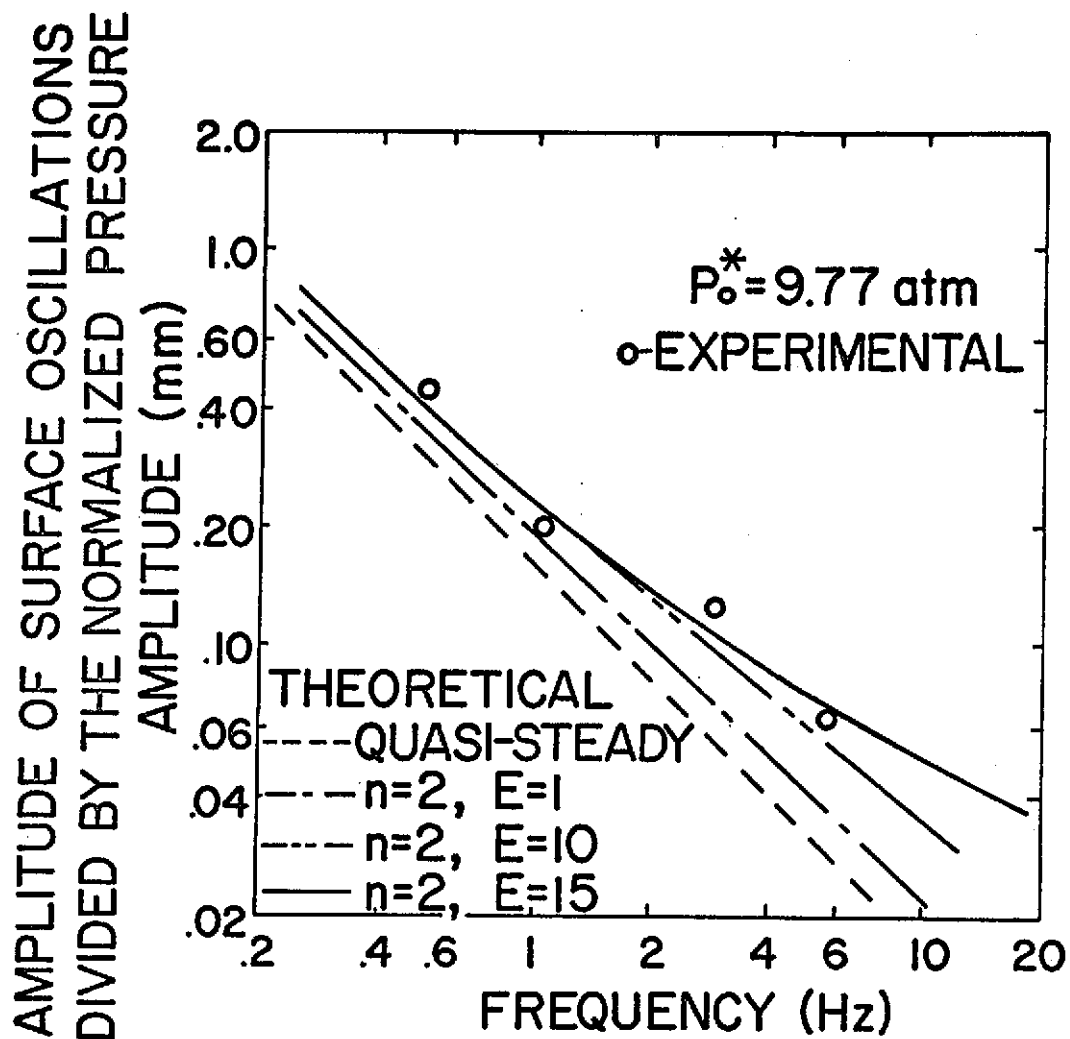


Figure 19 Theoretical and Experimental Magnitude of the Liquid Surface Oscillations as a Function of Frequency at a Mean Pressure of 9.77 atm

transient results. The results for a dimensionless activation energy of 30 do not differ appreciably from the results for $E = 15$ in this frequency range and these two curves are shown as one, labelled $E = 15$. As shown in Figure 19, the theoretical curve with a dimensionless activation energy of 15 is in reasonably good agreement with the experimental results.

Figure 20 is a plot of the phase angle of the surface oscillation as a function of frequency at a mean pressure of 9.77 atm. At low frequencies, both the transient and the quasi-steady analyses indicate a 90° phase angle. At this condition the burning rate and pressure oscillations are in phase. As seen from Equation (69), for the burning rate in phase with the pressure, the surface oscillation must be 90° out of phase. Of course, the quasi-steady model does not predict any deviation from the 90° out of phase condition as frequency increases.

As in the case of the amplitude of the surface oscillation, the activation energy has a significant effect upon the predicted phase angle. Again a nondimensional activation energy of 15 agrees with the data reasonably well as shown in Figure 20. Note that the phase angles at these conditions are greater than 90° indicating that the burning rate oscillation was leading the pressure oscillation.

Since the steady state results, as shown in Figure 8, indicate that the gas phase reaction at 9.77 atm is second order, no theoretical predictions were made assuming a first order reaction at this mean pressure. A second set of data was taken at 1.18 atm where, from Figure 8, the gas phase reaction appears to be first order. These results are described in the next section.

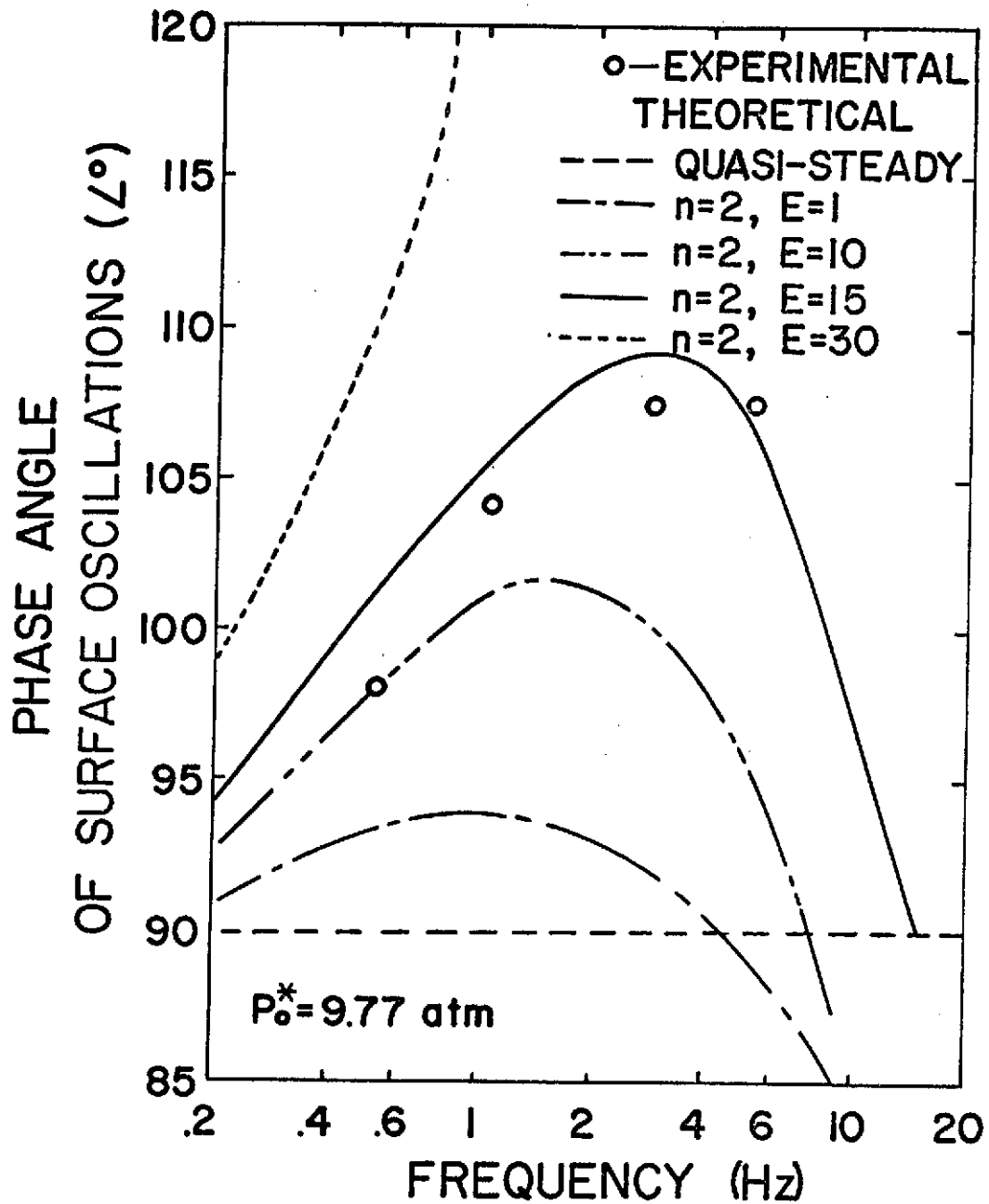


Figure 20 Theoretical and Experimental Phase Angle of the Liquid Surface Oscillations as a Function of Frequency at a Mean Pressure of 9.77 atm

4.2.4 Low Pressure Results

In order to investigate the effect of mean pressure on the oscillatory burning rate of hydrazine, a second series of data were taken at a mean pressure of 1.18 atm. At this mean pressure the steady results, as shown in Figure 8, indicate that the gas phase reaction is probably first order.

In Figure 21 the amplitude of the liquid surface oscillation is plotted as a function of frequency. The theoretical curves obtained from the transient model assume a first order reaction. At these conditions, the theoretical curve for $E = 1$, predicts a smaller surface oscillation amplitude than the totally quasi-steady analysis. However, both theoretical curves approach the quasi-steady results for low frequency.

The results shown in Figure 21 suggest that a higher activation energy than $E = 10$ is required to agree with the experimental data. However, the opposite conclusion is reached if the phase angle is considered as shown in Figure 22. The phase angle results suggest that a low activation energy, between 1 and 10, would best agree with the experimental data. Thus, the first order reaction theoretical results are not in good agreement with the experimental data at a mean pressure of 1.18 atm.

If the reaction is assumed to be second order at 1.18 atm, the theoretical steady strand burning rate is significantly less than the experimental result as seen from Figure 8. To adjust the steady burning rate, the results shown in Figure 8 were recorrelated by matching theory to the experimental results at 1.0

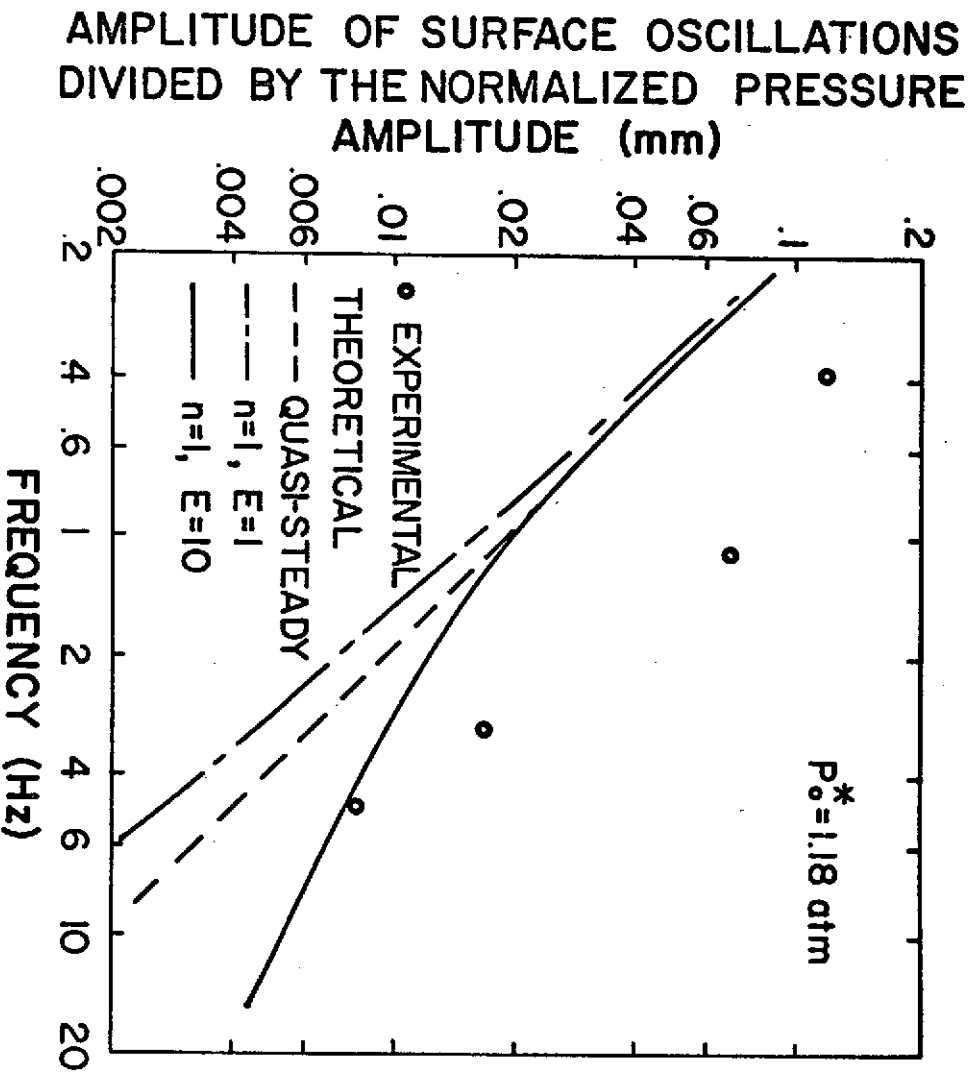


Figure 21 Theoretical ($n = 1$) and Experimental Magnitude of the Liquid Surface Oscillations as a Function of Frequency at a Mean Pressure of 1.18 atm

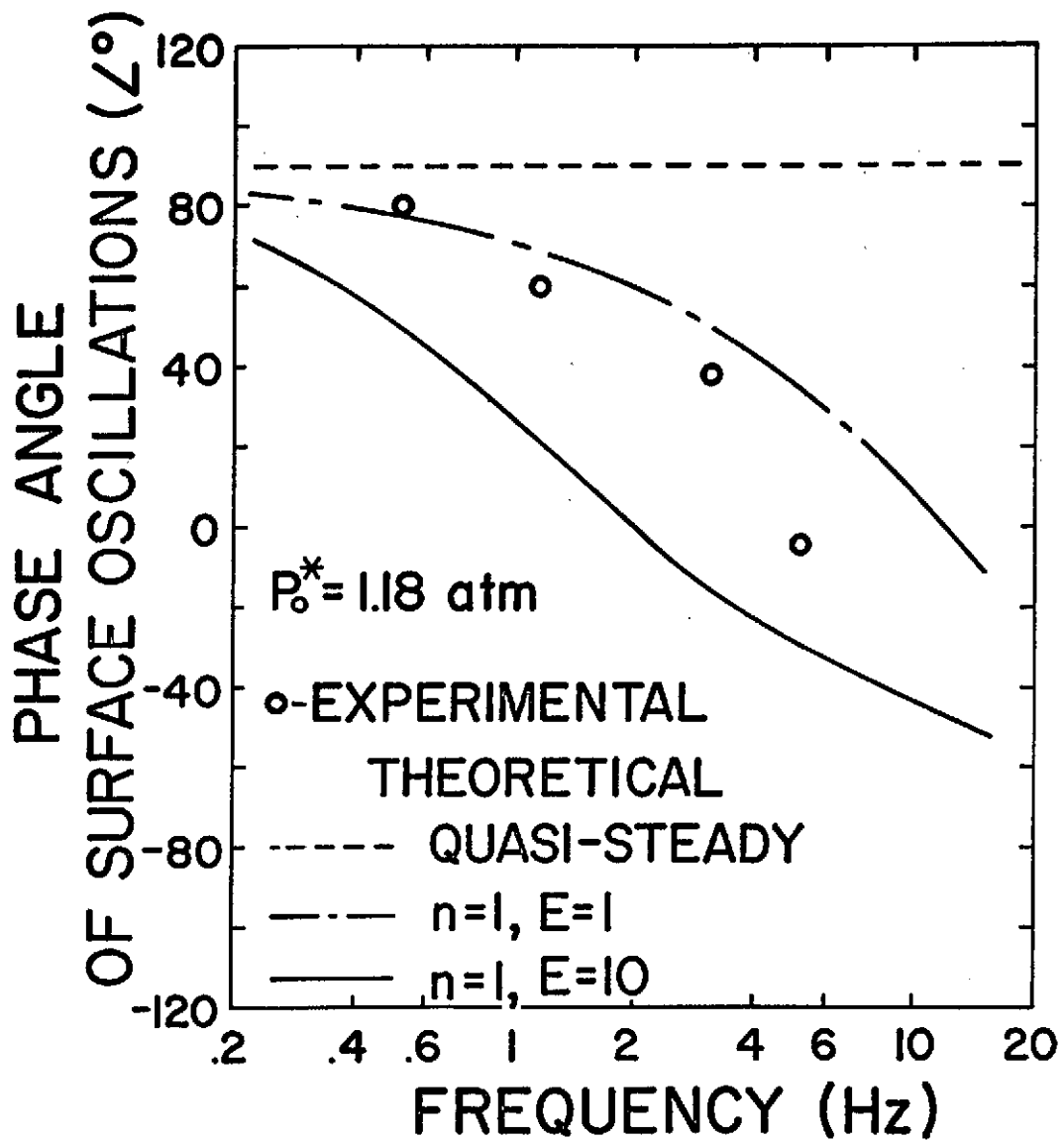


Figure 22 Theoretical ($n = 1$) and Experimental Phase Angle of the Liquid Surface Oscillations as a Function of Frequency at a Mean Pressure of 1.18 atm

atm for a second order gas phase reaction rather than at 6.7 atm. The parameters obtained from this match are listed in Table 3.

In Figure 23, the amplitude of the liquid surface oscillation is plotted as a function of frequency. A second order gas phase reaction with an activation energy of between 10 and 15 agrees well with the experimental data. The same conclusion is reached when considering phase angles as shown in Figure 24. Thus, as with the high pressure results, the theoretical model assuming a second order reaction with a nondimensional activation energy of about 15 is in good agreement with the experimental data. The corresponding dimensional activation energy of about 40 kcal is also in good agreement with the apparent activation energy of 36 kcal reported by McHale, et al., [49] from a kinetic study on hydrazine decomposition.

4.2.5 Additional Implications of the Theoretical Model

The preceding discussion has indicated that the theoretical model is in good agreement with all available experimental results on the oscillatory burning of hydrazine. After gaining this confidence in the model, the model was used to predict the effects of various parameters of interest to engine designers on the oscillatory behavior of hydrazine. This section describes these results in detail.

4.2.5.1 Effect of Mean Pressure

One of the prime quantities of interest in the unsteady combustion case is the dimensionless oscillatory mass burning rate perturbation, r_1 , due to an oscillatory pressure perturbation of

Table 3

Additional Correlation Condition and Parameters
Used in the Theoretical Model

E	E* (kcal/mole)	Correlation Condition	
		n = 2	$P_o^* = 1.0 \text{ atm}$ $v_l^* = 0.021 \text{ cm/sec}$
		B* (cm ³ /gm-sec)	
1	2.673	1.806 x 10 ⁸	
10	26.73	2.353 x 10 ¹⁴	
15	40.08	1.052 x 10 ¹⁷	
30	80.16	2.375 x 10 ²⁴	

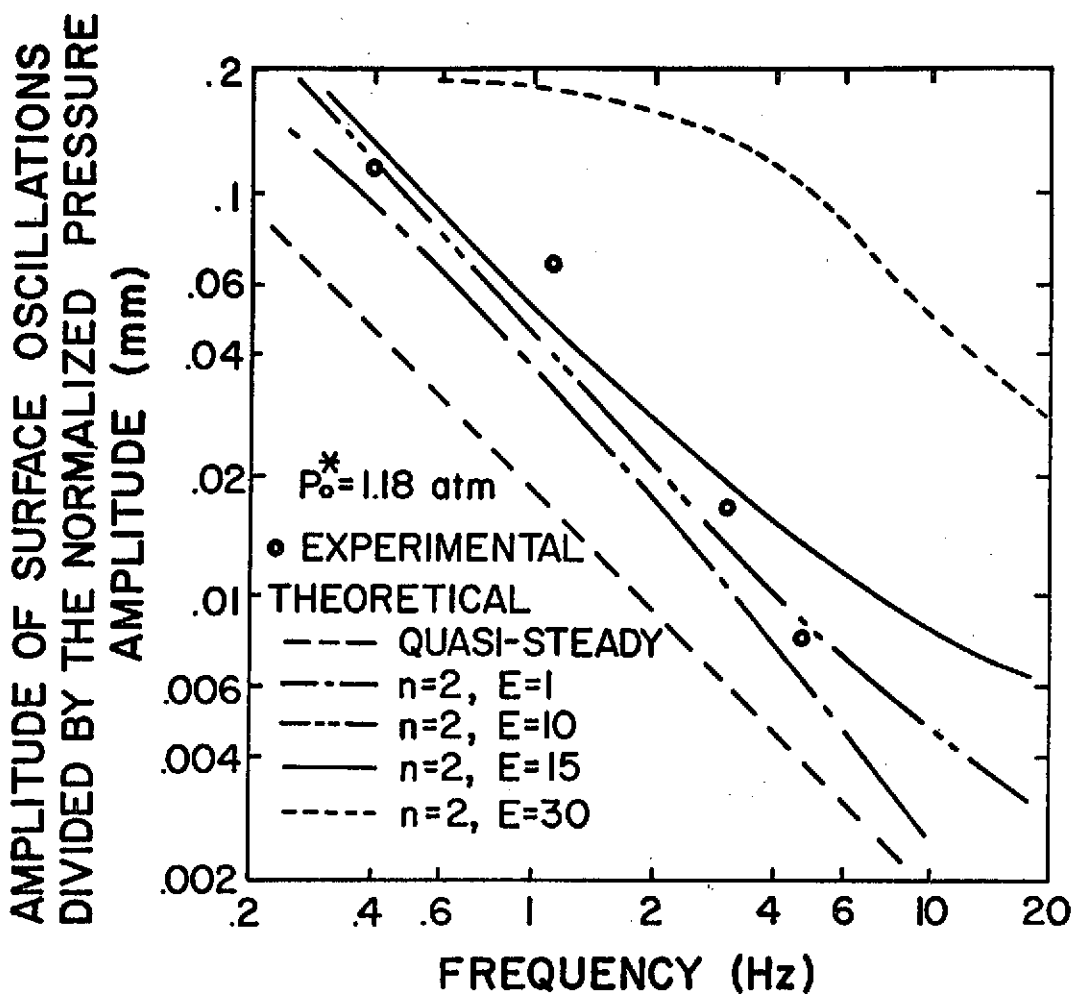


Figure 23 Theoretical ($n = 2$) and Experimental Magnitude of the Liquid Surface Oscillations as a Function of Frequency at a Mean Pressure of 1.18 atm

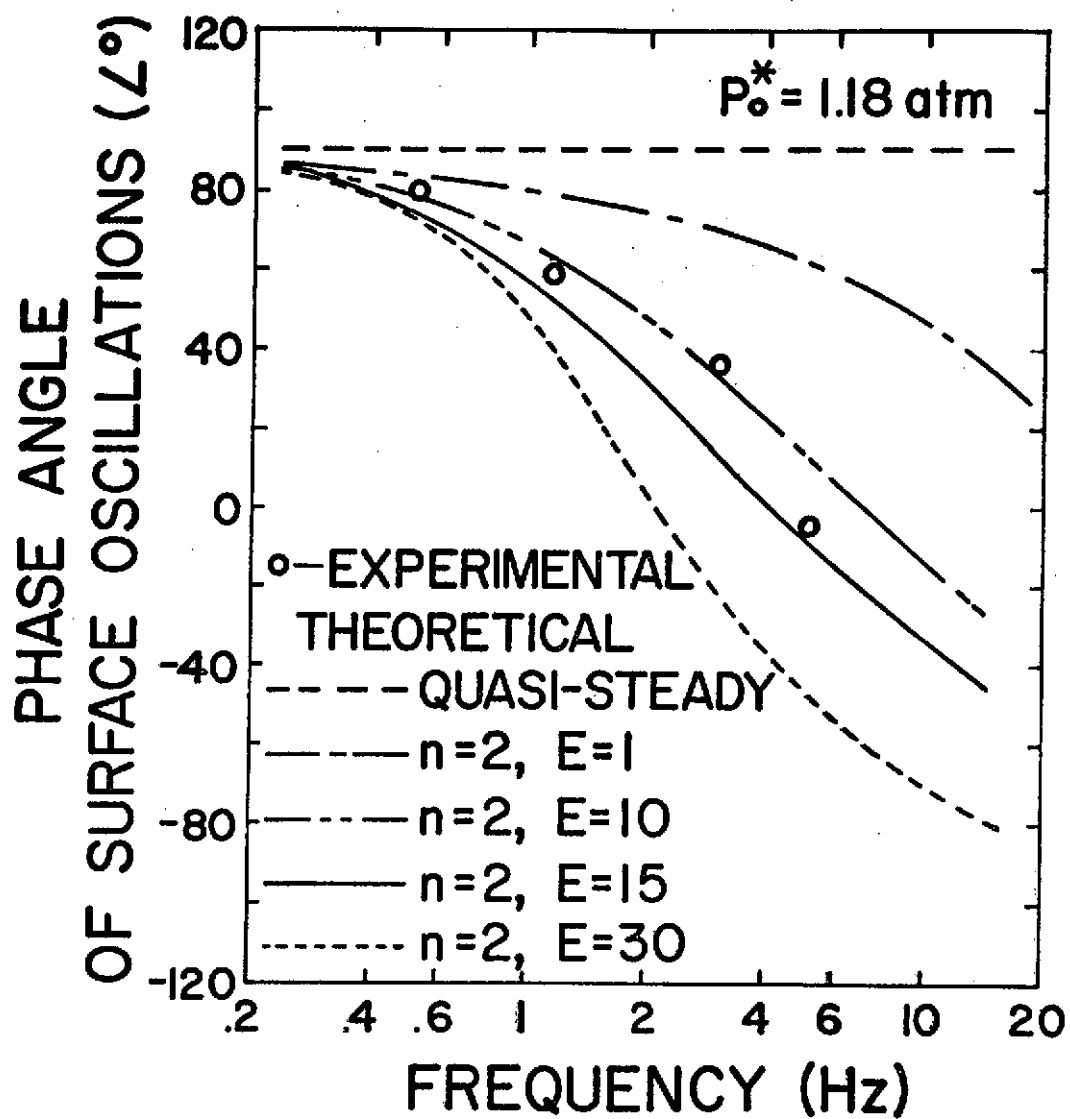


Figure 24 Theoretical ($n = 2$) and Experimental Phase Angle of the Liquid Surface Oscillations as a Function of Frequency at a Mean Pressure of 1.18 atm

amplitude ϵ . The next nine figures indicate the effect of mean pressure on the behavior of r_1 for various activation energies and a second order reaction.

Figures 25-27 show the amplitude and phase angle (with respect to the pressure oscillation) of r_1 for a dimensionless activation energy of 1 and mean pressures of 1, 10 and 100 atm, respectively, as a function of the dimensionless frequency of the pressure oscillation. At low frequencies the burning rate oscillation is in phase with the pressure oscillation, and the entire process, both liquid and gas phase, is quasi-steady. As the frequency approaches the characteristic frequency of the liquid phase thermal wave both the phase (with respect to the pressure oscillation) and the amplitude of r_1 begin to deviate from their quasi-steady value. The nondimensional characteristic frequency of the liquid phase thermal wave increased from about 10^{-4} at 1 atm to about 10^{-2} at 100 atm.

As the frequency increases beyond the characteristic liquid thermal wave frequency, gas phase transient effects become important. On Figures 25-27 two theoretical curves are shown. The solid curve neglects all transient gas phase effects but includes the effects of a transient liquid phase. The dashed curve includes the effects of both transient gas and liquid phases. As indicated in Figures 25-27 gas phase transient effects only become important for nondimensional frequencies on the order of 0.10. The quasi-steady gas phase analysis was obtained by taking the formal limit $\omega \rightarrow 0$ in the gas phase as described in Appendix C.

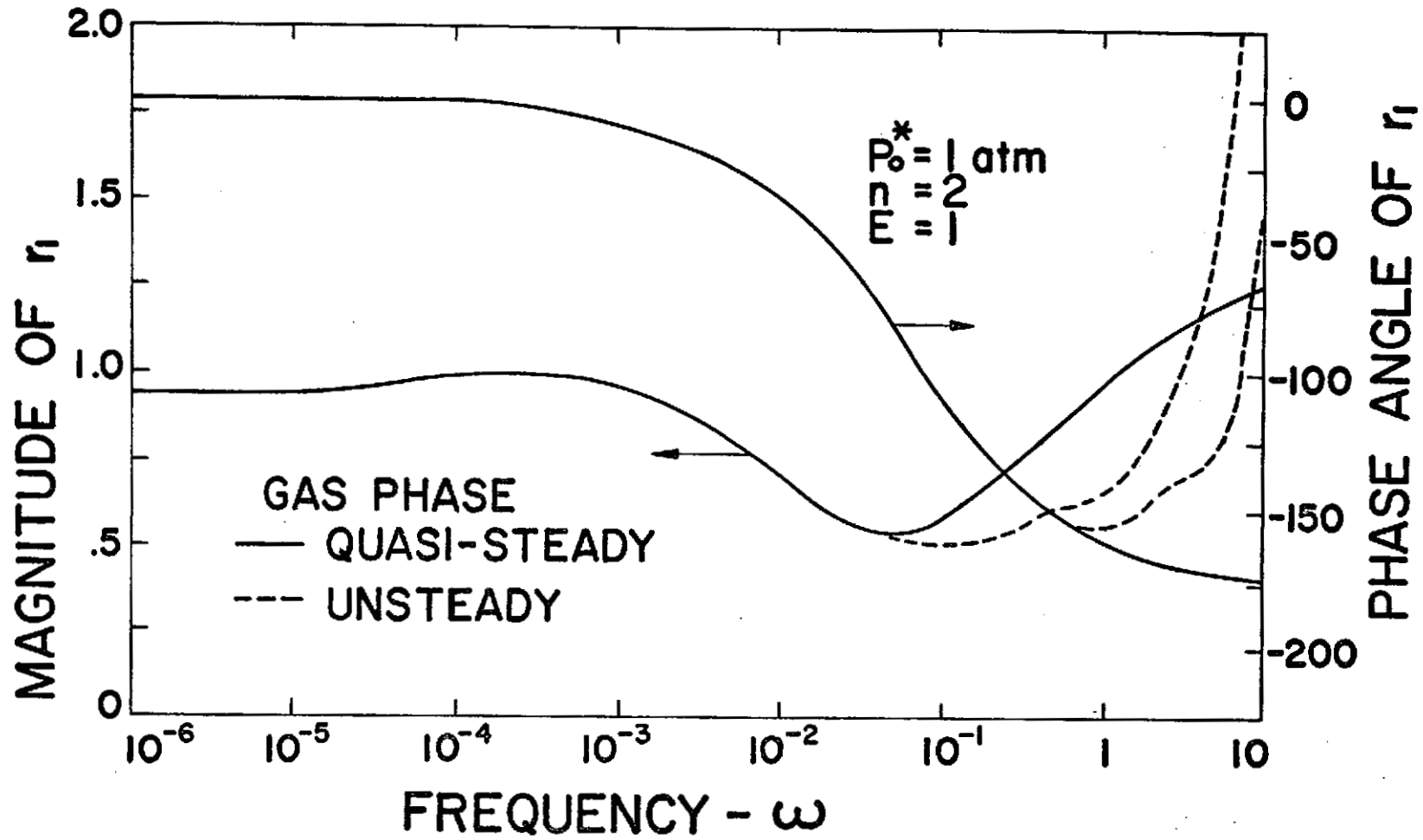


Figure 25 Burning Rate Oscillation Amplitude and Phase Angle as a Function of Frequency for $P_0^* = 1 \text{ atm}$, $n = 2$, $E = 1$

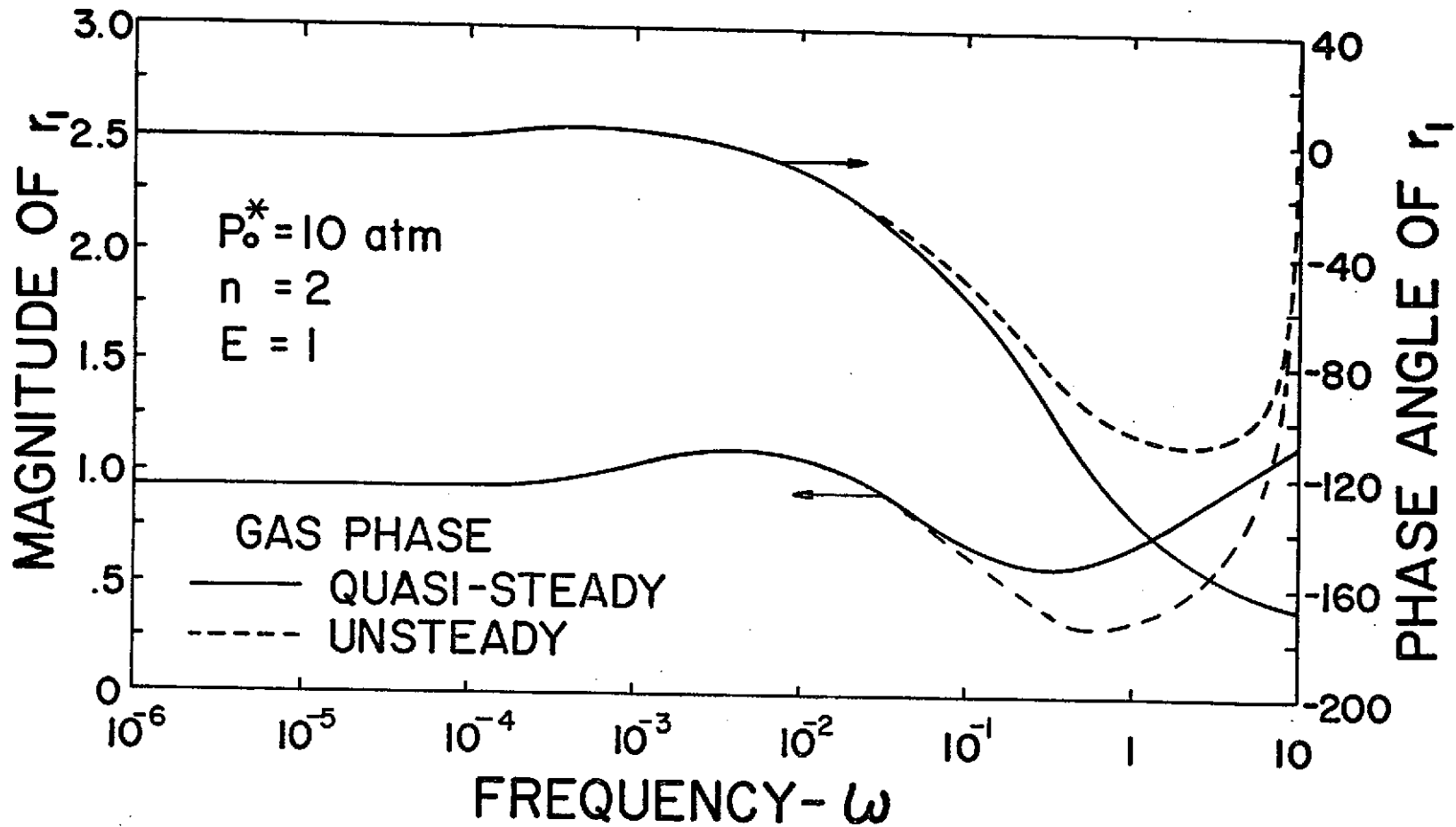


Figure 26 Burning Rate Oscillation Amplitude and Phase Angle as a Function of Frequency for $P_o^* = 10 \text{ atm}$, $n = 2$, $E = 1$

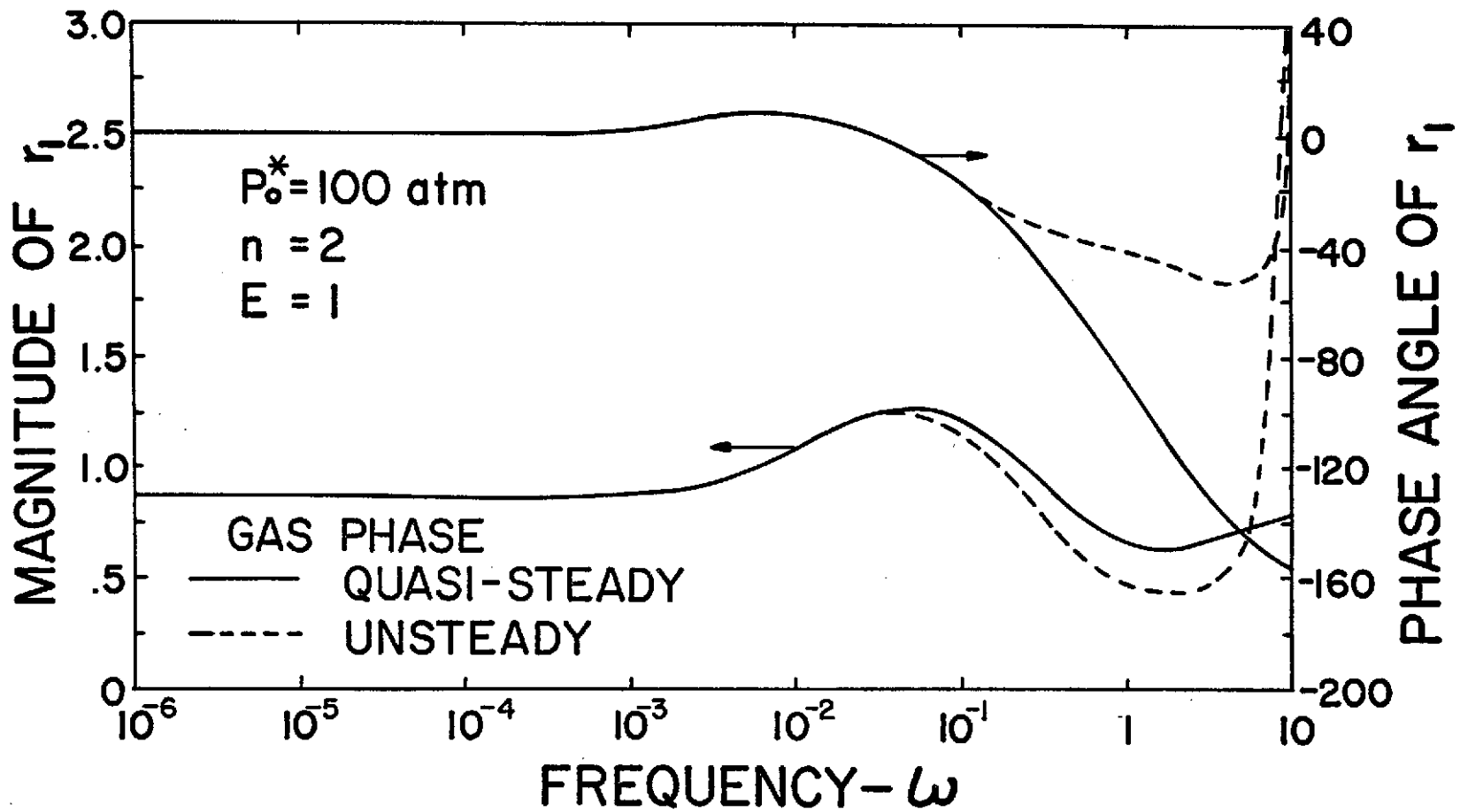


Figure 27 Burning Rate Oscillation Amplitude and Phase Angle as a Function of Frequency for $P_0^* = 100 \text{ atm}$, $n = 2$, $E = 1$

For $E = 1$, Figures 25-27 indicate that as the pressure increases the peak in the r_1 response curve due to liquid thermal effects becomes more pronounced. At low pressures the phase lag is negative for all frequencies of oscillation. As the pressure increases, however, the phase lag is at first positive and then goes negative as ω increases. This effect was found to be due to the shape of the hydrazine vapor pressure curve. Theoretically, the liquid surface temperature oscillation amplitude is relatively small. Thus, at low pressures a finite change in the pressure causes a relatively small change in the fuel mass fraction at the surface. At high pressures, the same change in pressure causes a significant change in the surface fuel mass fraction.

Similar trends were found for the case of $E = 10$ as shown in Figures 28-30. However, in this case the peak in the r_1 response curve becomes very pronounced as pressure increases.

For the case $E = 30$ somewhat different behavior was found. As illustrated in Figures 31-33 the peak in the r_1 response curve becomes less pronounced as pressure increases. However, as before, the phase angle tends to positive values as the pressure increases for a given frequency.

4.2.5.2 Effect of Conditioning Temperature

Another parameter which could be of importance with regard to oscillatory combustion response is the fuel conditioning temperature T_{∞}^* . The effect of increasing T_{∞}^* from 298 to 350 K was investigated at a mean pressure of 1 atm for a second order reaction with a nondimensional activation energy of 10. The results of these

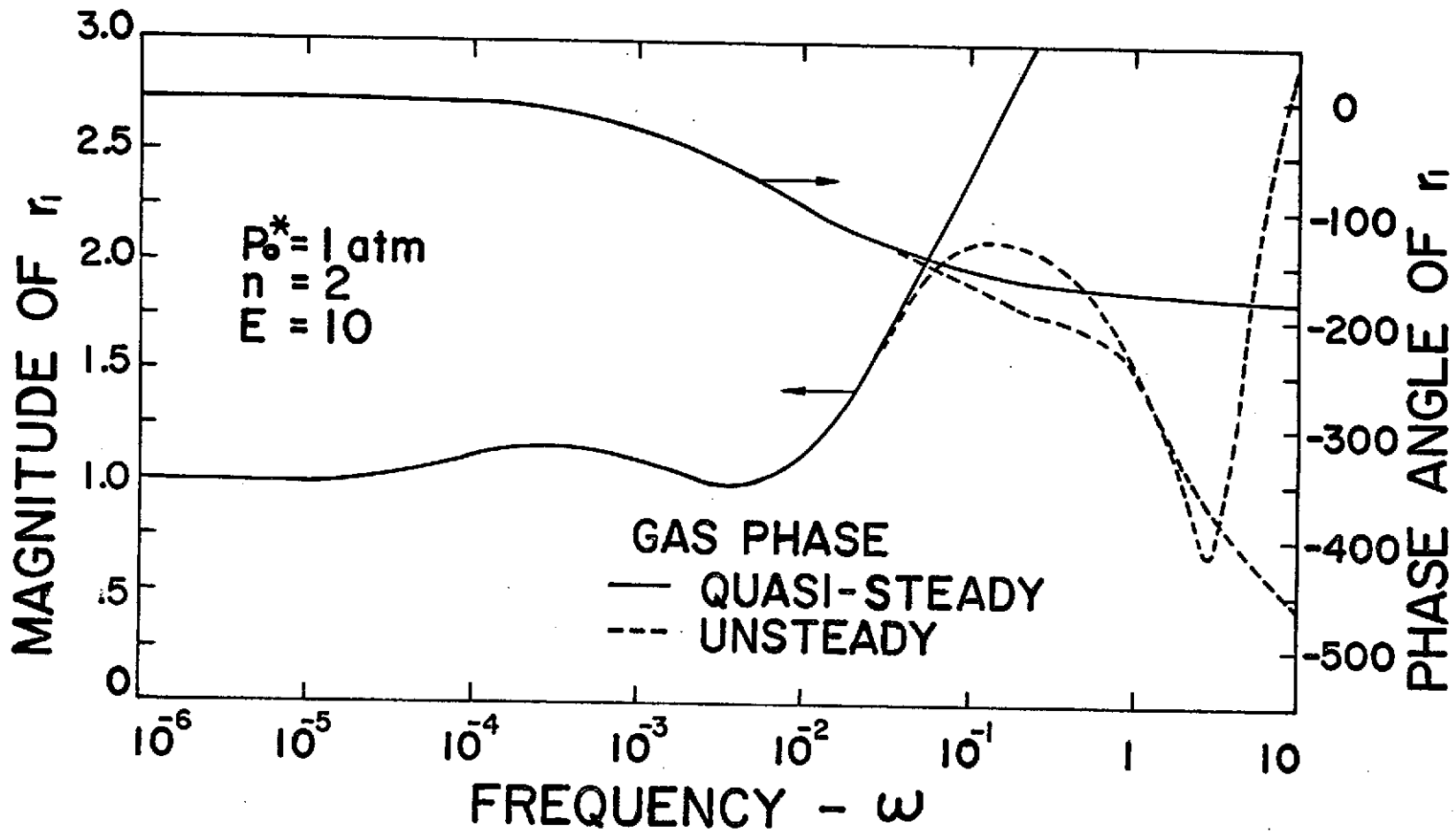


Figure 28 Burning Rate Oscillation Amplitude and Phase Angle as a Function of Frequency for $P_o^* = 1 \text{ atm}$, $n = 2$, $E = 10$

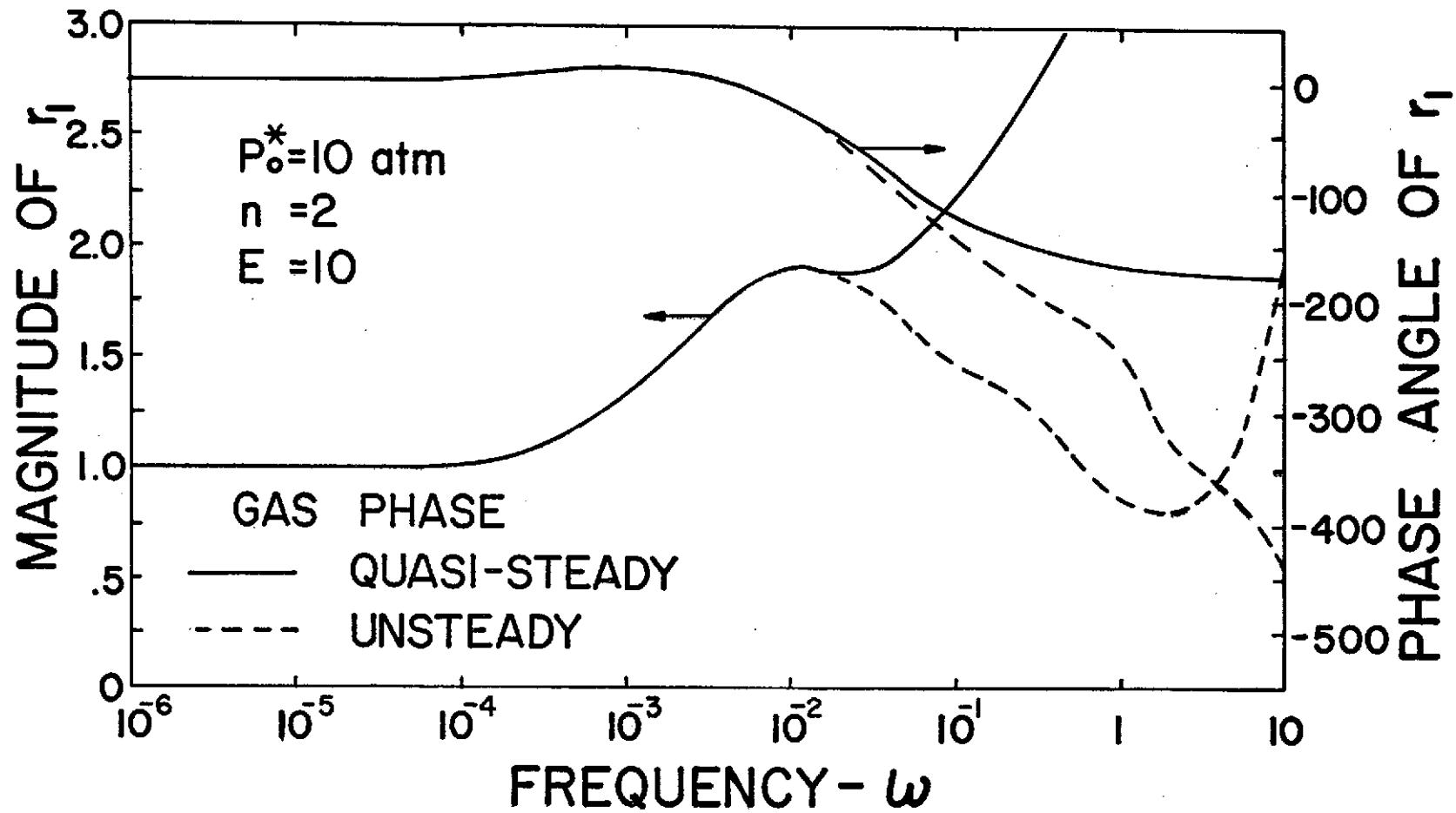


Figure 29 Burning Rate Oscillation Amplitude and Phase Angle as a Function of Frequency for $P_o^* = 10 \text{ atm}$, $n = 2$, $E = 10$

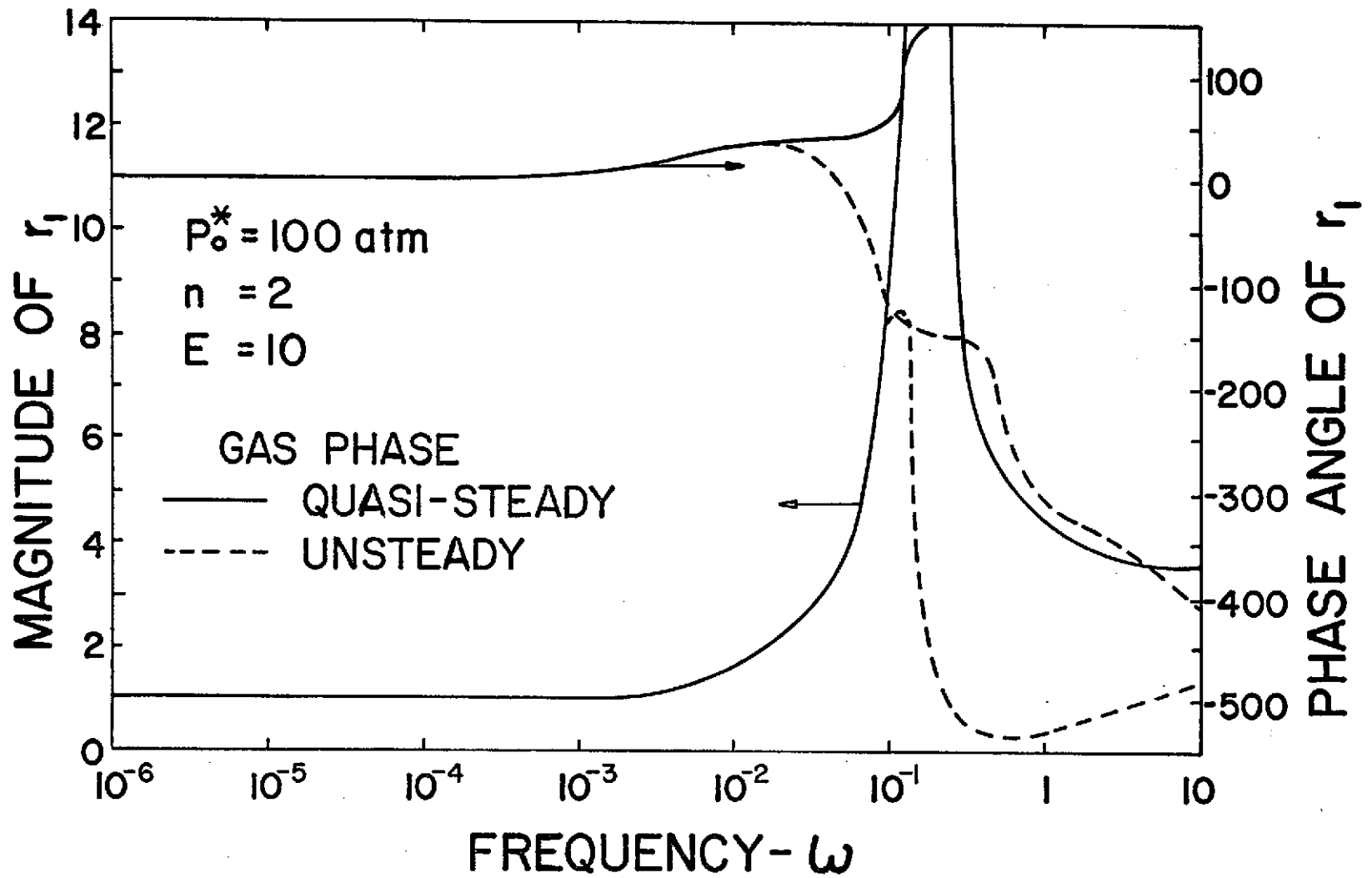


Figure 30 Burning Rate Oscillation Amplitude and Phase Angle as a Function of Frequency for $P_o^* = 100 \text{ atm}$, $n = 2$, $E = 10$

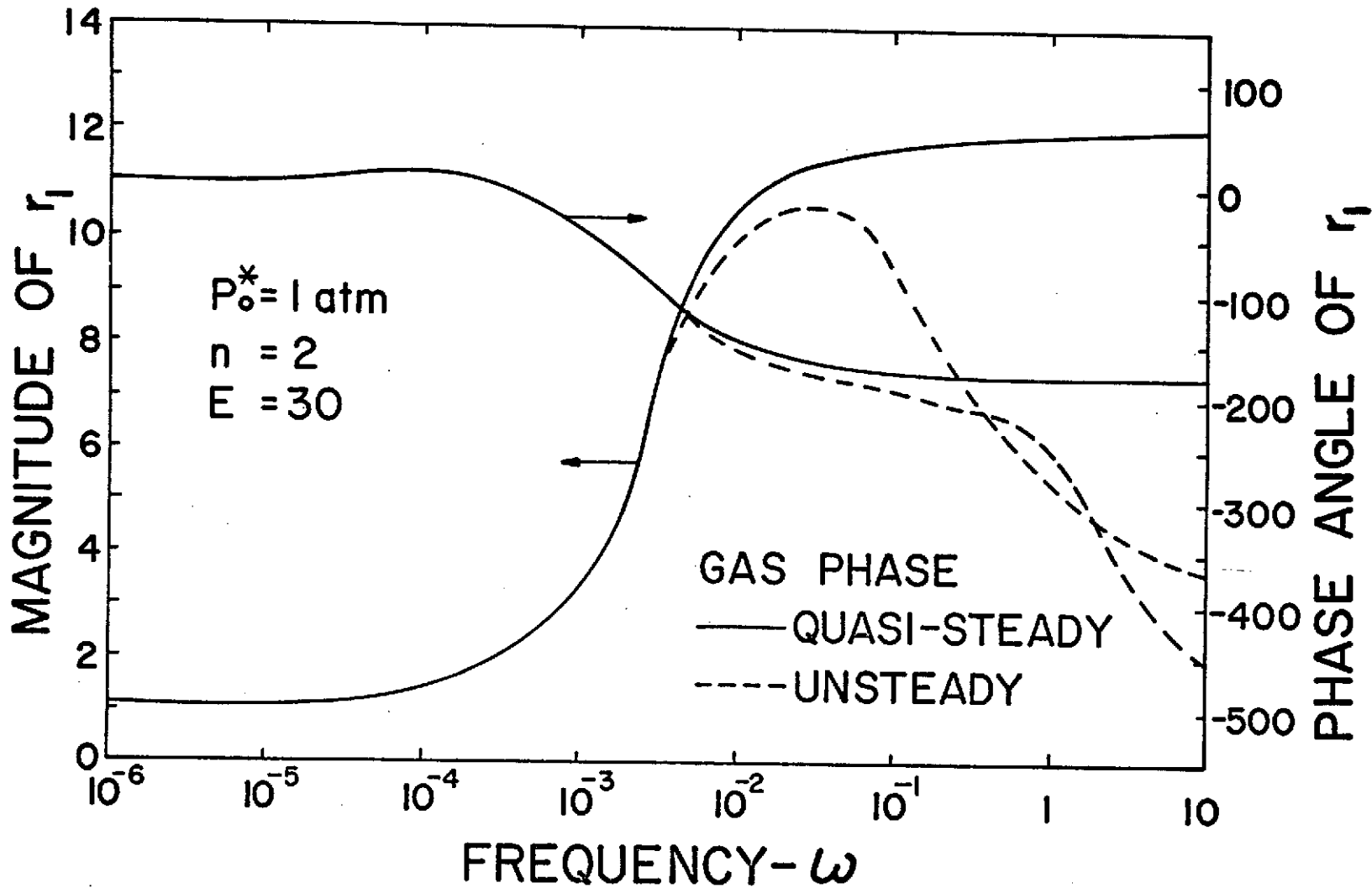


Figure 31 Burning Rate Oscillation Amplitude and Phase Angle as a Function of Frequency for $P_o^* = 1 \text{ atm}$, $n = 2$, $E = 30$

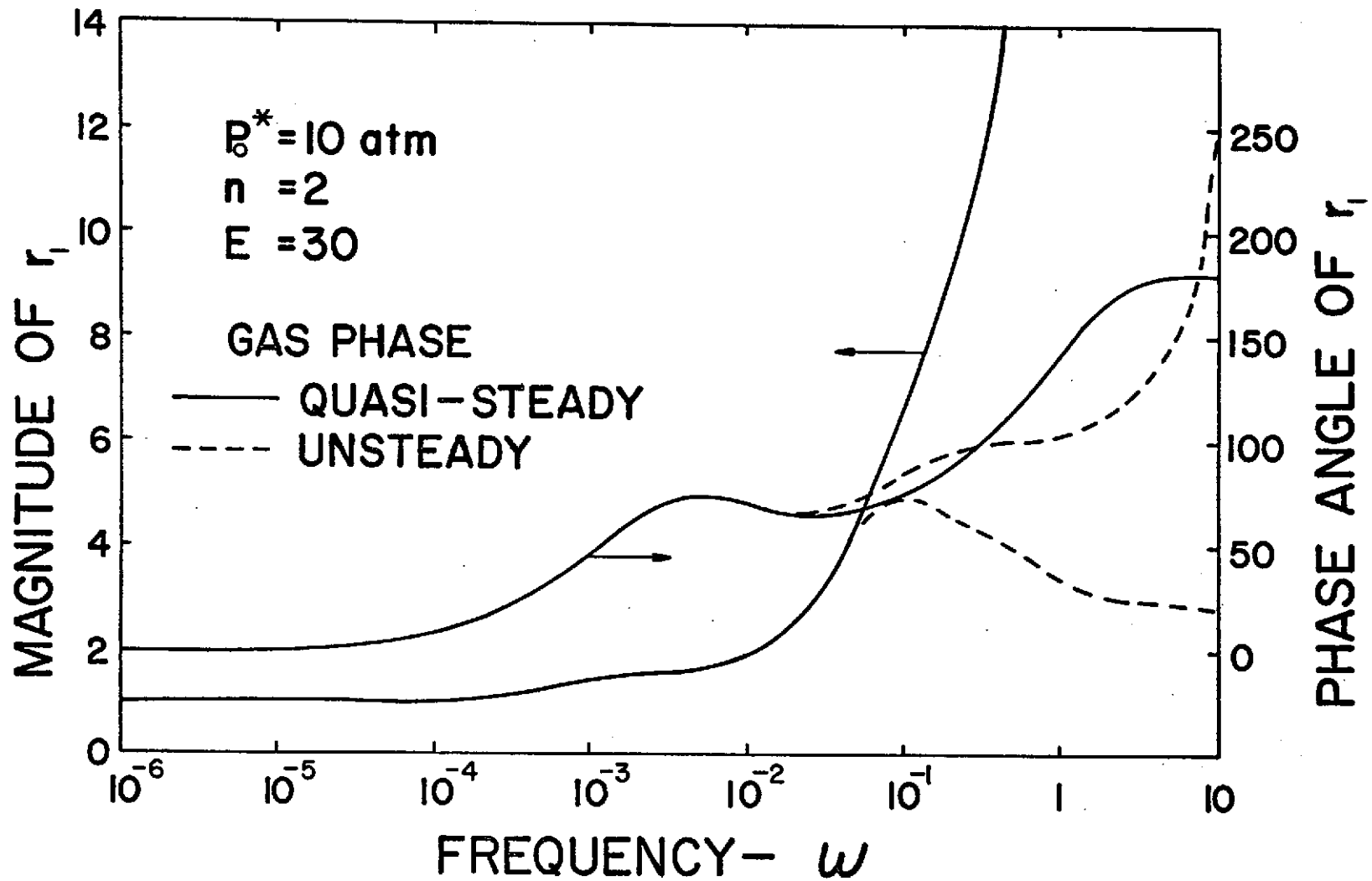


Figure 32 Burning Rate Oscillation Amplitude and Phase Angle as a Function of Frequency for $P_0^* = 10 \text{ atm}$, $n = 2$, $E = 30$

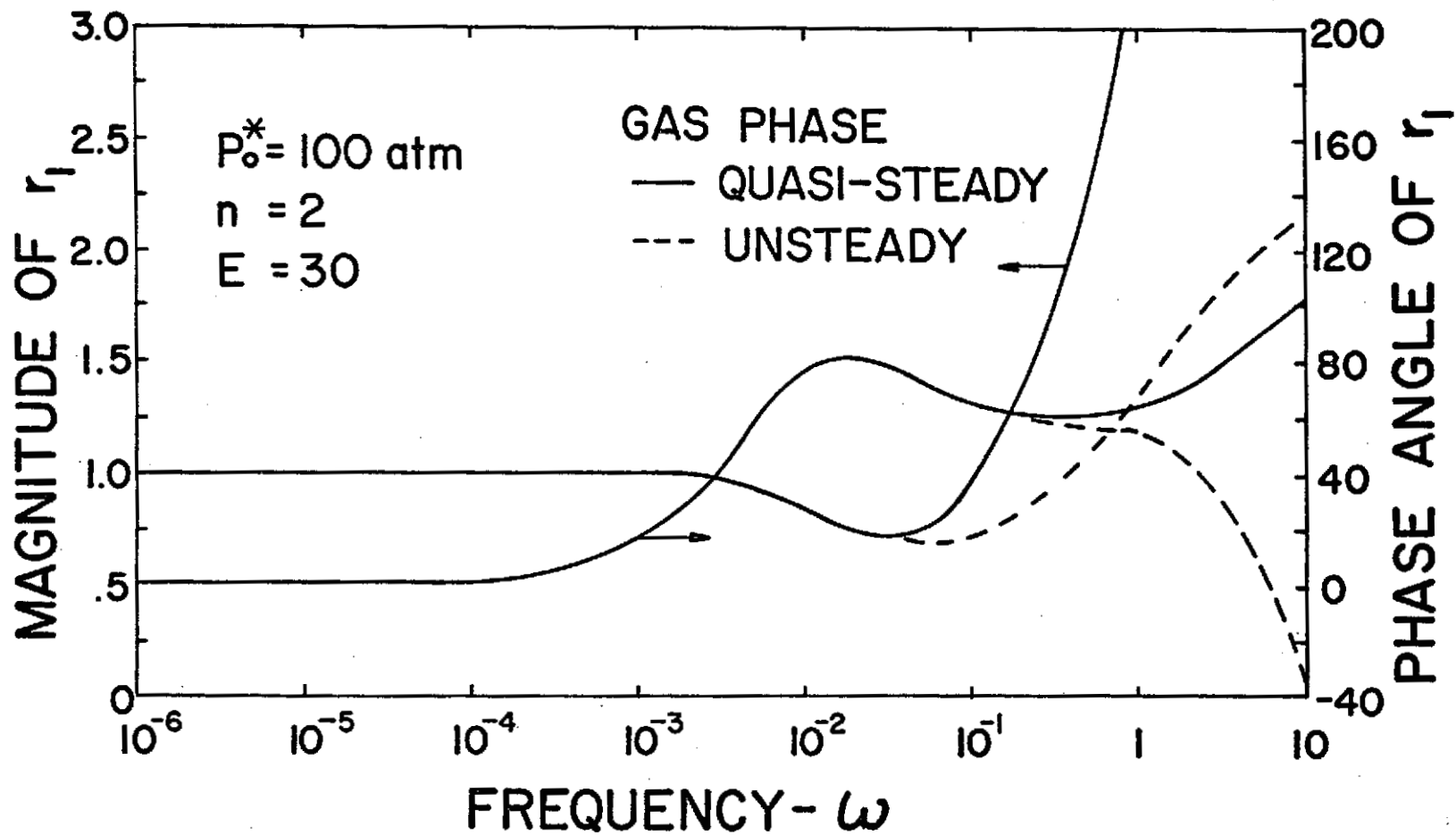


Figure 33 Burning Rate Oscillation Amplitude and Phase Angle as a Function of Frequency for $P_o^* = 100 \text{ atm}$, $n = 2$, $E = 30$

calculations are shown in Figure 34. Figure 34 was obtained by fixing all dimensional quantities but increasing the fuel conditioning temperature by 52 K. Of course, in order to satisfy overall conservation of energy the flame temperature had to be increased a corresponding amount. Increasing the flame temperature decreased the values of some of the nondimensional parameters of the problem, including the nondimensional activation energy.

By comparing Figure 34 with Figure 28 it is seen that the effect of increasing T_{∞} is to decrease somewhat the first peak in the r_1 response curve. However, the net overall effect is rather small.

4.2.5.3 Acoustic Admittance

The major parameter of interest to the designers in determining the stability characteristics of a combustion chamber is the real part of the acoustic admittance of the burning fuel. This quantity can be obtained from the present analysis as described in Appendix G.

The acoustic admittance varies with the distance from the liquid surface, but approaches a constant value for very large distances. As developed in Appendix G, the value shown here is the value at the true mathematical infinity.

Physically, the real part of the acoustic admittance represents that part of the gas phase velocity fluctuation which is in phase with the pressure fluctuation. Figures 35-37 show the real part of the acoustic admittance plotted as a function of frequency for various pressures for a second order reaction and nondimensional activation energies of 1, 10 and 30, respectively.

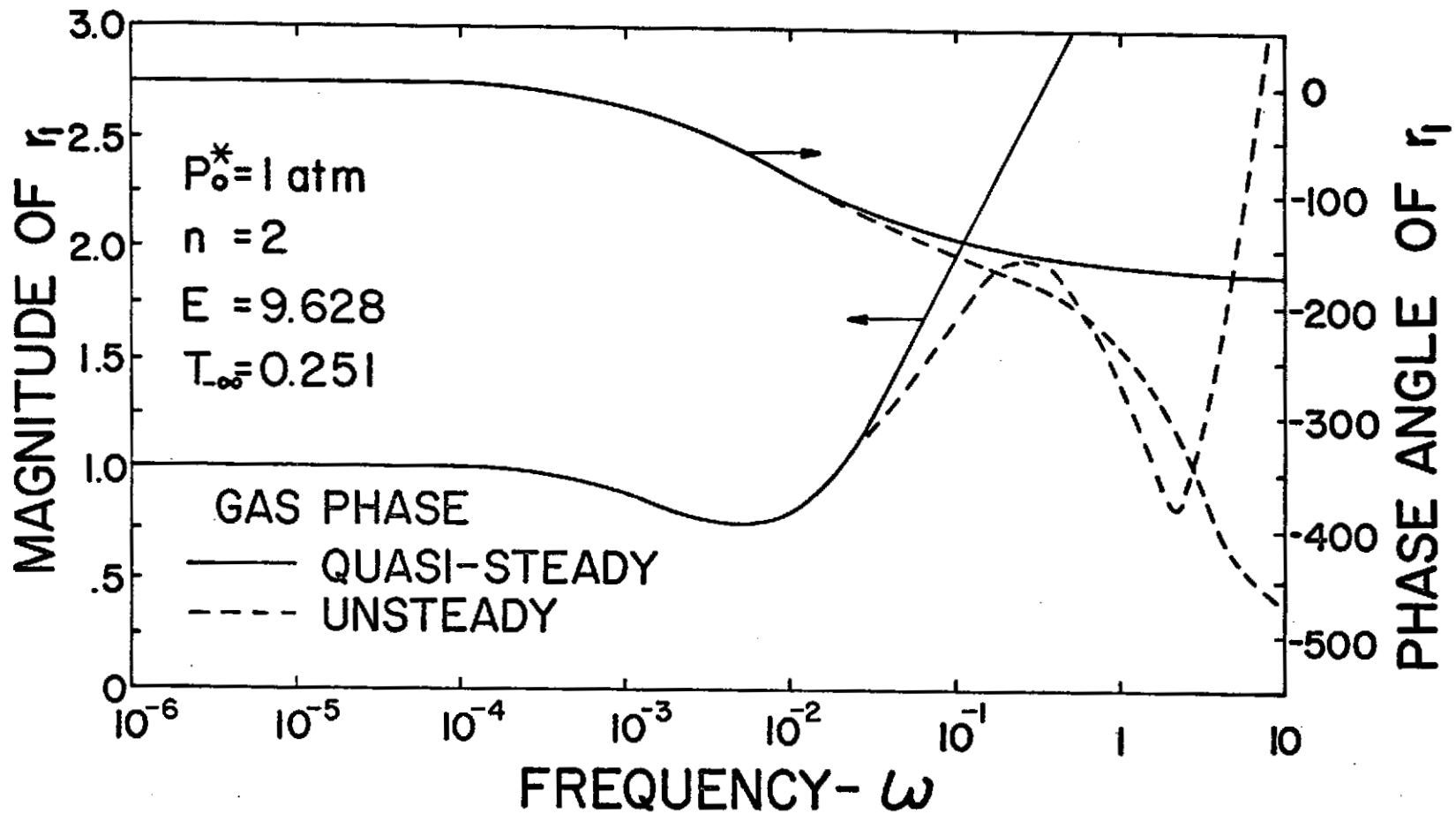


Figure 34 Burning Rate Oscillation Amplitude and Phase Angle as a Function of Frequency for $P_o^* = 1 \text{ atm}$, $n = 2$, $E = 9.628$, $T_{-\infty}^* = 350^\circ\text{K}$

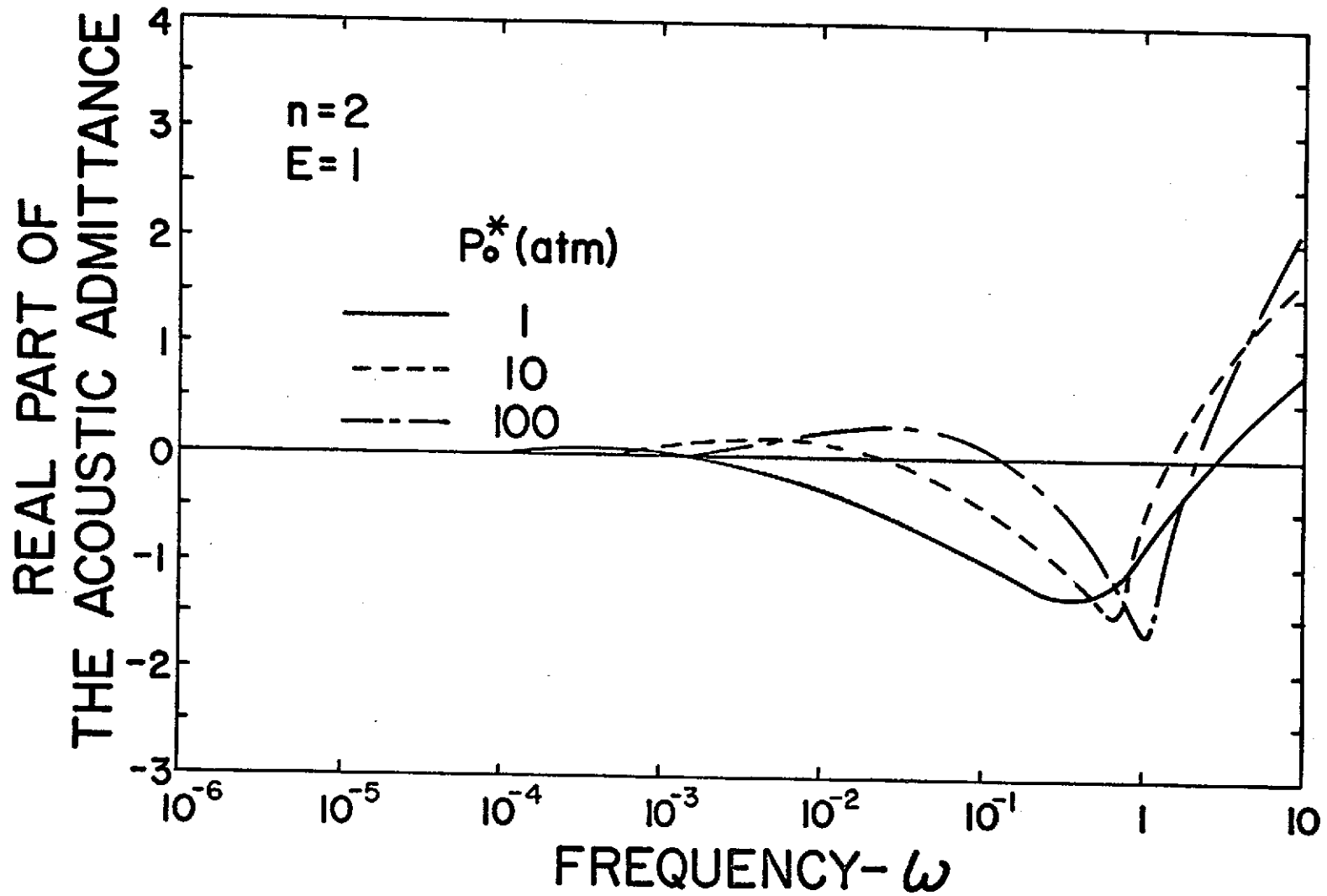


Figure 35 Real Part of the Acoustic Admittance as a Function of Frequency for $n = 2$, $E = 1$ and Various Pressures

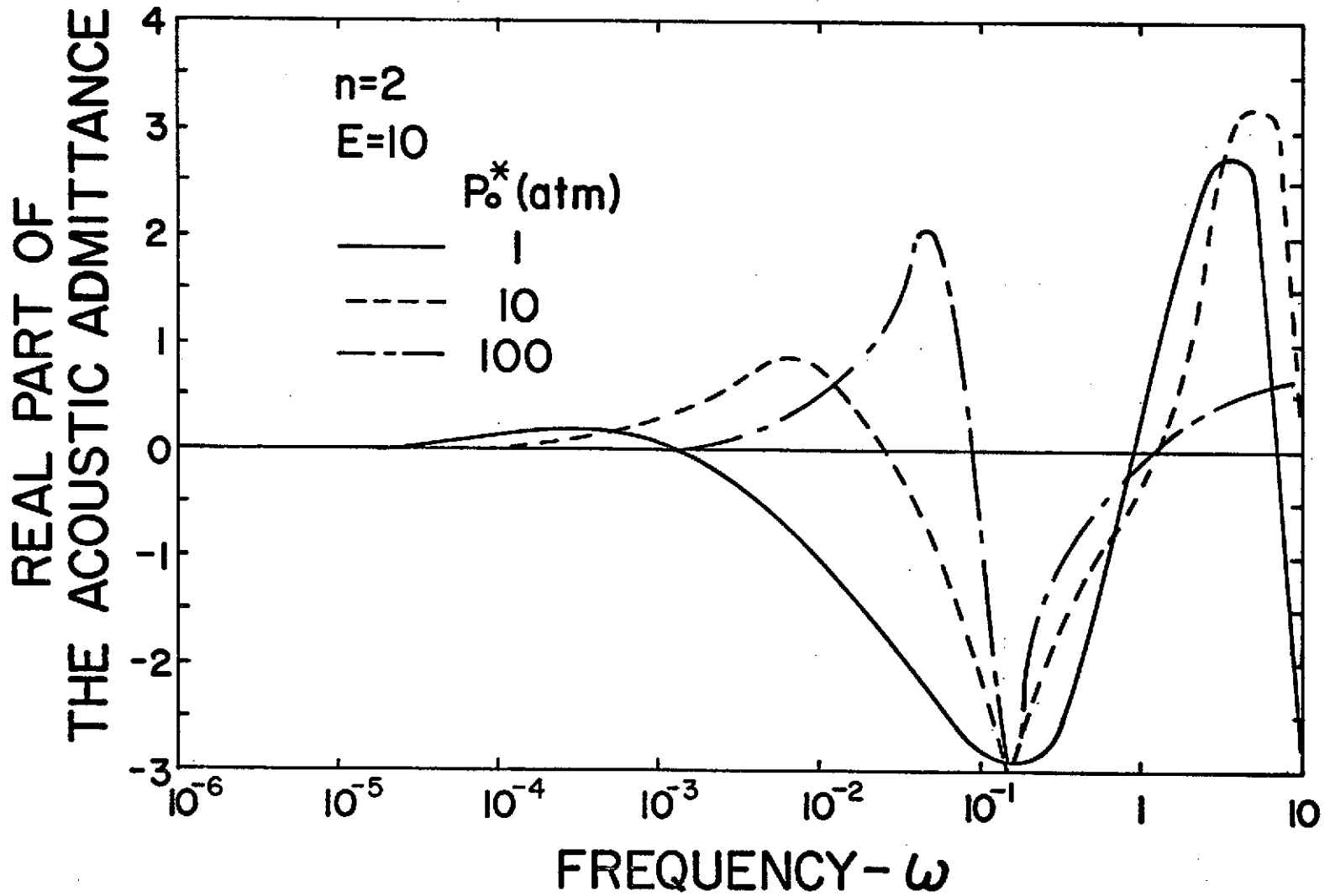


Figure 36 Real Part of the Acoustic Admittance as a Function of Frequency for $n = 2$, $E = 10$ and Various Pressures

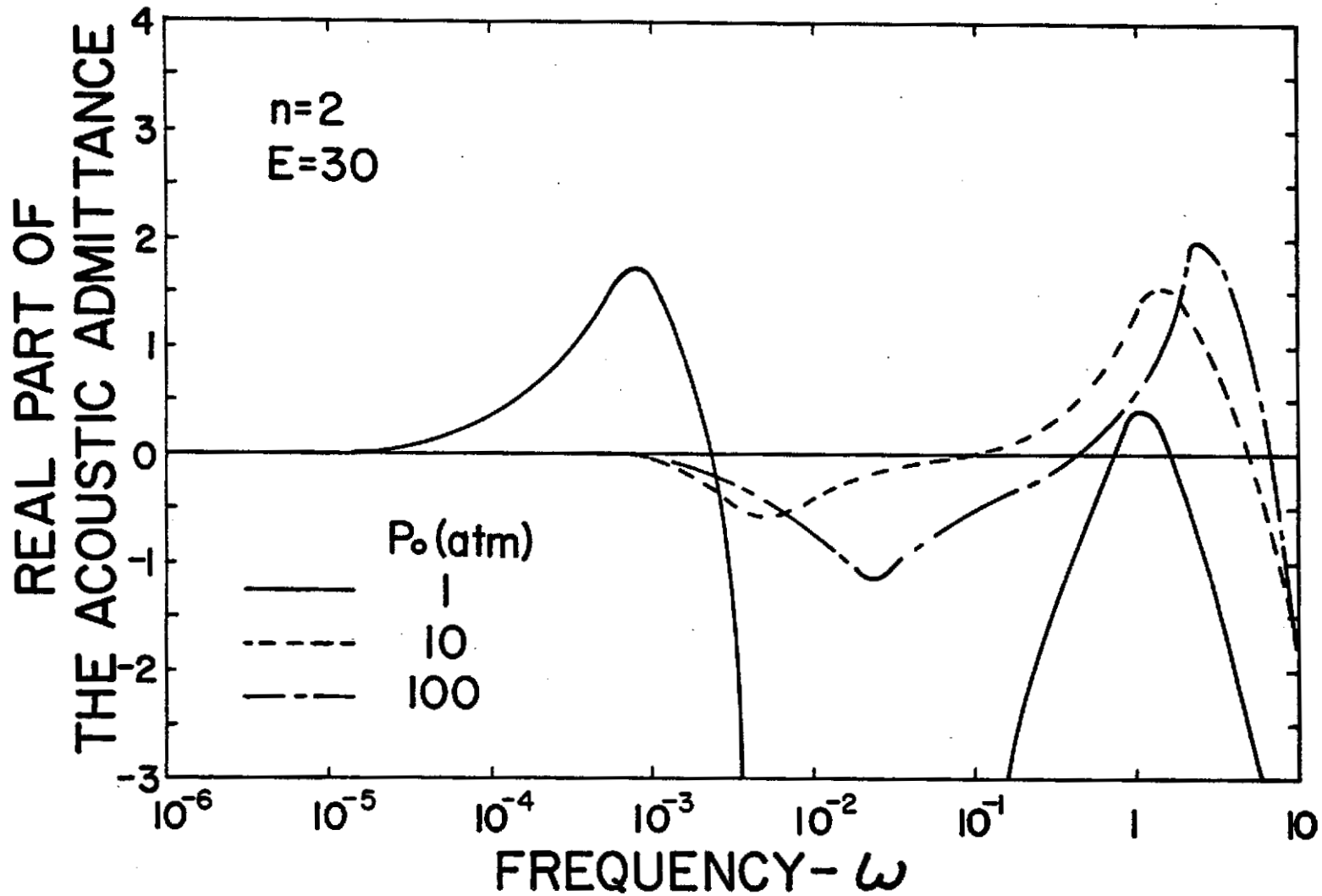


Figure 37 Real Part of the Acoustic Admittance as a Function of Frequency for $n = 2$, $E = 30$ and Various Pressures

As shown in Figure 35, the real part of the acoustic admittance is zero for low frequencies where the combustion process is quasi-steady. In this limit the mass burning rate for a second order reaction is linearly proportional to pressure. However, from the perfect gas relation, the gas phase density is also linearly proportional to pressure; therefore, the gas phase velocity is independent of pressure. Thus, the gas phase velocity fluctuation due to a pressure fluctuation is zero at low frequencies.

As the frequency increases, liquid phase thermal wave effects become important causing the real part of the acoustic admittance to deviate from its quasi-steady value. The curves shown in Figure 35 reach a maximum near the characteristic frequency of the liquid phase thermal wave then become negative as gas phase transient effects become important. The curves reach a minimum then become positive again for very high frequencies.

Reference [16] indicates that for instability to occur the real part of the acoustic admittance should be on the order of one. As shown in Figure 35 the real part of the acoustic admittance for $E = 1$ only becomes of the order one at very large frequencies for the pressures shown. Liquid phase thermal wave effects are not of sufficient magnitude to cause instability for $E = 1$.

Figure 36 shows a similar plot for $E = 10$. This figure indicates that as pressure increases a frequency range is reached where the real part of the acoustic admittance is one or greater. Also, with increasing pressure, the peaks in the curves due to liquid thermal wave effects move to higher frequencies.

Somewhat different behavior is evident from Figure 37. For $E = 30$, the real part of the acoustic admittance is of the order one or greater only for low pressures except for very high frequencies.

CHAPTER V

SUMMARY AND CONCLUSIONS

5.1 Summary

The present study was concerned with the strand combustion of hydrazine under both steady and oscillatory conditions. The specific objectives of the study were as follows:

1. Investigate the steady strand combustion characteristics of hydrazine experimentally to determine steady strand burning rates as functions of pressure, liquid concentration and tube diameter. Also investigate the liquid temperature distributions and liquid surface temperatures as a function of pressure during steady strand combustion.
2. Study the oscillatory combustion characteristics of hydrazine by experimentally determining the oscillatory burning rate as a function of mean pressure, and the frequency and amplitude of the imposed pressure oscillations.
3. Develop a theoretical model of the strand combustion system capable of predicting the observed experimental results under both steady and oscillatory conditions.

For the experimental program a steady strand combustor was used in the initial phases of the investigation. With this apparatus steady strand burning rates were measured over the pressure range of 0.32-42 atm and liquid temperatures were

obtained in the range of 1.0-20.5 atm. Liquid concentrations of from 92.6-99.4% N_2H_4 were studied in tube sizes of 4, 8 and 12 mm.

A modified version of the steady strand apparatus was constructed to provide a means of studying the oscillatory combustion of hydrazine. With this apparatus oscillatory burning rates were obtained in the mean pressure range of 1-10 atm with frequencies varying from 0.4-5.2 Hz and pressure amplitudes up to 35 % of the mean pressure.

A theoretical model of the system was developed. The major assumptions in the theoretical analysis were that the system was one dimensional, a one-step, irreversible reaction occurred in the gas phase and conventional low pressure phase equilibrium was adequate to describe the state of the liquid surface. While the liquid phase was assumed to have constant physical properties, a variable property gas phase solution was obtained through the use of a modified Howarth transformation. The resulting equations describing the combustion system were solved through the use of a perturbation analysis with the amplitude of the imposed pressure oscillations taken as the small perturbation parameter.

The zero order model described the steady strand combustion system. The predictions of this model were compared to the experimental steady strand results. The excellent agreement between theory and experiment justified the extension of this theory to include unsteady effects.

5.2 Conclusions

5.2.1 Steady Strand Combustion

The major conclusions of the steady strand portion of the study are as follows:

1. Addition of water to the liquid hydrazine reduces the burning rate. However, liquid purities of 98.6 and 99.4% yielded essentially the same burning rates.
2. The effect of tube diameter scales as the reciprocal of the tube diameter. By plotting steady strand burning rates as a function of the reciprocal of the tube diameter, linear plots were obtained allowing the determination of the fundamental strand burning rate.
3. The experimental results indicated that the strand burning rate has a pressure dependence of $1/2$ for subatmospheric pressures and a pressure dependence of 1 for pressures above atmospheric. This finding is in agreement with the results of previous investigations. [13-15] The theoretical model was matched to these results by assuming a first order decomposition reaction for subatmospheric pressures and a second order decomposition reaction for pressures greater than atmospheric.
4. The gas phase activation energy has very little effect upon the theoretically predicted steady strand burning rate for both a first and second order reaction.

5. The theoretical model, assuming constant liquid phase properties, agrees well with the experimental liquid temperature distributions.
6. The theoretical model is also in excellent agreement with the experimentally determined liquid surface temperatures justifying the low pressure phase equilibrium assumption.

5.2.2 Oscillatory Strand Combustion

The major conclusions of the oscillatory strand portion of this investigation are as follows:

1. As opposed to steady combustion, for oscillatory combustion the gas phase activation energy has a significant influence upon the predicted theoretical oscillatory burning rate. The theoretical results concerning both the amplitude and the phase angle of the liquid surface oscillations are in good agreement with the experimental results when a second order reaction with an activation energy of about 40 kcal ($E = 15$) is assumed.
2. Based upon the theoretical acoustic admittance, the model predicts that for activation energies in the range of 25-40 kcal ($E = 10-15$), the hydrazine combustion system exhibits a range of frequencies where instability could occur. As pressure increases, the instability range moves to higher frequencies and the system becomes less stable.

BIBLIOGRAPHY

1. Crocco, L. and Cheng, S. I., Theory of Combustion Instability in Liquid Propellant Rocket Motors, AGARDograph No. 8, Butterworths Scientific Publications, London, 1956.
2. Crocco, L., "Theoretical Studies on Liquid Propellant Rocket Instability," Tenth Symposium (International) on Combustion, The Combustion Institute, Pittsburgh, 1965, pp. 1101-1128.
3. Crocco, L., "Research on Combustion Instability in Liquid Propellant Rockets," Twelfth Symposium (International) on Combustion, The Combustion Institute, Pittsburgh, 1969, pp. 85-99.
4. Priem, R. J. and Heidmann, M. F., "Propellant Vaporization as a Design Criterion for Rocket-Engine Combustion Chambers," NASA TR R-67, 1960.
5. Priem, R. J. and Guentert, D., "Combustion Instability Limits Determined by a Nonlinear Theory and a One-Dimensional Model," NASA TN D-1409, 1962.
6. Priem, R. J., "Influence of the Combustion Process on Stability," NASA TN D-2957, 1965.
7. Allison, C. B. and Faeth, G. M., "Decomposition and Hybrid Combustion of Hydrazine, MMH and UDMH as Droplets in a Combustion Gas Environment," Combustion and Flame, Vol. 19, No. 2, October 1972, pp. 213-226.
8. Dykema, O. W. and Greene, S. A., "An Experimental Study of RP-1, UDMH, and N_2H_4 Single Droplet Burning in Air and in Oxygen," Progress in Astronautics and Rocketry, Vol. 2, Academic Press, New York, 1960, pp. 299-324.
9. Rosser, W. A., Jr., "The Decomposition Burning of Monopropellant Drops: Hydrazine, Nitromethane, and Ethyl Nitrate," Progress Report No. 20-305, Jet Propulsion Laboratory, Pasadena, California, January 1957.
10. Lawver, B. R., Kosvic, T. C. and Breen, B. P., "Effects of Additives on the Combustion of Hydrazine," AFRPL-TR-67-288, January 1968, Dynamic Science Corporation, Monrovia, California.
11. Kosvic, T. C. and Breen, B. P., "Study of Additive Effects on Hydrazine Combustion and Combustion Instability at High Pressure," AFRPL-TR-69-12, November 1969, Dynamic Science Corporation, Monrovia, California.
12. Adams, G. K. and Stocks, G. W., "The Combustion of Hydrazine," Fourth Symposium (International) on Combustion, Williams and Wilkins, Baltimore, 1953, pp. 239-248.

13. Gray, P. and Kay, J. C., "Stability of the Decomposition Flame of Liquid Hydrazine," Research, London, Vol. 8, 1955, pp. 53-55.
14. Gray, P., Lee, J. C., Leach, H. A. and Taylor, D. C., "The Propagation and Stability of the Decomposition Flame of Hydrazine," Sixth Symposium (International) on Combustion, Reinhold, New York, 1956, pp. 255-263.
15. Antoine, A. C., "The Mechanism of Burning of Liquid Hydrazine," Eighth Symposium (International) on Combustion, Williams and Wilkens, Baltimore, 1962, pp. 1057-1059.
16. Harrje, D. T. (Ed.), Liquid Propellant Rocket Combustion Instability, NASA SP-194, 1972.
17. Williams, F. A., "Response of a Burning Fuel Plate to Sound Vibrations," AIAA Journal, Vol. 3, No. 11, November 1965, pp. 2112-2124.
18. Strahle, W. C., "Periodic Solutions to a Convective Droplet Burning Problem: The Stagnation Point," Tenth Symposium (International) on Combustion, The Combustion Institute, Pittsburgh, 1965, pp. 1315-1325.
19. Strahle, W. C., "Unsteady Reacting Boundary Layer on a Vaporizing Flat Plate," AIAA Journal, Vol. 3, No. 6, June 1965, pp. 1195-1198.
20. Strahle, W. C., "New Considerations on Causes for Combustion Instability in Liquid Propellant Rockets," Combustion Science and Technology, Vol. 2, 1970, pp. 29-40.
21. Heidmann, M. F. and Wieber, P. R., "Analysis of Frequency Response Characteristics of Propellant Vaporization," AIAA Paper No. 66-604, 1966.
22. T'ien, J. S. and Sirignano, W. A., "Unsteady Thermal Response of the Condensed-Phase Fuel Adjacent to a Reacting Gaseous Boundary Layer," Thirteenth Symposium (International) on Combustion, The Combustion Institute, Pittsburgh, 1971, pp. 529-539.
23. Fristrom, R. M. and Westenberg, A. A., Flame Structure, McGraw-Hill Book Company, New York, 1965, pp. 170-174.
24. Steinberger, R., "Mechanism of Burning of Nitrate Esters," Fifth Symposium (International) on Combustion, Reinhold, New York, 1955, pp. 205-211.
25. Hildenbrand, D. L., Whittaker, A. G. and Euston, C. B., "Burning Rate Studies I. Measurement of the Temperature Distribution in Burning Liquid Strands," Journal of Physical Chemistry, Vol. 58, 1954, pp. 1130-1133.

26. Whittaker, A. G., Donovan, T. M. and Williams, H., "Burning Rate Studies. Part 7. Onset of Turbulent Combustion of Liquids Contained in Small Tubes," Journal of Physical Chemistry, Vol. 62, 1958, pp. 908-912.
27. Chervinsky, A. P., Sirignano, W. A., Harrje, D. T. and Varma, A. K., "Axisymmetric Jet Diffusion Flame in an External Oscillating Stream," Sixth ICRPG Combustion Conference, CPIA Publication No. 192, December 1969, pp. 171-180.
28. Hart, R. W. and McClure, F. T., "Combustion Instability: Acoustic Interaction with a Burning Propellant Surface," Journal of Chemical Physics, Vol. 30, No. 6, June 1959, pp. 1501-1514.
29. Krier, H., T'ien, J. S., Sirignano, W. A. and Summerfield, M., "Nonsteady Burning Phenomena of Solid Propellants: Theory and Experiments," AIAA Journal, Vol. 6, No. 2, February 1968, pp. 278-285.
30. Friedly, J. C. and Petersen, E. E., "Influence of Combustion Parameters on Instability in Solid Propellant Motors: Part I. Development of Model and Linear Analysis," AIAA Journal, Vol. 4, No. 9, September 1966, pp. 1604-1610.
31. Denison, M. R. and Baum, E., "A Simplified Model of Unstable Burning in Solid Propellants," ARS Journal, August 1961, pp. 1112-1122.
32. T'ien, J. S., "Oscillatory Burning of Solid Propellants Including Gas Phase Time Lag," Combustion Science and Technology, Vol. 5, 1972.
33. Zel'dovich, Y. B., "Chain Reactions in Hot Flames - An Approximate Theory for Flame Velocity," International Chemical Engineering, Vol. 2, 1962, pp. 227-235.
34. Culick, F. E. C., "A Review of Calculations for Unsteady Burning of a Solid Propellant," AIAA Journal, Vol. 6, No. 12, December 1968, pp. 2241-2255.
35. Williams, F. A., "Response of a Burning Solid to Small Amplitude Pressure Oscillations," Journal of Applied Physics, Vol. 33, November 1962, pp. 3153-3166.
36. Culick, F. E. C., "Calculation of the Admittance Function for a Burning Surface," Astronautica Acta, Vol. 13, 1967, pp. 221-237.
37. Williams, F. A., Combustion Theory, Addison-Wesley, Reading, Massachusetts, 1965, Chapter 1.
38. Faeth, G. M., "High-Pressure Liquid-Monopropellant Strand Combustion," Combustion and Flame, Vol. 18, 1972, pp. 103-113.

39. Audrieth, L. F. and Ogg, B. A., The Chemistry of Hydrazine, John Wiley and Sons, New York, 1951.
40. Hottel, H. C. and Sarofim, A. F., Radiation Transfer, McGraw-Hill, New York, 1967, p. 237.
41. Davidson, N., Statistical Mechanics, McGraw-Hill, New York, 1962, p. 160.
42. Harshman, R. C., "The Physical and Chemical Properties of the Alkyl Hydrazines," Jet Propulsion, April 1957, pp. 398-400.
43. Lewis, G. N. and Randall, M., Thermodynamics, 2nd Ed., Revised by Pitzer, K. S. and Brewer, L., McGraw-Hill, New York, 1961.
44. Svehla, R. A., "Estimated Viscosities and Thermal Conductivities of Gases at High Temperatures," NASA Technical Report R-132, 1962.
45. Scott, D. W., Oliver, G. D., Gross, M. E., Hubbard, W. N. and Huffman, H. M., "Hydrazine: Heat Capacity, Heats of Fusion and Vaporization, Vapor Pressure, Entropy and Thermodynamic Functions," Journal of the American Chemical Society, Vol. 71, July 1949, pp. 2293-2297.
46. Jones, W. H. (Chairman), JANAF Thermochemical Tables, Dow Chemical Company, Midland, Michigan.
47. Hieber, W. and Woerner, A., Z. Elektrochem., Vol. 40, 1934, p. 252.
48. Chang, E. T. and Gokcen, N. A., "Thermodynamic Properties of Hydrazine, UDMH and Their Mixtures," Journal of Physical Chemistry, Vol. 72, 1968, p. 2557.
49. McHale, E. T., Knox, B. E. and Palmer, H. B., "Determination of the Decomposition Kinetics of Hydrazine Using a Single-Pulse Shock Tube," Tenth Symposium (International) on Combustion, The Combustion Institute, 1965, pp. 341-351.

APPENDIX A

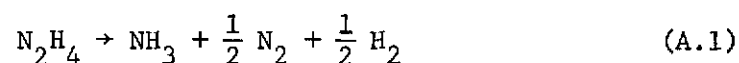
CHECK OF THE ASSUMPTIONS OF THE ANALYSIS

A.1 Estimation of Radiation Effects During Strand Burning

An estimation of the effect of radiation can be made by comparing the energy reaching the liquid surface due to radiation to the total amount of energy reaching the liquid surface. In the steady state the total amount of energy reaching the liquid surface is equal to the product of the liquid density, the fuel burning rate and the heat required to raise the temperature of the liquid to the surface temperature and vaporize the fuel at the surface temperature.

To get a rough estimation of the amount of heat reaching the liquid surface due to radiation, the combustion system was taken to be an infinite cylinder of the decomposition flame products at the adiabatic flame temperature of the fuel. The walls of the cylinder were assumed to be transparent. The shape factor and mean beam length were taken from Hottel and Sarofim [40].

The fuel decomposition products were taken to be those suggested by Audrieth and Ogg [39]; namely



The only emitter is the system in NH_3 with a mole fraction of 0.5. Using the corresponding partial pressure and the mean beam length, the emissivity was taken from Hottel and Sarofim [40]. The heat due to radiation reaching the liquid surface was then the product of the shape factor, the gas emissivity, the Stefan-Boltzmann constant and the adiabatic flame temperature raised to the fourth power.

By comparing the radiation heat transfer to the total heat transfer in the above manner, it was found that the radiation effect was always less than 1% of the total. This result is

not surprising since hydrazine has a low adiabatic flame temperature.

A.2 Phase Equilibrium Assumption

The equilibrium assumption at the liquid surface can be justified if the rate at which molecules from the gas phase strike the liquid surface is much greater than the fuel burning rate. The number of molecules striking the liquid surface per unit time was estimated using kinetic theory.

The rate at which molecules from the gas phase strike the liquid surface was estimated using the following equation derived from kinetic theory [41]

$$\Phi = P \sqrt{\frac{M}{2\pi RT}} \quad (\text{A.2})$$

where Φ is the rate at which molecules strike the surface per unit area, P is the pressure, M is the molecular weight and T is the surface temperature.

Using the experimentally determined surface temperature as a function of pressure in Equation (A.2), Φ was compared to the experimental burning rate at various pressures. It was found that Φ was always between two and three orders of magnitude greater than the burning rate at any given pressure. Thus the assumption of phase equilibrium at the surface is justified.

A.3 Constant Total Pressure Assumption

The constant total pressure assumption is really two assumptions, namely that the Mach number of the flow is much less than unity and that the wavelength of any periodic pressure disturbance

is long compared to the distance from the outer edge of the reaction zone to the liquid surface. The Mach number was estimated to be in the range of 0.001-0.002 and is much less than unity. This section of Appendix A, therefore, deals with estimating the frequency where the long wavelength assumption breaks down.

To estimate this frequency assume that the temperature profile is linear between the surface temperature and the flame temperature. Then the total heat transfer to the liquid surface can be expressed as

$$q_S^* = \left(\lambda^* \frac{dT^*}{dx^*} \right)_S = \lambda^* \frac{T_f^* - T_S^*}{x_f^* - x_S^*} = \rho_\ell^* v_\ell^* L^* \quad (\text{A.3})$$

All quantities in Equation (A.3) are known either as thermodynamic properties or as experimentally measured parameters except the distance from the outer edge of the reaction zone to the surface, $(x_f^* - x_S^*)$.

The parameter, $(x_f^* - x_S^*)$, was computed from Equation (A.3) as a function of pressure. It was found that $(x_f^* - x_S^*)$ is greater than 0.10 of the wavelength of any periodic pressure disturbance for frequencies above about 50,000 Hz.

APPENDIX B

FORM OF THE ZERO ORDER ENERGY EQUATION FOR LARGE η

The only equation which must be integrated for the zero order problem is Equation (46) which is rewritten here.

$$\frac{d^2 T_o}{d\eta^2} - \frac{dT_o}{d\eta} + Aq^{1-n} T_o^{1+\delta-n} (1-T_o)^n \exp\left[\frac{-E}{T_o}\right] = 0 \quad (\text{B.1})$$

To find the form of Equation (B.1) for large η let

$$T_o = 1 - \xi T_o^{(1)} \quad (\text{B.2})$$

where ξ is a small parameter. Combining Equation (B.1) and Equation (B.2) yields

$$\xi \frac{d^2 T_o^{(1)}}{d\eta^2} - \xi \frac{dT_o^{(1)}}{d\eta} - \xi^n Aq^{1-n} \exp(-E) T_o^{(1)n} = 0 \quad (\text{B.3})$$

The solution of Equation (B.3) depends on the order of the reaction, n . For $n = 1$, the solution of Equation (B.3) is straightforward.

$$T_o^{(1)} = C_1 \exp\left(\frac{1 - \sqrt{1+4A\exp(-E)}}{2} \eta\right) \quad (\text{B.4})$$

The growing exponential part of the solution to Equation (B.3) is rejected since $T_o^{(1)}$ must approach zero for large η from Equation (47). C_1 in Equation (B.4) is an unknown constant.

Combining Equation (B.2) and Equation (B.4) results in

$$T_o = 1 - C \exp\left(\frac{1 - \sqrt{1+4A\exp(-E)}}{2} \eta\right) \quad (\text{B.5})$$

For $n = 1$, where

$$C = \xi C_1 \quad (\text{B.6})$$

and is an unknown constant.

For $n = 2$, Equation (B.3) can be solved by stretching the η coordinate such that

$$\eta = \xi^a \mu \quad (\text{B.7})$$

where a is a constant determined by proper matching.

Substituting Equation (B.7) into Equation (B.3) yields

$$\xi^{1-2a} \frac{d^2 T_o^{(1)}}{d\mu^2} - \xi^{1-a} \frac{dT_o^{(1)}}{d\mu} - \xi^2 A \exp(-E) (T_o^{(1)})^2 / q = 0 \quad (\text{B.8})$$

A proper match of the terms in Equation (B.8) is only obtained by balancing convection and reaction; the diffusion term is of higher order. Then $a = -1$ and the resulting equation is

$$\frac{dT_o^{(1)}}{d\mu} = - \frac{A}{q} \exp(-E) (T_o^{(1)})^2 \quad (\text{B.9})$$

solving Equation (B.9)

$$T_o^{(1)} = \left(\frac{A}{q} \exp(-E) \mu - C_1 \right)^{-1} \quad (\text{B.10})$$

where C_1 is an unknown constant.

From Equation (B.2) and Equation (B.7)

$$T_o = 1 - \xi / \left(\xi \frac{A}{q} \exp(-E) \eta - C_1 \right) \quad (\text{B.11})$$

or

$$T_o = 1 - \left(\frac{A}{q} \exp(-E) \eta - C \right)^{-1} \quad (\text{B.12})$$

for $n = 2$, where

$$C = C_1 / \xi \quad (\text{B.13})$$

and is an unknown constant.

APPENDIX C

SOLUTION METHOD FOR THE FIRST ORDER PROBLEM

The first order problem is given by Equations (60-66) and Equation (68). The problem can be simplified somewhat by noting that the solution of Equation (61) can be represented by

$$\theta_1 = K_1 \exp\left[\frac{1 - \sqrt{1+4i\omega}}{2}\eta\right] + \theta_{1P}(\eta) \quad (C.1)$$

where K_1 is the unknown constant in the homogeneous solution and θ_{1P} represents the particular solution. In arriving at Equation (C.1) the growing exponential part of the homogeneous solution was rejected since, physically, neither the temperature nor the fuel mass fraction fluctuations can grow exponentially with increasing η . In general θ_{1P} must be determined numerically. However, for large η , using Equation (47) in Equation (61),

$$\theta_{1P}(\eta) \rightarrow \frac{\gamma-1}{\gamma} \quad (C.2)$$

Equation (C.2) also follows from Equation (68).

Using Equation (C.1) in Equation (62) the first order problem reduces to the following equation

$$\frac{d^2 T_1}{d\eta^2} - \frac{dT_1}{d\eta} + pT_1 = r_1 b + K_1 c + d \quad (C.3)$$

where

$$p = qw_o \left[\left(\frac{1+\delta-n}{T_o} \right) - \frac{n}{1-T_o} + \frac{E}{T_o^2} \right] - i\omega \quad (C.4)$$

$$b = \frac{dT_o}{d\eta} \quad (C.5)$$

$$c = - \frac{nw_o}{1-T_o} \exp\left(\frac{1 - \sqrt{1+4i\omega}}{2}\eta\right) \quad (C.6)$$

$$d = - \frac{d^2 T_o}{d\eta^2} - qw_o(n-1) - \frac{\gamma-1}{\gamma} i\omega T_o - \frac{nw_o}{1-T_o} \theta_{1P} \quad (C.7)$$

The boundary conditions can also be reduced to the following:

$$\left(\frac{dT_1}{d\eta} \right)_{\eta=0+} = r_1 f + g T_1(0) + h \quad (C.8)$$

$$K_1 + \theta_{1P}(0) = j T_1(0) + k \quad (C.9)$$

$$K_1 \ell + \left(\frac{d\theta_{1P}}{d\eta} \right)_{\eta=0+} = r_1 m + K_1 + \theta_{1P}(0) - T_1(0) + \left(\frac{dT_1}{d\eta} \right)_{\eta=0+} - h \quad (C.10)$$

where

$$f = \frac{\rho \ell \lambda \ell}{2\delta_1^2 i\omega} [T_o(0) - T_{-\infty}] [\sqrt{1+4i\omega\delta_1} - 1] + T_o(0)(1-\beta) + L \quad (C.11)$$

$$g = 1-\beta + \frac{\rho \ell \lambda \ell}{2\delta_1} (1 + \sqrt{1+4i\omega\delta_1}) \quad (C.12)$$

$$h = - \left(\frac{dT_o}{d\eta} \right)_{\eta=0+} \quad (C.13)$$

$$j = \frac{aqL_1}{T_o^2(0)} \exp \left[\frac{-L_1}{T_o(0)} \right] + 1 \quad (C.14)$$

$$k = T_o(0) - 1 \quad (C.15)$$

$$\ell = (1 - \sqrt{1+4i\omega})/2 \quad (C.16)$$

$$m = 1 - T_o(0) - q \quad (C.17)$$

The outer boundary condition remains as specified by Equation (67) or Equation (68).

The equations representing the quasi-steady gas phase problem can be obtained by setting $\omega = 0$ in Equations (61 and 62). These equations can be summarized as follows:

$$\theta_1 = K_1 \quad (C.18)$$

since

$$\theta_{1P} = 0$$

and

$$\frac{d^2 T_1}{d\eta^2} - \frac{dT_1}{d\eta} + p_s T_1 = r_1 b + K_1 c_s + d_s \quad (C.19)$$

where

$$p_s = qw_o \left[\left(\frac{1+\delta-n}{T_o} \right) - \frac{n}{1-T_o} + \frac{E}{T_o^2} \right] \quad (C.20)$$

$$c_s = - \frac{nqw_o}{1-T_o} \quad (C.21)$$

$$d_s = - \frac{d^2 T_o}{d\eta^2} - qw_o (n-1) \quad (C.22)$$

The boundary conditions remain the same except

$$\ell_s = \theta_{1P}(0) = \left(\frac{d\theta_{1P}}{d\eta} \right)_{\eta=0+} = 0 \quad (C.23)$$

Since the equations for the complete unsteady and quasi-steady problems are similar except for the values of the coefficients, the general solution method as discussed in the following is applicable to either case.

The first order problem reduces to the solution of one linear, second order, ordinary differential equation, Equation (C.3), with two unknown constants r_1 and K_1 . The four boundary conditions permit unique values of the unknown constants to be found as well as the desired solution out of the family of solutions of the second order, ordinary differential equation.

Exploiting the linearity of Equation (C.3), let

$$T_1 = \hat{T}_1 + r_1 T_1^* + K_1 \bar{T}_1 \quad (C.24)$$

Then Equation (C.3) can be separated into three equations

$$\frac{d^2 \hat{T}_1}{d\eta^2} - \frac{d\hat{T}_1}{d\eta} + pT_1 = d \quad (C.25)$$

$$\frac{d^2 T_1^*}{d\eta^2} - \frac{dT_1^*}{d\eta} + pT_1^* = b \quad (C.26)$$

$$\frac{d^2 \bar{T}_1}{d\eta^2} - \frac{d\bar{T}_1}{d\eta} + p\bar{T}_1 = c \quad (C.27)$$

The boundary conditions, Equations (C.8-C.10 and 67) can also be separated as follows:

$$\left(\frac{d\hat{T}_1}{d\eta} \right)_{\eta=0+} = g\hat{T}_1(0) + h \quad (C.28)$$

$$\left(\frac{dT_1^*}{d\eta} \right)_{\eta=0+} = gT_1^*(0) + f \quad (C.29)$$

$$\left(\frac{d\bar{T}_1}{d\eta} \right)_{\eta=0+} = g\bar{T}_1(0) \quad (C.30)$$

$$\theta_{1P}(0) = j\hat{T}_1(0) + k \quad (C.31)$$

$$0 = jT_1^*(0) \quad (C.32)$$

$$1 = j\bar{T}_1(0) \quad (C.33)$$

$$\left(\frac{d\theta_{1P}}{d\eta} \right)_{\eta=0+} = \theta_{1P}(0) - \hat{T}_1(0) + \left(\frac{d\hat{T}_1}{d\eta} \right)_{\eta=0+} - h \quad (C.34)$$

$$0 = m - T_1^*(0) + \left(\frac{dT_1^*}{d\eta} \right)_{\eta=0+} \quad (C.35)$$

$$l = 1 - \bar{T}_1(0) + \left(\frac{d\bar{T}_1}{d\eta} \right)_{\eta=0+} \quad (C.36)$$

and as $\eta \rightarrow \infty$

$$\hat{T}_1 \rightarrow \hat{C} \quad (C.37)$$

$$T_1^* \rightarrow C^* \quad (C.38)$$

$$\bar{T}_1 \rightarrow \bar{C} \quad (C.39)$$

where \hat{C} , C^* and \bar{C} are constants.

The three differential equations, Equations (C.25-C.27), each have a particular and a homogeneous solution. However, since the homogeneous equations are identical, the homogeneous solutions are identical. Breaking the equations into homogeneous and particular parts, let

$$\hat{T}_1 = \hat{T}_{1P} + \hat{K}T_{1H} \quad (C.40)$$

$$T_1^* = T_{1P}^* + K^*T_{1H} \quad (C.41)$$

$$\bar{T}_1 = \bar{T}_{1P} + \bar{K}T_{1H} \quad (C.42)$$

where \hat{K} , K^* and \bar{K} are unspecified constants. The differential equations, Equations (C.25-C-27) become

$$\frac{d^2 T_{1H}}{d\eta^2} - \frac{dT_{1H}}{d\eta} + pT_{1H} = 0 \quad (C.43)$$

$$\frac{d^2 \hat{T}_{1P}}{d\eta^2} - \frac{d\hat{T}_{1P}}{d\eta} + p\hat{T}_{1P} = d \quad (C.44)$$

$$\frac{d^2 T_{1P}^*}{d\eta^2} - \frac{dT_{1P}^*}{d\eta} + p T_{1P}^* = b \quad (C.45)$$

$$\frac{d^2 \bar{T}_{1P}}{d\eta^2} - \frac{d\bar{T}_{1P}}{d\eta} + p \bar{T}_{1P} = c \quad (C.46)$$

The constants \hat{K} , K^* and \bar{K} are chosen such that one of the boundary conditions at $\eta=0$, Equations (C.8-C.10) is satisfied. The remaining two boundary conditions at $\eta = 0$ are used to determine r_1 and K_1 .

At this point one must choose which boundary condition to use to determine \hat{K} , K^* and \bar{K} . The solution of the system of equations, Equations (C.43-46) should be unique and thus independent of the choice of boundary condition. It was verified that the choice has no effect on the final computed results by using all three boundary conditions, Equations (C.8-C.10), in turn and computing, numerically, the solution. Equation (C.9) is chosen as the boundary condition to be used here for illustration purposes.

Separating Equations (C.31-C.33) using Equations (C.40-C.42) yields

$$\hat{K} = \frac{\theta_{1P}(0) - k - j \hat{T}_{1P}(0)}{j T_{1H}(0)} \quad (C.47)$$

$$K^* = - T_{1P}^*(0) / T_{1H}(0) \quad (C.48)$$

$$\bar{K} = \frac{1 - j \bar{T}_{1P}(0)}{j T_{1H}(0)} \quad (C.49)$$

Summarizing thus far, the solution method consists of solving Equations (C.43-C.46) numerically for $T_{1H}(\eta)$, $\hat{T}_{1P}(\eta)$, $T_{1P}^*(\eta)$

and $\bar{T}_{1P}(\eta)$. Equations (C.47-C.49) are then used to determine \hat{K} , K^* and \bar{K} . Next, Equations (C.40-C.42) are used to find $\hat{T}_1(\eta)$, $T_1^*(\eta)$, and $\bar{T}_1(\eta)$. Finally, Equations (C.28-C.30) and Equations (C.34-C.36) are recombined to produce two equations involving two unknown constants, r_1 and K_1 . These equations are:

$$r_1 \left[-m - \left(\frac{dT_1^*}{d\eta} \right)_{\eta=0+} \right] + K_1 \left[\ell - 1 + \bar{T}_1(0) - \left(\frac{d\bar{T}_1}{d\eta} \right)_{\eta=0+} \right] = \theta_{1P}(0) - \hat{T}_1(0) + \left(\frac{d\hat{T}_1}{d\eta} \right)_{\eta=0+} - h - \left(\frac{d\theta_{1P}}{d\eta} \right)_{\eta=0+} \quad (C.50)$$

$$r_1 \left[\left(\frac{dT_1^*}{d\eta} \right)_{\eta=0+} - f \right] + K_1 \left[\left(\frac{d\bar{T}_1}{d\eta} \right)_{\eta=0+} - g\bar{T}_1(0) \right] = g\hat{T}_1(0) + h - \left(\frac{d\hat{T}_1}{d\eta} \right)_{\eta=0+} \quad (C.51)$$

Equations (C.50-C.51) permit unique values of r_1 and K_1 to be determined.

The first order problem is reduced to the solution of five second order, ordinary differential equations, Equations (C.43-C.46) and the solution of Equation (61) for $\theta_{1P}(\eta)$. As with the zero order problem, these equations were solved by integrating to the liquid surface from some large, but finite, η . Asymptotic analysis was used to determine the analytical form of the solutions for large η . These analytical equations were then used to generate starting values for the numerical solution. The asymptotic analysis is discussed in the following.

The form of $\theta_{1P}(\eta)$ for large η has already been discussed. For the complete unsteady gas phase problem, the form is given by Equation (C.2). For the quasi-steady gas phase problem the form of

θ_{1P} for all η is given by

$$\theta_{1P} = 0 \quad (C.52)$$

For T_{1H} , \hat{T}_{1P} , T_{1P}^* and \bar{T}_{1P} the form of the solutions depends on the reaction order, n . For $n = 1$ and $\delta = 0$, it can be shown that for large η

$$p \rightarrow -A \exp(-E) - i\omega = -p_\infty \quad (C.53)$$

$$d \rightarrow -\left(\frac{\gamma-1}{\gamma}\right)i\omega - A \exp(-E)\theta_{1P} \quad (C.54)$$

$$b \rightarrow 0 \quad (C.55)$$

$$c \rightarrow -A \exp(-E) \exp\left[\frac{1 - \sqrt{1+4i\omega}}{2} \eta\right] \quad (C.56)$$

Substituting Equations (C.53-C.56) into Equations (C.43-C.46) it is found that for large η

$$T_{1H} = \exp\left[\frac{1 - \sqrt{1+4p_\infty}}{2} \eta\right] \quad (C.57)$$

$$\hat{T}_{1P} = \exp\left[\frac{1 - \sqrt{1+4p_\infty}}{2} \eta\right] + \frac{\left(\frac{\gamma-1}{\gamma}\right)i\omega + A \exp(-E)\theta_{1P}}{A \exp(-E) + i\omega} \quad (C.58)$$

$$T_{1P}^* = T_{1H} \quad (C.59)$$

$$\bar{T}_{1P} = \exp\left[\frac{1 - \sqrt{1+4p_\infty}}{2} \eta\right] + \left[\frac{A \exp(-E) + \left(\frac{1 - \sqrt{1+4i\omega}}{2}\right)^2 - \left(\frac{1 - \sqrt{1+4i\omega}}{2}\right)}{A \exp(-E) + i\omega} \right] \exp\left[\frac{1 - \sqrt{1+4i\omega}}{2} \eta\right] \quad (C.60)$$

For $n = 2$ and $\delta = 0$, it can be shown that for large η

$$p \rightarrow -i\omega \quad (C.61)$$

$$d \rightarrow -\frac{\gamma-1}{\gamma} i\omega \quad (\text{C.62})$$

$$b \rightarrow 0 \quad (\text{C.63})$$

$$c \rightarrow 0 \quad (\text{C.64})$$

and thus

$$T_{1H} = \exp \left[\frac{1 - \sqrt{1+4i\omega}}{2} \eta \right] \quad (\text{C.65})$$

$$\hat{T}_{1P} = \exp \left[\frac{1 - \sqrt{1+4i\omega}}{2} \eta \right] + \frac{\gamma-1}{\gamma} \quad (\text{C.66})$$

$$T_{1P}^* = T_{1H} \quad (\text{C.67})$$

$$\bar{T}_{1P} = T_{1H} \quad (\text{C.68})$$

In deriving Equations (C.57-C.60) and Equations (C.65-C.68) growing exponentials were disregarded in order to satisfy Equations (C.37-C.39). The constants in the homogeneous solutions were normalized to unity since they were already considered in the constants \hat{K}_1 , K^* and \bar{K} .

Summarizing, Equation (61) is first solved to find $\theta_{1P}(\eta)$ using Equation (C.2) to generate starting values for large η . If the gas phase is assumed to be quasi-steady then θ_{1P} is set equal to zero for all η . Next, Equations (C.43-C.46) are solved using the appropriate starting values, Equations (C.57-C.60) for $n = 1$ or Equations (C.65-C.68) for $n = 2$. Equations (C.47-C.49) are then used to find \hat{K} , K^* and \bar{K} . Next \hat{T}_1 , T_1^* , and \bar{T}_1 are found using Equations (C.40-C.42). It should be mentioned at this point that the first and second derivatives of \hat{T}_1 , T_1^* and \bar{T}_1 can be found from equations similar to

Equations (C.40-C.42). r_1 and K_1 are then determined from Equations (C.50-C.51). Finally, Equation (C.24) is used to find T_1 .

APPENDIX D

PHYSICAL PROPERTIES

The references for the physical properties required in the calculations are shown on Table 4. The correlations used to compute the properties are discussed in the following.

The specific heat of the fuel in both the gas and liquid phases were assumed constant. The gas phase specific heat was evaluated at a temperature of 900°K.

The gas phase thermal conductivity λ_{∞}^* was evaluated at the adiabatic flame temperature. For this calculation the gas phase mixture was assumed to be made up of 50% N_2H_4 , 25% NH_3 , 12.5% N_2 and 12.5% H_2 on a molar basis.

The liquid phase thermal conductivity was assumed constant. It was evaluated from the liquid thermal diffusivity which was found to give the best fit of the zero order theory to the experimental results on liquid phase temperature distributions. This value of liquid thermal diffusivity was found to be $1.26 \times 10^{-3} \text{ cm}^2/\text{sec}$ as discussed in Section 4.1.1.

The adiabatic flame temperature, T_{∞}^* , was calculated allowing for all relevant dissociation reactions. The thermochemical properties required for this calculation were taken from the JANAF Tables. [46]

The heat of vaporization of the fuel was evaluated from the overall conservation of energy relation. By specifying the temperature at the cold end of the liquid, the final gas phase temperature, the heat capacities of the gas and liquid, and the heat of combustion, the overall conservation of energy in the steady state could only be satisfied by proper selection of the heat of vaporization. The value used is shown in Table 1.

Table 4

References for Physical Properties

Property	References	
	N_2H_4	Combustion Products
h^o	42	43
ρ_ℓ^*	39	--
$\lambda_{\infty o}^*$	44 ^a	44
C_p	45	--
C_ℓ	39	--

^aComputed, Method of Reference [44]

The constants in the Clausius-Clapeyron equation were determined from a least squares fit to the existing data on vapor pressures as a function of liquid temperature for hydrazine.

[45, 47-48] The values found are listed in Table 1.

APPENDIX E

SURFACE MASS FRACTION USING THE INFINITE
ACTIVATION ENERGY ASSUMPTION

If an infinite gas phase activation energy is assumed rather than a unity Lewis number, the zero order equation relating surface fuel mass fraction to surface temperature, Equation (16), is different. In this Appendix, the theoretical development of an equation analogous to Equation (16) is presented for an infinite activation energy flame.

The theoretical development follows closely that given in Reference [38]. Faeth [38] used a molar basis for his analysis and assumed that both the specific heat and thermal conductivity of the gas phase were linear functions of temperature. In the analysis presented here, a mass basis is used and the specific heat is assumed constant but thermal conductivity is a function of temperature.

Since the reaction is confined to a flame surface, the steady state energy and species conservation equations can be written as

$$\rho^*v^*[C_p(T^* - T_s^*) + L^*] = \lambda^* \frac{dT^*}{dx^*} \quad (E.1)$$

$$\rho^*v^*[Y_F - 1] = \rho^*D \frac{dY_F}{dx^*} \quad (E.2)$$

With the assumption of infinite activation energy, the outer boundary condition can rigorously be applied at the outer edge of the flame zone, x_F^* , since the flame is infinitely thin.

Thus, the boundary conditions are

$$\begin{aligned} x^* = 0, & \quad Y_F = Y_{F,S} & \quad T = T_s^* \\ x^* = x_F^*, & \quad Y_F = 0 & \quad T = T_\infty^* \end{aligned} \quad (E.3)$$

The quantity λ^*/ρ^*D is only a weak function of composition and is assumed constant. [38]

Dividing Equation (E.1) by Equation (E.2) to eliminate spatial derivatives and integrating, using the boundary conditions, Equation (E.3) yields

$$Y_{F,S} = 1 - \left[\frac{L^*}{C_p (T_\infty^* - T_s^*) + L^*} \right] \frac{\lambda^* / (\rho^* D C_p)}{\quad} \quad (E.4)$$

Equation (E.4) then replaces Equation (16) if an infinite activation energy is assumed.

APPENDIX F

DEVELOPMENT OF THE TOTALLY QUASI-STEADY ANALYSIS

The totally quasi-steady analysis neglects both transient liquid and gas phase effects. The analysis was done by using the experimental data on the fundamental strand burning rate of hydrazine as a function of pressure shown in Figure 8 and fitting it to the following empirical equation for pressures greater than atmospheric.

$$v_{\ell}^* = u_0^* + u_1^* P_0^* = \frac{dx_s^*}{dt^*} \quad (F.1)$$

where u_0^* and u_1^* are constants.

Assume the pressure, P_0^* , varies sinusoidally with time such that

$$P_0^* = P_{00}^* + P_{01}^* \cos \omega^* t^* \quad (F.2)$$

where P_{00}^* and P_{01}^* are also constants. Substituting Equation (F.2) into (F.1) and integrating yields

$$x_s^* = (u_0^* + u_1^* P_{00}^*) t^* + \frac{u_1^* P_{01}^*}{\omega^*} \sin \omega^* t^* \quad (F.3)$$

Equation (F.3) is the totally quasi-steady theoretical prediction of liquid surface movement. The first term on the right hand side of Equation (F.3) represents the steady regression of the liquid surface for constant pressure. The second term represents the oscillatory motion of the liquid surface under oscillatory pressure conditions. Note that the amplitude of the oscillating component of the liquid surface motion is an inverse function of frequency, and that the phase angle of the surface oscillation with respect to the pressure oscillation is constant and equal to 90° .

APPENDIX G

DEVELOPMENT OF THE ACOUSTIC ADMITTANCE EXPRESSION

In order to determine the acoustic admittance of the combustion system, the gas phase velocity perturbation due to a pressure perturbation of amplitude ϵ must be known. The solution of the equations developed from the present theoretical model do not explicitly yield the gas phase velocity perturbation. However, this parameter can be found from other output parameters of the theory as developed in the following.

Rewriting Equation (21) here for convenience

$$r = \rho v + \frac{\partial}{\partial t} \int_{x_s(t)}^x \rho \, dx \quad (G.1)$$

but

$$\rho = \frac{P}{T} \quad (G.2)$$

and therefore

$$rT = Pv + T \int_{x_s(t)}^x \frac{1}{T} \left[-\frac{P}{T} \frac{\partial T}{\partial t} + \frac{\partial P}{\partial t} \right] dx - \rho_s \dot{x}_s \quad (G.3)$$

Perturbing Equation (G.3) using Equation (45) and rearranging yields to zero order in ϵ

$$v_0 = T_0 \quad (G.4)$$

and to first order in ϵ

$$v_1 = T_0(r_1 - 1) + T_1 - i\omega T_0 \int_0^{\phi} \frac{T_0 - T_1}{T_0} d\eta - \frac{i\omega x_{s1} T_0}{T_0(0)} \quad (G.5)$$

where to first order

$$dx = T_0 \, d\eta \quad (G.6)$$

and

$$\Phi = \int_0^{\eta} T_o \, d\eta \quad (G.7)$$

The acoustic admittance is defined as

$$A_b = \left(\frac{v_1}{v_o} \right)_{x \rightarrow \infty} = \left(\frac{v_1}{v_o} \right)_{\eta \rightarrow \infty} \quad (G.8)$$

Using Equations (G.4 and G.5) the real part of the acoustic admittance, which is the quantity of interest as discussed in Section 4.2.5.3, is

$$A_{b,R} = r_{1,R} - 1 + \frac{T_{1,R}}{T_o} + \omega \int_0^{\Phi} \frac{T_{1,I}}{T_o} \, d\eta + \frac{\omega x s_{1,I}}{T_o(0)}. \quad (G.9)$$

The real part of the acoustic admittance discussed in Section 4.2.5.3 was determined from Equation (G.9) evaluated at η equal to infinity. The parameters in Equation (G.9) were taken from the numerical solution of the first order problem except for large η where the asymptotic representations of the parameters were used.

APPENDIX H

EXPERIMENTAL DATA

Table 5

Hydrazine Steady Strand Burning Rates

Pressure (atm)	Liquid Purity (%)	Tube Inside Diameter (mm)	Burning Rate x 10 ² (cm/sec)
0.36	99.4	12.0	1.61
0.72	99.4	12.0	2.01
1.00	99.4	12.0	2.42
8.10	99.4	12.0	8.74
13.8	99.4	12.0	16.1
25.0	99.4	12.0	26.2
39.1	99.4	12.0	44.5
0.33	98.6	12.0	1.55
0.40	98.6	12.0	1.60
1.00	98.6	12.0	2.40
2.72	98.6	12.0	4.25
3.40	98.6	12.0	5.00
5.44	98.6	12.0	6.50
6.70	98.6	12.0	8.61
12.9	98.6	12.0	16.72
20.4	98.6	12.0	25.8
28.9	98.6	12.0	35.5
39.1	98.6	12.0	48.2
0.40	98.6	8.0	1.72
1.00	98.6	8.0	2.55
3.40	98.6	8.0	5.15
6.70	98.6	8.0	8.81
12.9	98.6	8.0	17.3
20.4	98.6	8.0	25.9
0.40	98.6	4.0	2.20
1.00	98.6	4.0	3.25
3.40	98.6	4.0	5.95
6.70	98.6	4.0	9.80
12.9	98.6	4.0	17.5
20.4	98.6	4.0	26.0
0.34	95.6	12.0	1.41
1.00	95.6	12.0	1.89
3.41	95.6	12.0	3.65
11.6	95.6	12.0	6.30
37.8	95.6	12.0	12.5
0.37	92.6	12.0	1.25
1.00	92.6	12.0	1.70
4.05	92.6	12.0	3.30
17.0	92.6	12.0	6.10
36.8	92.6	12.0	10.6

Table 6

Hydrazine Liquid Surface Temperatures

Pressure (atm)	Surface Temperature (K)
0.51	351.8
0.82	362.1
1.00	367.0
3.37	407.5
6.60	426.2
10.1	440.3
13.0	458.7
17.2	469.0
19.8	470.3

Table 7

Hydrazine Liquid Surface Oscillation Amplitude and Mean Burning
Rate at a Mean Pressure of 1.54 atm and a Frequency of 1.32 Hz
for Various Pressure Amplitudes

ϵ	x_{s1}^*/ϵ (mm)	$v_{\dot{m}}^* \times 10^2$ (cm/sec)
0.051	0.077	0.311
0.103	0.075	0.309
0.153	0.076	0.311
0.198	0.074	0.312
0.245	0.080	0.315
0.298	0.086	0.329
0.335	0.089	0.335

Table 8

Hydrazine Liquid Surface Oscillation Amplitude and Phase Angle at a Mean Pressure of 9.77 atm for Various Frequencies

ω^* (Hz)	x_{S1}^*/ϵ (mm)	ϕ ($^\circ$)
0.52	0.445	98.1
1.05	0.201	104.2
2.88	0.102	107.4
5.19	0.065	107.6

Table 9

Hydrazine Liquid Surface Oscillation Amplitude and Phase Angle at a Mean Pressure of 1.18 atm for Various Frequencies

ω^* (Hz)	x_{S1}^*/ϵ (mm)	ϕ ($^\circ$)
0.40	0.121	80.1
1.01	0.068	59.8
3.12	0.017	37.1
4.85	0.008	-4.4